Modeling and Analysis of a Horizontal Direct Chill Casting Process

Garðar Garðarsson

Faculty of Industrial,- Mechanical Engineering and Computer Science
University of Iceland

Modeling and Analysis of a Horizontal Direct Chill Casting Process

Garðar Garðarsson

60 ECTS thesis submitted in partial fulfilment of a
Magister Scientiarum degree in Mechanical Engineering

Thesis committee
Brynjar Örn Arnarson, M.Sc.
Halldór Pálsson, Ph.D.
Magnús Þór Jónsson, Ph.D.
Þröstur Guðmundsson, Ph.D.

Faculty Representative
Halldór Guðmundsson, M.Sc.

Faculty of Industrial, - Mechanical Engineering and Computer Science
School of Engineering and Natural Sciences
University of Iceland
Reykjavik, May 2012

Modeling and Analysis of a Horizontal Direct Chill Casting Process
60 ECTS thesis submitted in partial fulfilment of a *Magister Scientiarum* degree in Mechanical Engineering

Faculty of Industrial,- Mechanical Engineering and Computer Science
School of Engineering and Natural Sciences
University of Iceland
VRII, Hjardarhagi 2-6
107 Reykjavik
Iceland

Telephone: 525 4000

Bibliographic information:
Garðar Garðarsson, 2012, Modeling and Analysis of a Horizontal Direct Chill Casting Process, Master's thesis, Faculty of Industrial,- Mechanical Engineering and Computer Science, University of Iceland, pp. 85.

Printing: Háskólaprent
Reykjavik, Iceland, May 2012

Abstract

The objective of this study is to investigate bleedouts in Horizontal Direct Chill casting process and to make a complete finite volume model of such process. The casting machine that was investigated and used as a reference for the numerical model, was the HDC casting machine at Alcoa Fjarðaál in Iceland. One of Fjarðaál‘s main production problems are bleedouts in the HDC casting machine and the consequences of recurrent bleedouts is production loss. To analyse the problem, historical data were examined and measurements were performed in the process. The numerical model was used to support the research. To simulate the current state, measurements were used to construct the numerical model.

It was focused on examining the main control parameters in the casting process and their impact on the probability of bleedouts. The goal was to identify which control parameter is most critical and realise how it is possible to reduce number of bleedouts or prevent it. The study showed that the temperature of the aluminium alloy is the most sensitive control parameter. Furnace exchange has also a influence on bleedouts, it includes discrepancy between furnaces.

Útdráttur

Markmið þessarar rannsóknar var að rannsaka blæðingar í láréttu sísteypuferli (HDC) sem framleiðir melmisstangir úr áli og að búa til nákvæmt reiknilíkan af slíku ferli. Steypuvélin sem var rannsökuð og notuð sem viðmið fyrir líkansmíðina, var lárétt steypuvél Alcoa Fjarðaáls á Íslandi. Eitt helsta framleiðsluvandamál Fjarðaáls eru blæðingar í láréttu steypuvélinni og afleiðingar síendurtekinna blæðinga er framleiðslutap. Til að greina vandamálið voru söguleg gögn skoðuð og mælingar framkvæmdar í ferlinu. Reiknilíkanið var notað til að styðja við rannsóknina. Til að ná að herma núverandi ástand voru mælingar notaðar til að byggju upp reiknilíkanið.

Lögð var áherslu á að skoða helstu stýribreytur í steypuferlinu og áhrif þeirra á líkindi blæðinga. Takmarkið var að finna hvaða stýribreyta væri mikilvægust fyrir ferlið og átta sig á því hvernig mögulega væri hægt að fækka blæðingum eða koma í veg fyrir þær. Rannsóknin leiddi það í ljós að álhitastigið væri viðkvæmasta stýribreytan. Ofnaskipti hafa einnig áhrif á blæðingar, það felur helst í sér ósamræmi milli ofna.

Table of Contents

List of Figures

List of Tables

Abbreviations

DC: Direct chill

VDC: Vertical direct chill

HDC: Horizontal direct chill

CFD: Computational fluid dynamics

FVM: Finite volume model

CBF: Change between furnaces

Acknowledgements

This study was performed under the supervision of Professor Magnús Þór Jónsson and co-supervised by Associate Professor Halldór Pálsson, both at the Department of Industrial Engineering, Mechanical Engineering and Computer Science at the University of Iceland, and by Þröstur Guðmundsson PhD. Material Engineer at HRV Engineering. The fourth member of the thesis committee was Brynjar Örn Arnarson from Alcoa Fjarðaál. I deeply thank them for all their assistance and support during the study.

Alcoa Fjarðaál receive my greatest gratitude for sponsoring the work and to supply excellent assistance, both in terms of workspace and support from staff. I want to especially thank all the employees in the casthouse who provided all the help needed with smile on their face. I want to deliver a special appreciation to Ásgrímur Sigurðsson who was my main contact with Alcoa Fjarðaál.

Last but not least I thank my family for all the support during this project and the years of study preceding it.

1 Introduction

Direct-chill (DC) casting of aluminum was invented between 1936 and 1938 almost simultaneously in Germany (W. Roth, VAW) and in USA (W.T. Ennor, ALCOA). This technology was based on the existing methods for copper and aluminium alloys suggested by Zunkel (1935) and Junghans (1933). The fundamental DC process is classified as one of the most important discoveries that led to the modern aluminium production. (Nadella R. , Eskin, Du, & Katgerman, 2007). The DC process has been classified into vertical direct chill (VDC) and horizontal direct chill (HDC) casting processes. VDC process has become the fundamental casting process in the aluminum industry but in recent years the HDC process is attracting attention all over the world (Dawood, 2001). The HDC process has many advantages in comparison with the VDC process, such as lower investment cost, potential for continuous casting, higher flexibility and so on (Wertli, 1986). The HDC process has however some characteristic technical problems due to gravity effects, which results in asymmetric cross-section and inhomogeneous microstructures in the product (Zhao, Cui, Dong, & Zhang, 2007).

Macrosegregation and bleedouts are considered as major defects in DC castings and these two defects are connected through the solidification phenomena. Macrosegregations are defects related to surface quality, such as drag marks, hot tears and cold shuts. Bleedout happens when the molten alloy have melted through the solid layer of the alloyed bar and aluminium alloy liquid flows freely out of the molds (Nadella R. , Eskin, Du, & Katgerman, 2007) (Suyitno, Eskin & Katgerman, 2006) (Suyitno, Kool & Katgerman, 2004). The DC casting process is controlled by varying casting parameters, the main casting parameters are the casting speed (the speed at which the solid is withdrawn from the mold), the temperature of the aluminium alloy and the flow rate of cooling water (Nadella R. , Eskin, Du, & Katgerman, 2007). The casting speed is an important variable during DC casting, since it determines the productivity of the process. Casting speed exerts a dominant influence on the macrosegregation and it is well known from earlier studies that the severity of macrosegragation increases with the casting speed (Nadella, Eskin, & Katgerman, 2006) (Gariepy & Caron, 1991). The cooling water flow rate is however the casting parameter that has minimal effect on the macrosegregation (Gariepy & Caron, 1991).

The aim of this study is to investigate bleedouts in a HDC casting process and construct a complete numerical model of the solidification process. Many studies have been conducted with VDC casting processes and it is a well known process. Much fewer studies have been conducted with HDC casting processes and the solidification process in HDC casting is not well known phenomena. The intention to construct a numerical model was to be able to understand the solidification phenomena better. Specially, the following research questions will be addressed:

- Is it possible to construct a complete numerical model of the solidification process?
- Which casting parameter(s) are most critical for the solidification process?

The solidification in a HDC casting process begins when aluminium alloy liquid flows through water cooled molds. Once the liquid metal solidifies, a solid shell is formed close to the wall of the molds, due to the heat flow from the liquid metal to the cooling water in the molds (primary cooling). While the outer part of the alloyed bar is now solid, the inner core is still a liquid or semi-solid (mushy zone). Once the secondary cooling outside of the molds takes effect, the alloyed bar will freeze all the way to the core. Bleedouts occurs when the cooling process has not functioned properly. (Sigurðsson, 2012) (Nadella R. , Eskin, Du, & Katgerman, 2007).

The casting machine that was investigated and used as a reference for the numerical model, was the HDC casting machine at Alcoa Fjarðaál in Iceland. Fjarðaál‘s HDC casting machine is the largest and most prolific machine of its kind in the world (Fjarðaál A. , 2011). In Fjarðaál‘s casthouse there are three casting machines, two value-added machines and one traditional sow caster for pure aluminium. The value-added machines are rod mill, producing continuous cast rods, and a HDC casting machine, producing complete aluminium alloy. The HDC casting machine is designed to produce pure aluminium or alloy and the final product can be delivered in three forms; T-bar and two types of foundry ingots. Currently it is focused on producing aluminium alloy ingots. The speciality of the HDC casting machine is the potential to do long continuous (many days) castings. The production rate can be great when producing large quantities of the same product. However, it is impractical when producing small quantities. One of Fjarðaál‘s main production problems are bleedouts in the HDC casting machine when casting the ingots. When bleedout occurs, sometimes it is possible to block the bleeding bar(s) and continue casting, but most of the time it is necessery to stop the casting process. Tidying up and preparing for next casting, called turnaround, can take up to 48 hours in the worst bleedout cases. In ordinary controlled stops, the turnaround is usually 14-20 hours. Another fact is that bleedout castings are on average shorter than castings without bleedouts. Based on this the uptime of the machine is much lower than it should be and it is clear that repeatedly bleedouts is causing production loss for Fjarðaál (Sigurðsson, 2012). To prevent bleedouts it is necessary to understand why it occurs and realise which casting parameter(s) are most critical for the solidification process. Once the root cause is found, it is possible to find solutions to prevent bleedouts. Current targets are to be able to cast continuously for 1-2 weeks, followed with a 12-24 hours for preventive maintenance and turnaround of the machine. Current casting averages are around 4-5 days, with current longest cast of just over 6 days. The results of this thesis activity are expected to help with extending further the average casting durations.

In order to analyse the casting parameters, historical data were examined. In Fjarðaál all casting parameters are continuously registered and stored in a database. Based on this database, the history of bleedouts were analysed, each bleedout casting was examined and compared to castings without bleedouts. The focus was on examining the instability in the casting parameters and it was identified which casting parameters were critical when bleedout occurs. Change between furnaces were also examined and whether there are links between bleedouts and those changes. To maintain continuous casting process, it requires two furnaces and at regular interval it is needed to change between those furnaces. To validate the numerical model, further measurements were performed on the process. Temperature distribution of the aluminium alloy in tundish was measured, the effects of the primary cooling was measured and the effects of secondary cooling was measured. To test the functionality of the numerical model, known case was simulated and results

compared. With this comparison it was possible to see if the calculation in the numerical model was correct. For accuracy of the results, mesh comparison was examined. It is best to have the mesh as rough as possible to minimize the calculation time but without affecting the accuracy of the results. The optimum mesh was found by comparing results for meshes with different coarseness and different shape. Last but not least, the cooling conditions in the model was adapted to the measurements of the primary cooling and secondary cooling. Thus, a numerical model of the HDC casting process was created and validated. This numerical model was then used to understand the solidification in this process.

2 Methods and Materials

2.1 Horizontal Direct Chill Casting

Figure 1 shows a schematic picture of HDC casting process. Two furnaces are used to prepare the aluminum alloy for casting. The preparation involves creating the right chemical composition and reaching the right temperature. It is poured from one furnace at a time while the other one is being prepared. Using this approach it is possible to do a long continuous casting and if the aluminium alloy is well prepared in the furnace, the change between furnaces should not affect the casting process. When poured from the furnaces, the aluminium alloy flows along launders and finally ends in a tundish, which is kind of a reservoir for the aluminium alloy, before the aluminium alloy leaks out of the tundish due to gravity and through the mold. The launders and the tundishes are well insulated, with a insulated lid to prevent loss of heat, because the aluminium alloy must have a predetermined temperature at the tundish.

A conveyor belt pulls the solidified bar out of the molds and it controls the casting speed of the process. The conveyor belt runs the bars through a sawing chamber where the bars are cut into correct length. At the end of the conveyor belt a robot stacks the ingots onto pallets, pallets are strapped prior to transportation of the finished product (after sawing the bars are called ingots). Finally the pallets are moved into the warehouse, ready for delivery. (Sigurðsson, 2012).

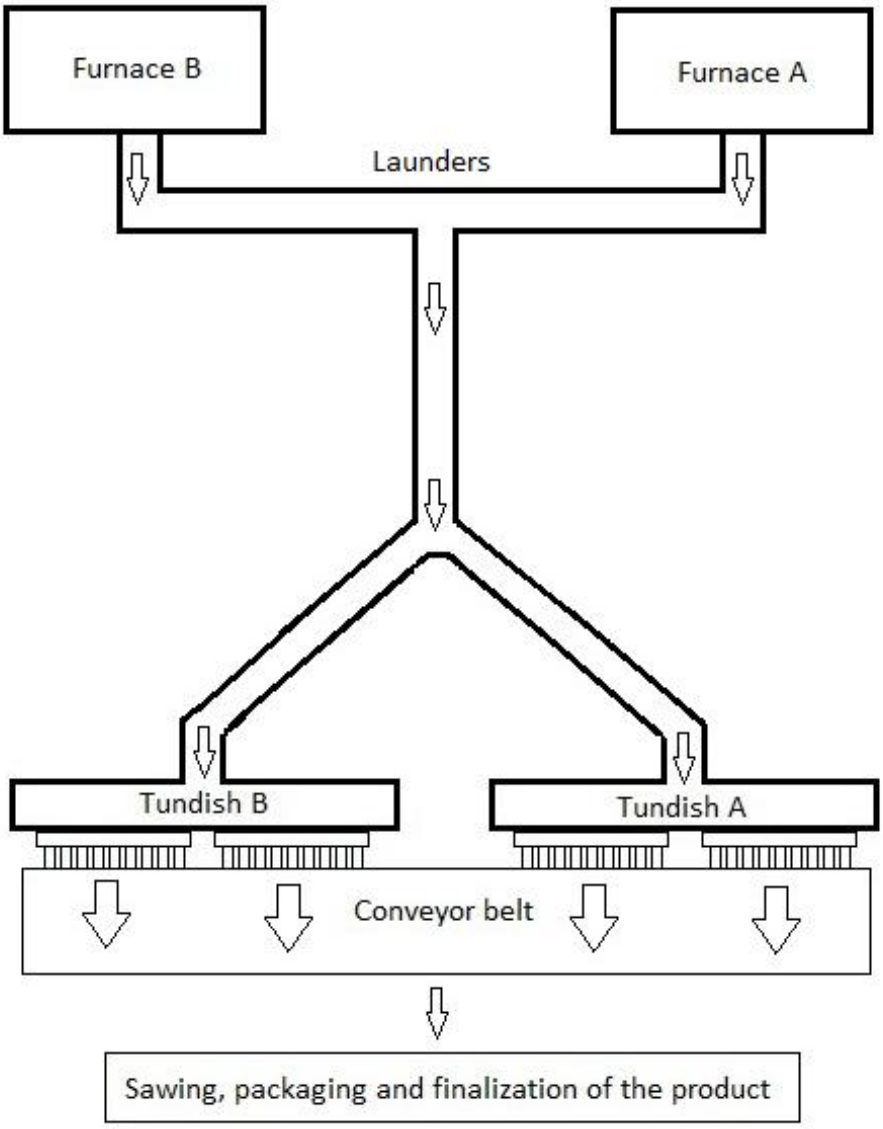

Figure 1 : Schematic figure of a HDC casting process

Figure 2 shows graphically how the aluminium alloy leaks out of the tundish through the mold. At the bottom of the tundish there are holes and narrow insulated pipes connect the mold to these holes. Due to gravity, the aluminium alloy flows through these pipes and into the mold. The mold cools down the alloyed bar and changes the aluminum alloy from liquid phase to solid form. When the bar leaves the mold, it has reached its final shape and the conveyor belt pulls the bar out of the mold at constant velocity (Sigurðsson, 2012).

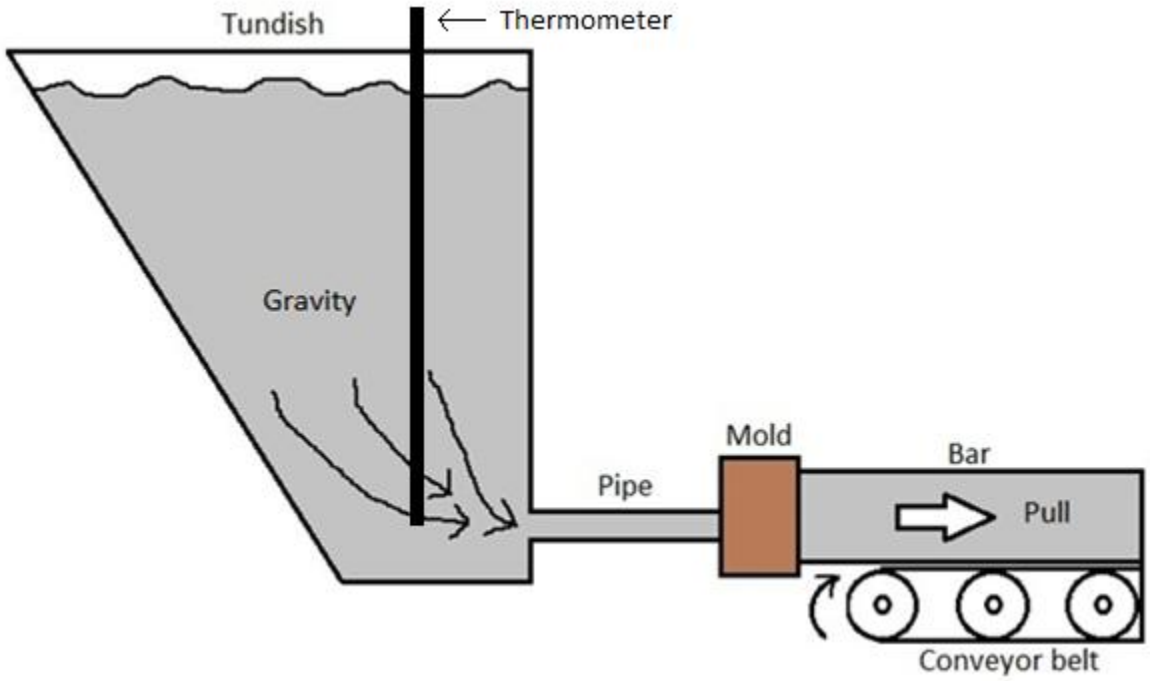

Figure 2 : Aluminium alloy flowing from tundish through the mold. Black vertical line show the location of a thermometer measuring the temperature of the alloy before entering the mold. (Sigurðsson, 2012).

The cooling of an alloyed bar is separated into primary cooling which occurs inside the molds and secondary cooling which occurs outside the molds. The cooling water flows into the molds and absorbs heat from the alloyed bar through the wall of the molds (primary cooling) and then the cooling water injects out of the molds directly to the bar (secondary cooling). The primary cooling is divided into two different cooling zones, zone 1 where the alloyed bar is in direct contact with the mold and zone 2 where there is an air gap between the alloyed bar and the mold. The reason for the air gap is that when the aluminum alloy begin to solidify on the surface, next to the molds and the alloyed bar shrinks together. Figure 3 shows a schematic of the air gap and the different cooling zones for an alloyed bar (Krane & Vusanovic, 2009).

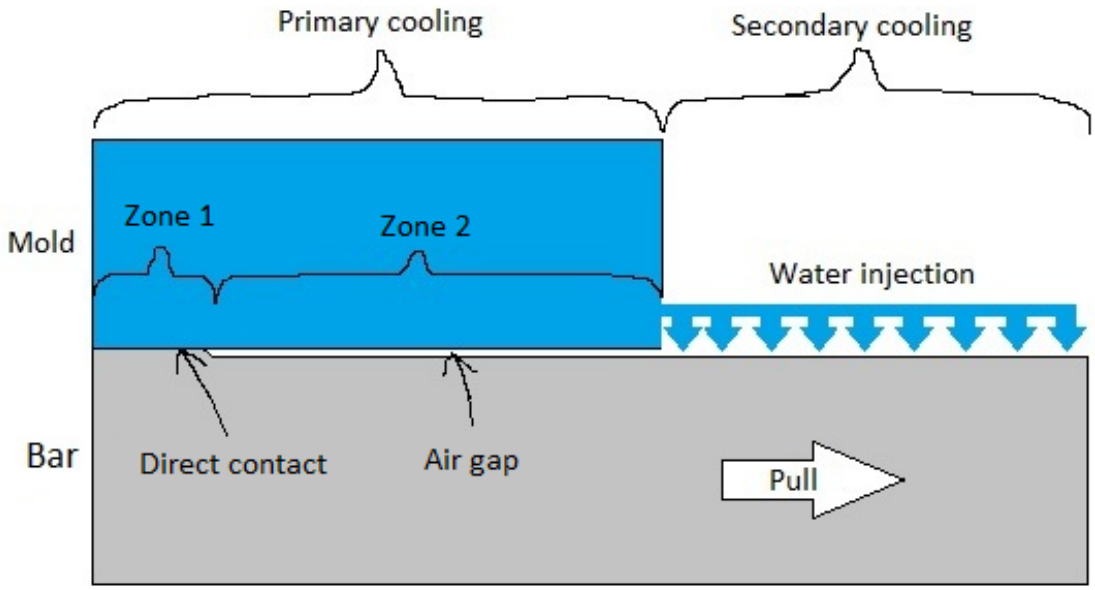

Figure 3 : Different cooling zones for an alloyed bar **(Krane & Vusanovic, 2009)**. *Zones 1 and 2 belongs to the primary cooling inside the mold and the secondary cooling is the water injection at bar's surface.*

The heat transfer varies by different cooling zones. The greatest heat transfer occurs in the secondary cooling where the water is in direct contact to the bar. At first contact the cooling water boils and the heat transfer reaches its maximum (Grandfield & McGlade, 1996) (Zuidema, Katgerman, Opstelten, & Rabenberg, 2001). The second largest heat transfer occurs in zone 1 where the alloyed bar is in direct contact to the mold. The least heat transfer occurs in zone 2 where an air gap acts as an insulation between the alloyed bar and the mold (Krane & Vusanovic, 2009). At the end of the secondary cooling there is some residual heat left in the alloyed bars, but that heat dissipates slowly into the air after the cooling processes itself. A Sankey diagram of the heat transfer can be seen in figure 4, which shows how it is relatively distributed at various points in the process. The Sankey diagram is based on measurements.

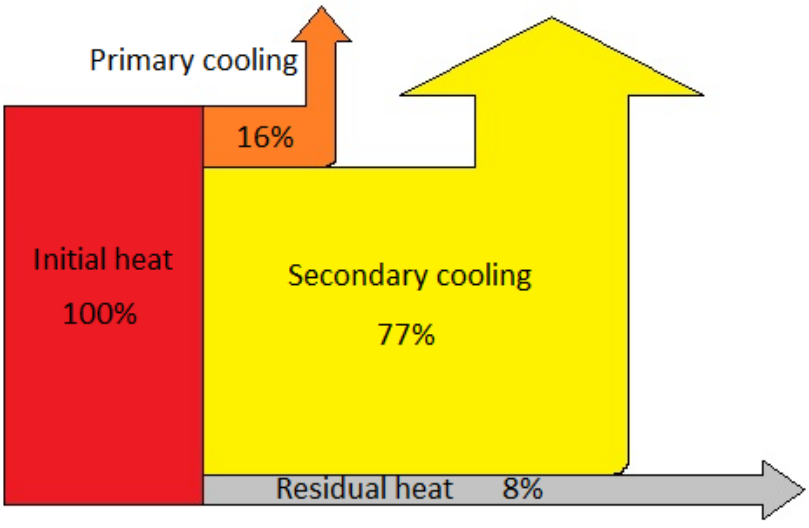

Figure 4 : Sankey diagram – relative distribution of heat transferred in alloyed bar

Figure 5 shows cross section of alloyed bar and an example of how it solidifies during the cooling process. The aluminium alloy starts to solidify in the primary cooling part (inside the molds) and a solid shell is formed close to the mold walls. While the outer part of the alloyed bar is now solid, the inner core is still liquid and semi solid/liquid (Nadella R. , Eskin, Du, & Katgerman, 2007). The semi solid/liquid zone is called mushy zone, where the liquid fraction is more than 0 and less than 1, but this zone is critical for the occurrence of some defects such as bleedouts (Suyitno, Kool & Katgerman, 2004). The secondary cooling ensures that the alloyed bar will solidify all the way to the core.

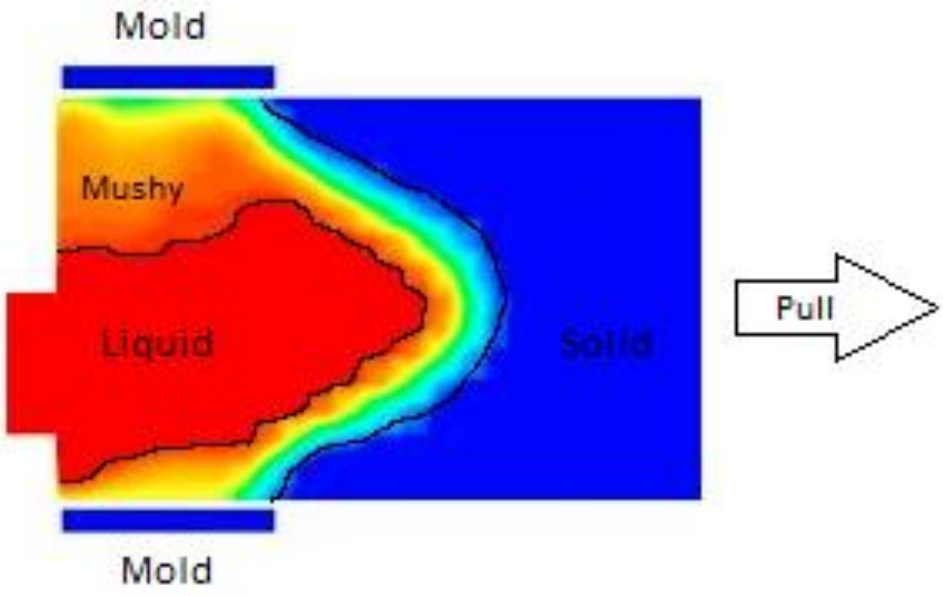

Figure 5 : Solidification of an alloyed bar. This figure is obtained from the model created in this study.

The process is controlled by varying casting parameters and these casting parameters control the quality of the product and performance. The parameters can influence each other so it is important to synchronize them to maintain a proper balance to achieve long continuous casting. The main casting parameters are the casting speed, temperature of the aluminium alloy, cooling water rate, the temperature of the cooling water and the lubrication rate. The casting speed is navigated by the velocity of the conveyor belt that pulls the bars out of the molds. It is easy to control this velocity and changes will immediately be detected. The temperature of the aluminium alloy in the tundishes is the same as the initial temperature of the aluminium alloy when it enters the molds. It can be difficult to control this parameter but change between furnaces can affect it and the temperature can suddenly change during the exchange. Then the aluminium alloy must be either cooled or heated but it may take some time. Since this is a difficult parameter to control, the operators usually try to keep the temperature within certain range. Cooling water rate and lubrication rate are easy to control and changes will be detected immediately. Temperature of the cooling water can be controlled rather easily and the changes will not be detected immediately (Sigurðsson, 2012).

2.2 Bleedouts

Bleedouts occurs when the cooling process has not functioned properly. There are two cases possible, either the cooling is too fast for the existing conditions or the cooling is too slow for the existing conditions. These conditions can suddenly change, for example if the temperature of the aluminium alloy changes or the casting speed is changed. When the cooling is too fast, the aluminium alloy solidifies too early inside the mold and the mold gets clogged. When the mold gets clogged either the alloyed bar gets stuck in the mold or the aluminium alloy flows through but no alloyed bar will be formed. When the cooling is too slow the alloyed bar is unable to solidify all the way to the core and the hot aluminium alloy in the core melts through the solid outer layer. In both cases the consequences are that the aluminium alloy flows uncontrolled through the molds and into the pit below (Sigurðsson, 2012) (Nadella R. , Eskin, Du, & Katgerman, 2007).

Figures 6 - 8 show photographs of bleedout cases. Figure 6 shows a case where large amount of alloy flows into the pit below because of bleedout. Figure 7 shows a bar where bleedout had occured through the bottom surface. Inside the bar the shape of the mushy zone can be shown as well as a hole through the bottom surface. Figure 8 shows a bar where bleedout had started and then stopped. The secondary cooling did prevent this bleedout. The bar is upside down and it can be shown that the bleedout occurred in the bottom surface and at the bottom of the side.

Figure 6: Photograph of a bleedout where large amount of alloy flows into the pit below.

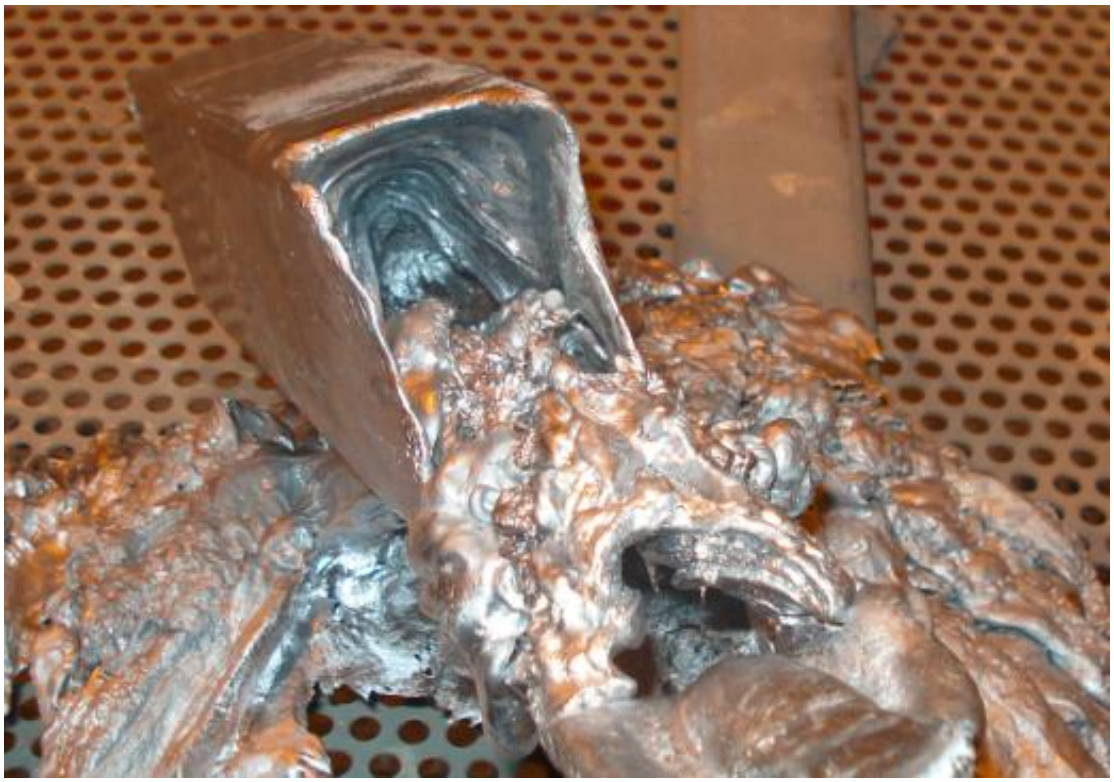

Figure 7 : Photograph of a bleedout bar. The bleedout occurred in the bottom surface, a hole can be seen through the bottom. Inside the bar the shape of the mushy zone can be shown.

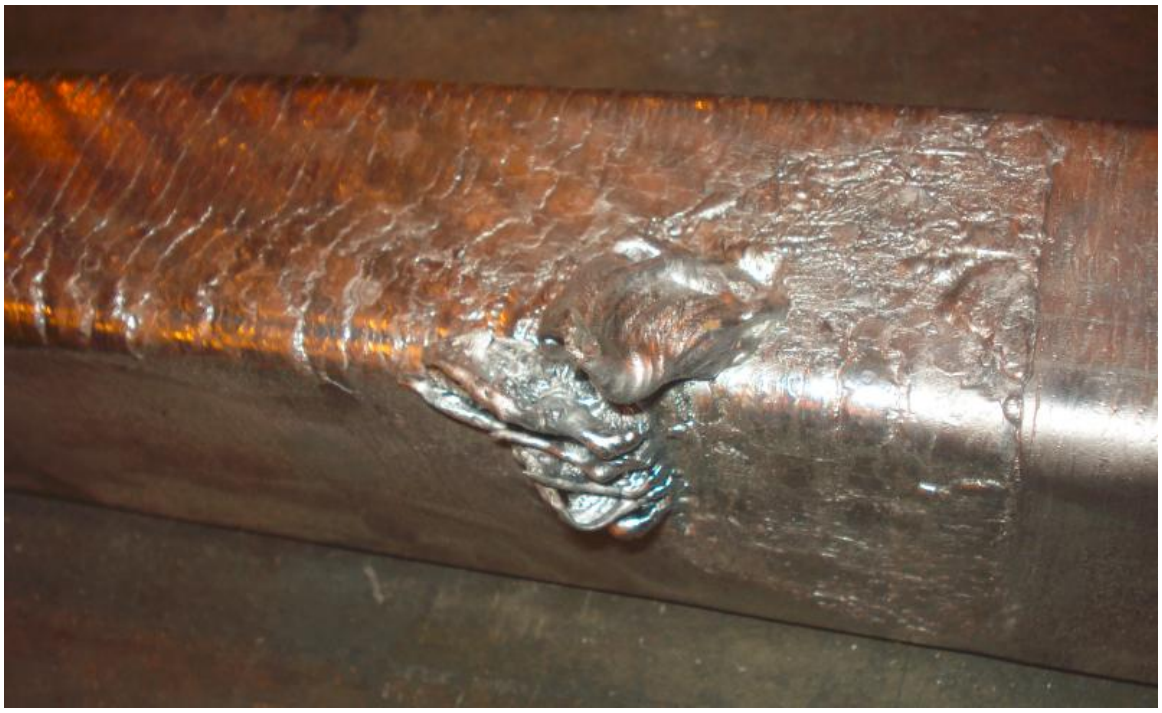

Figure 8 : Photograph of a bleedout bar. Here the bleedout was not serious and stopped automatically. The bar is upside down, the bleedout occurred in the bottom surface and at the bottom of the side.

2.3 Verification Measurements

Measurements were performed in the process in order to support the numerical model and make it possible to simulate the current state as accurately as possible. The measurements were also used to explore some theories about the process. All measurements were performed at least three times and in each measurement every measuring point was measured five times. To ensure consistency between the measurements, the same measuring instruments were used. Different thermometers were used, in each case the most suitable thermometer was chosen, all with estimated error of ± 1,1°C (Sigurðsson, 2012).. The three different thermometers will be called thermometer1, thermometer2 and thermometer3 for separation. All estimated errors were taken into account when processing the measurements.

Tundish – Temperature distribution

Measurements were performed in the tundishes to measure the temperature of the aluminium alloy and check whether the temperature distributions were uneven. In advance it was considered that the highest temperature was in the middle and the lowest temperature at the ends. If this were true, the alloyed bars have different initial temperature when entering the mold and it creates discrepancy between the alloyed bars. These measurements were also examined to check if it is acceptable to have just one thermometer at each tundish constantly logging, located at the ends.

In these measurements, thermometer1 was dipped into the aluminium alloy in several different locations and comparison made. Figure 9 shows where the temperature of the aluminium alloy in tundish is measured and figure 10 shows the measuring instruments used in this measurements

Figure 9 : Thermometer1 dipped into the aluminium alloy in tundish.

Figure 10 : Thermometer1, logger and measuring device in use.

Cooling water – Temperature difference

Each mold has four water intakes located at the ends as seen in figure 11. The water is ejected from the molds through thin pipes that are uniformly distributed around each bar, see figure 12. The water temperature at the intakes is known parameter (stored in the database) and the water temperature at the outlets is unknown parameter, so it had to be measured.

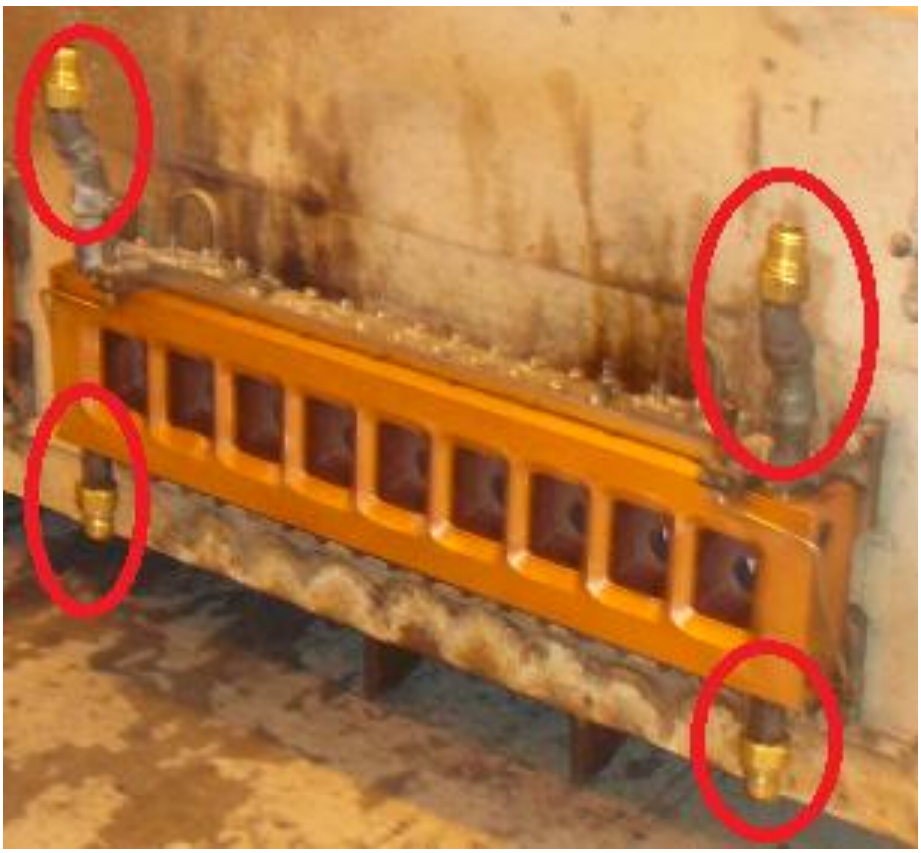

Figure 11 : Molds – water intakes, marked with red circles.

Figure 12 : Molds – holes for water outlet.

Measurements were made to make it possible to estimate the temperature change of the cooling water in the molds. Thermometer2 was inserted into the water outlets to measure the water temperature before the water leaves the molds, see thermometer2 in figure 13.

Figure 13 : Thermometer2 and measurement device.

By knowing the temperature difference, it is possible to calculate the heat transfer in the molds, see formula for heat transfer,

$$Q = \dot{m} C_p \Delta T \qquad (1)$$

where $\dot{m}$ is the amount of cooling water, C_p is the specific heat capacity of the cooling water at given temperature and ΔT is the temperature change of the cooling water (Holman, 2002). This heat transfer was used as reference in the numerical model, so the heat transfer in the molds could be simulated.

Bars – Temperature distribution

Measurements were performed to estimate the temperature distribution at the bars surface as a function of distance from the molds. The purpose was to determine how fast the bars are cooled in the secondary cooling. Also there was a theory that the cooling varies by location in the molds. To understand what effect the cooling water has on the temperature distribution, measurements were performed for different amount of cooling water and different initial temperature of the cooling water.

Twenty bars were measured as can be seen in figure 14. Five bars were chosen from each mold which should show if there is any difference between bars, based on location in the molds. Each bar was measured five times, it is total one hundred measurements for each condition.

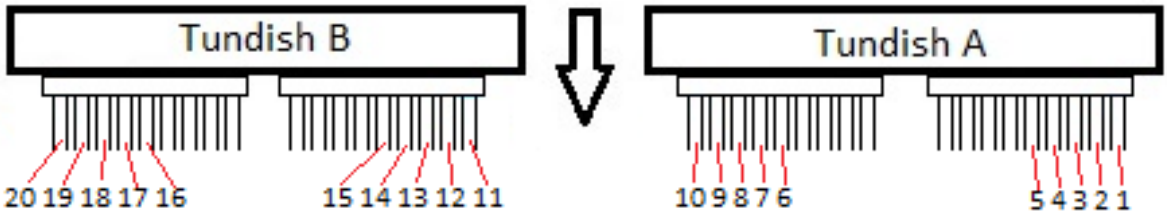

Figure 14 : Bars measured for temperature distribution.

Figure 15 shows the cross section of an alloyed bar and the exact location of the measuring points, it is the same location at each bar measured. Accuracy of the measuring points was: middle ± 5mm. Figure 16 shows how the measurements were logged in the casting direction. Thermometer3 was located at the middle of the bars, right up to the molds, and then it followed the bar for 20-30cm. Thermometer3 can be seen in figure 17.

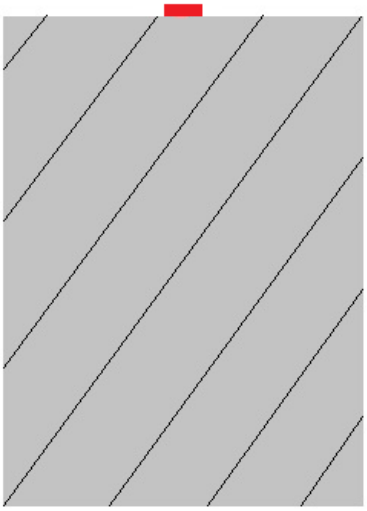

Figure 15 : Cross section of an alloyed bar, the red line denotes location of the measurement in each bar.

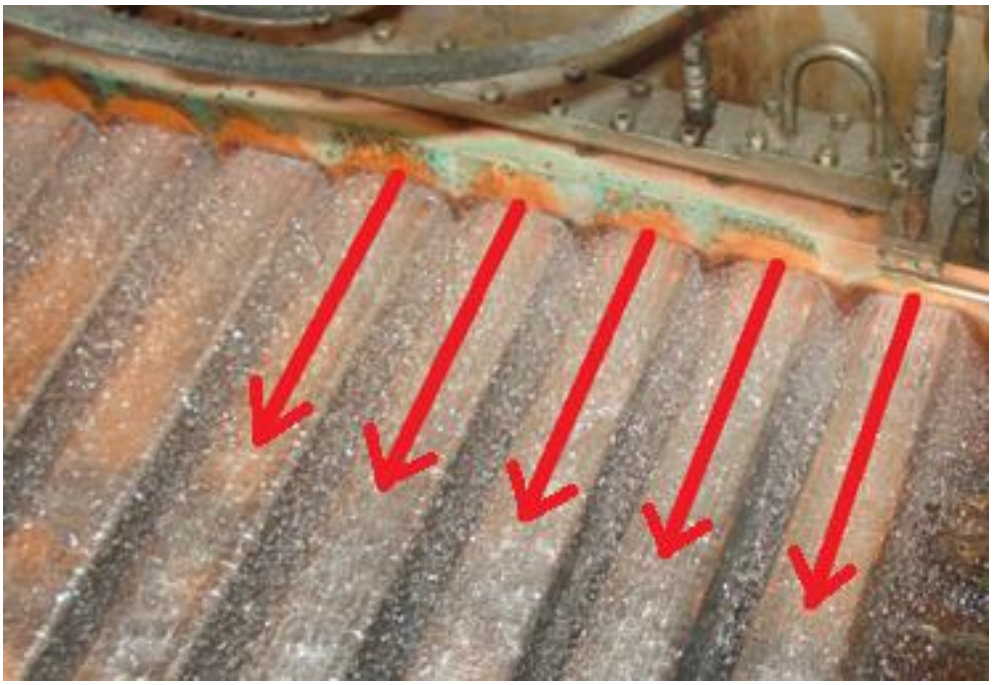

Figure 16 : Measuring temperature distribution, arrows show measuring direction.

Figure 17 :Thermometer 3, logger and measuring instrument.

The results of the measurements were used as reference in the numerical model, so the heat transfer in the secondary cooling could be simulated.

2.4 Numerical Model

ANSYS FLUENT was used to construct a numerical model of the solidification process. FLUENT is a computational fluid dynamics (CFD) software package to simulate fluid problems. It uses the finite-volume method (FVM) to solve the governing equations for fluid flow. It provides the capability to use different physical models such as incompressible or compressible, inviscid or viscous, laminar or turbulent, etc. A broad range of mathematical models for transport phenomena is combined with the ability to model complex phenomena, for example multiphase flow, energy, radiation, heat exchange, solidification, melting and acoustics. FLUENT‘s key strength is the ability to use variety of models to model complex phenomena (ANSYS, 2009). FVM discretization is based upon an integral form of the partial differential equations (PDE) to be solved (e.g. conservation of mass, momentum, or energy). The PDE is written in a form which can be solved for a given finite volume or cell. The computational domain is discretized into finite volumes and then for every volume the governing equations are solved. The resulting system of equations usually involves fluxes of the conserved variable, and thus the calculation of fluxes is very important in FVM (Versteeg & Malalasekera, 2007).

CFD codes are structured around the numerical algorithms and the two main parts are called preprocessor and solver (Versteeg & Malalasekera, 2007). Preprocessing is the first

step in building and analysing a flow model. It includes building the model, generating a mesh and entering the flow data to define the problem. Building the model includes creating the geometry, either in 2D or 3D as appropriate, and defining the boundary conditions. If the geometry is symmetric somehow, it is suitable to solve the calculations for only one half of the symmetry to save calculation time in the solver.

Preprocessor:

A model of half alloyed bar was created, a slice was taken vertically through the center of the bar. It was assumed that left side and right side are similar. The alloyed bar itself was created 150mm long. The inflow pipe, from reservoir (tundish) to the mold, was also created. All dimensions were based on measurements performed in Fjarðaál‘s casthouse. The first 100mm of the alloyed bar was considered as critical region since the bleedouts occurs there and the rest of the geometry doesn‘t really matter. The reason for creating 150mm long bar and the inflow pipe, is to ensure that boundary conditions at the ends (inflow & outflow) will not affect the results in the most important region. By testing different lengths for the bar in the model, it was revealed that 150mm would be a suitable length, the shorter the simpler calculations. A 1000mm long bar gave the same results as a 150mm long bar. 100mm–140mm long bars gave different results than 150mm long bar. The model was also tested without the inflow pipe and it gave completely different results. Figures 18 and 19 show the geometry used in the model. The inflow pipe is in two parts and the location of the molds is shown with transparent blue lines.

Figure 20 shows the boundaries for the boundary conditions. At the inlet, inflow was defined at certain temperature and certain velocity. The temperature of the aluminium alloy in tundish, was defined as the inlet temperature. The inlet velocity was calculated from the casting speed. The wall of the inflow pipe and the bottom of the mold were defined as isolation with no heat flux or heat loss. Cooling was defined at the surface of the bar, including in the mold. The cooling was divided into many cooling zones, based on the different cooling. Heat transfer coefficient was defined for each cooling zone. Primary cooling (inside the mold) has two cooling zones. The secondary cooling (outside the mold) has many cooling zones, since the cooling decreases further from the mold. At the outlet, outflow was defined and the velocity was the same as the casting speed.

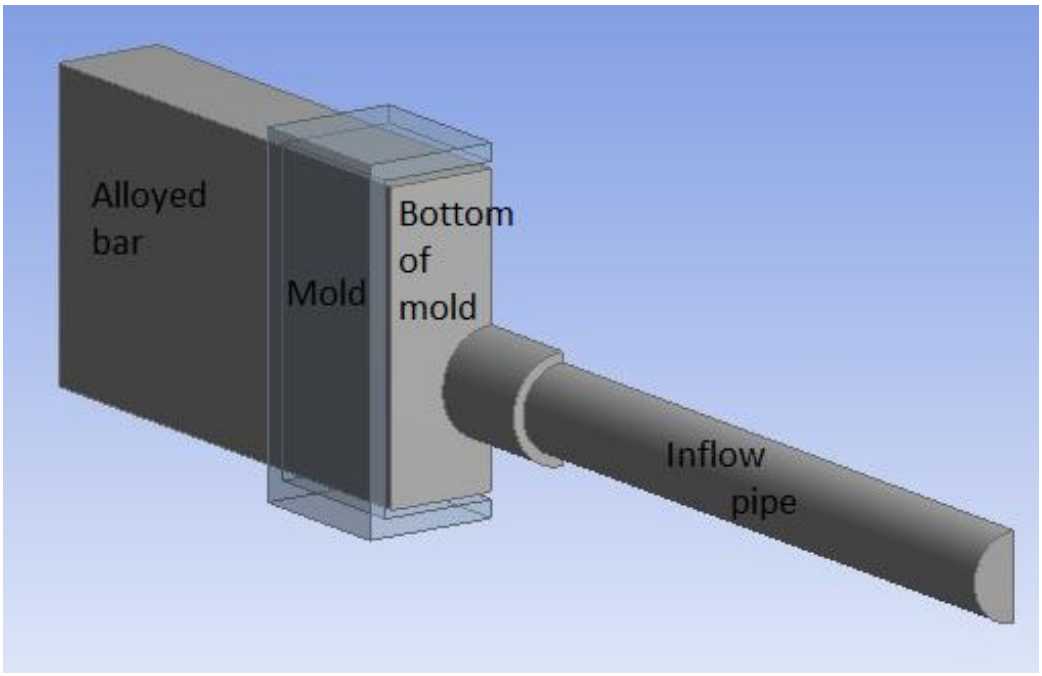

Figure 18 : The geometry used in the numerical model, 3D view 1.

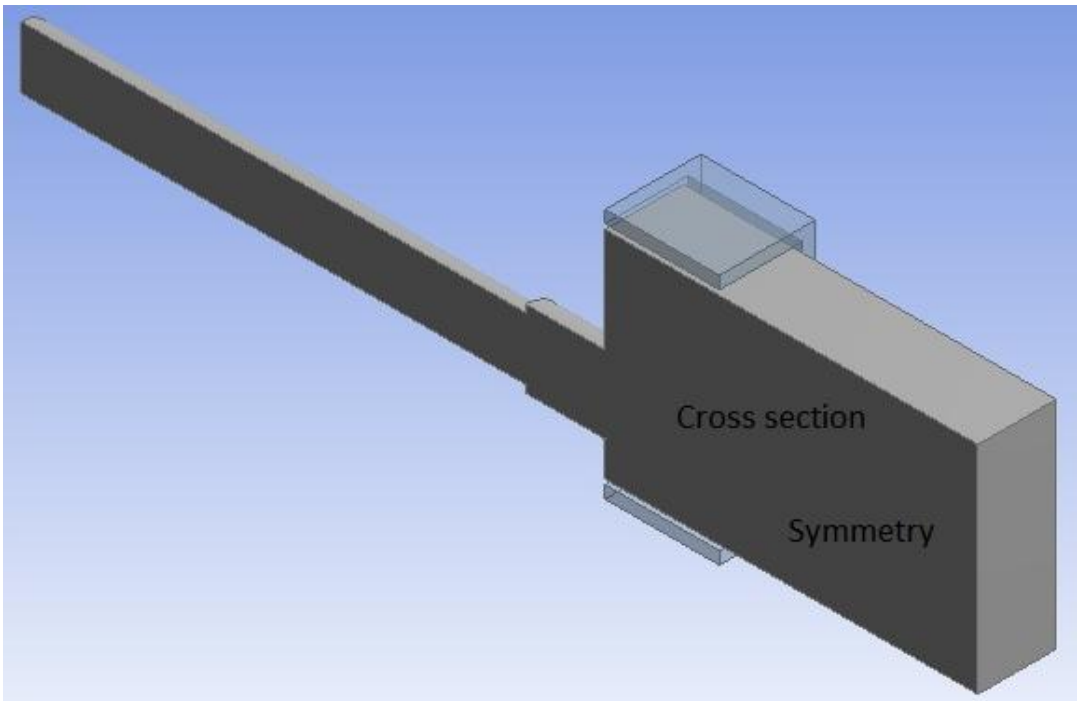

Figure 19 : The geometry used in the numerical model, 3D view 2.

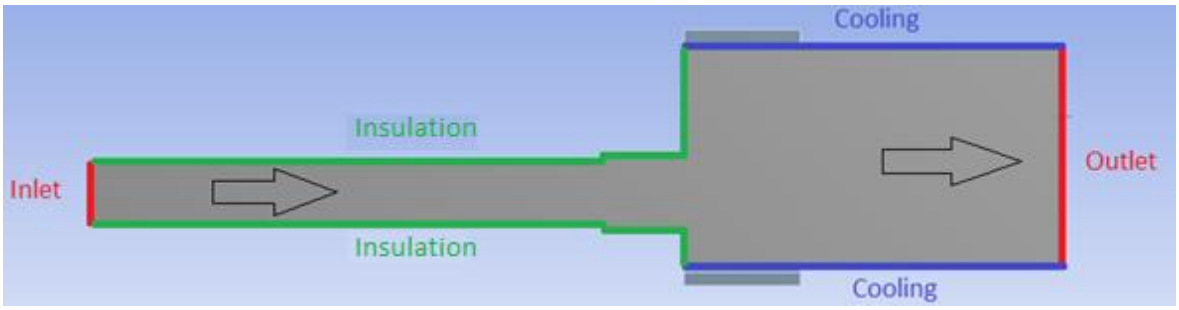

Figure 20 : Boundaries for the boundary conditions. Arrows show casting direction.

To get good results, it is important to apply mesh that is fine enough. Too few cells lead to inaccurate results and too many cells may result in long solver runs. It is important to have many cells close to walls and boundaries that matters and where there are fast changes, for example solidification. It is good to have few cells at big regions where there are no changes, as long as it does not affect the results. In this case the mesh was created rather coarse, except close to the cooling boundaries and the wall of the inflow pipe, there were more cells. The mesh was also adapted at the solidification zone, which means more cells were created. The mesh chosen had approximately 50000 cells, see figures 21 and 22. Experiments were performed with the mesh and many versions tested. Mesh with more cells than this did not lead to better solutions, it gave the comparable solution. Mesh with fewer cells than this did lead to worse solution.

Figure 21 : The mesh chosen, viewing the symmetry surface.

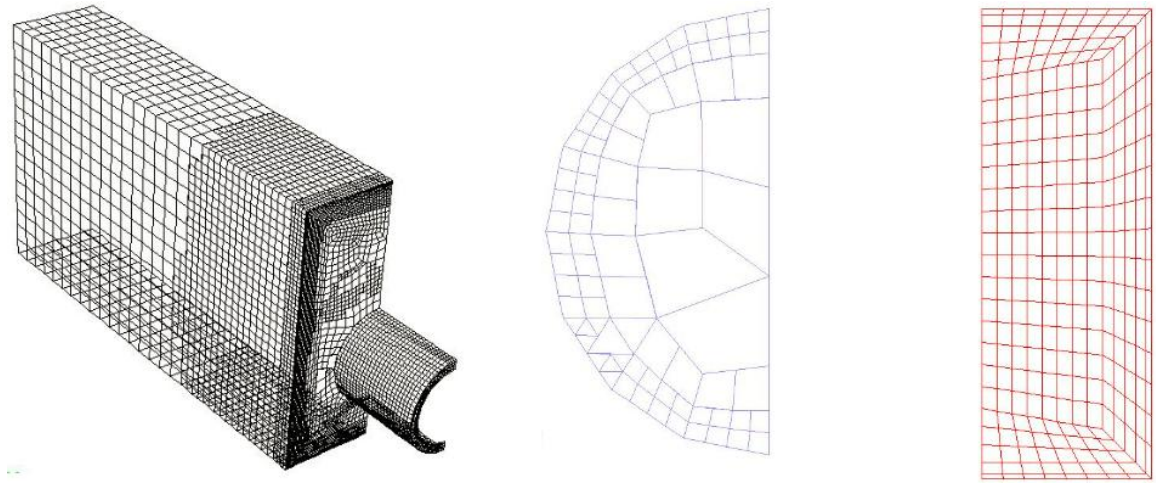

Figure 22 : The mesh chosen. From the left is listed; 3D view of the mesh, the inlet and the outlet.

Solver:

The second main element in CFD codes is the solver. The CFD solver does the flow calculations and produces the results (Versteeg & Malalasekera, 2007). Figure 23 shows roughly how the algorithm of the numerical approach works. The solver iterates the solution until the accuracy is satisfied. First the solution is initialized and then a solution is calculated. If the solution does not converge, solution parameters are modified and new solution is calculated. If the solution converges, accuracy is checked. If the accuracy is not enough, solution parameters are modified and new solution is calculated. This is repeated until the sufficient accuracy is achieved.

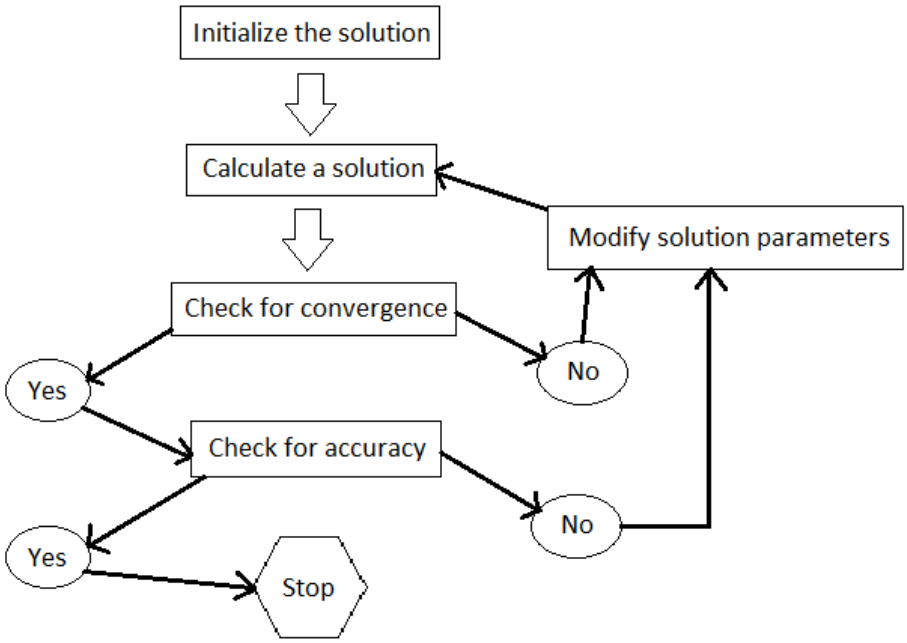

Figure 23 : Functionality of the algorithm of numerical approach, standard method in FLUENT.

The solver needs to be configured correctly to get correct results. In this case pressure-based solver was used, laminar flow was expected and the program was solved transient. When the program is solved transient, it is expected that no steady-state solution exists. In complex cases such as solidification&melting, there is rarely a steady-state solution. The built-in models in FLUENT used, was the energy model and the solidification&melting model. Since the solidification&melting model was used, pulling velocity needed to be defined. Pulling velocity pulls the material when the liquid fraction is less than 1, otherwise it would stop. As settings for the solution methods, the gradient was least squares cell based, the pressure was standard, the momentum was second order upwind and the energy was second order upwind. In all flow problems, FLUENT solves conservation equations for mass and momentum. When there is heat transfer involved, an additional equation for energy conservation is solved.

The equation for conservation of mass can be written as follows:

$$\frac{\delta\rho}{\delta t} + \nabla \cdot \left(\rho\vec{V}\right) = 0 \qquad (2)$$

where ρ is density, t is time and $\vec{V}$ is overall velocity vector (ANSYS, 2009).

The equation for conservation of momentum can be written as follows:

$$\frac{\delta}{\delta t}\left(\rho\vec{V}\right) + \nabla \cdot \left(\rho\vec{V}\vec{V}\right) = -\nabla p + \nabla(\bar{\bar{\tau}}) + \rho\vec{g} + \vec{F} \qquad (3)$$

where p is the static pressure, $\bar{\bar{\tau}}$ is the stress tensor, $\rho\vec{g}$ is the gravitational body force and $\vec{F}$ is the external body force.

The stress tensor is given by

$$\bar{\bar{\tau}} = \mu\left[(\nabla\vec{v} + \nabla\vec{v}^{\mathrm{T}}) - \frac{2}{3}\nabla \cdot \vec{v}I\right] \qquad (4)$$

where μ is the dynamic viscosity, I is the unit tensor and the second term on the right hand side is the effect of volume dilation (ANSYS, 2009).

The energy equation can be written as follows:

$$\frac{\delta}{\delta t}(\rho E) + \nabla \cdot \left(\vec{V}(\rho E + p)\right) = \nabla \cdot \left(k_{eff}\nabla T - \sum_j h_j \vec{J_j} + \left(\bar{\bar{\tau}}_{eff} \cdot \vec{v}\right)\right) + S_h \qquad (5)$$

where k_{eff} is the effective conductivity ($k + k_t$, where k_t is the turbulent thermal conductivity) and $\vec{J_j}$ is the diffusion flux of species j. Since laminar flow is used k_t is zero. The first three terms on the right-hand side is the conduction energy transfer, species diffusion, and viscous dissipation. S_h includes the heat of chemical reaction and E can be defined as

$$E = h - \frac{p}{\rho} + \frac{v^2}{2} \quad (6)$$

where h is the enthalpy. The enthalpy of the material is computed as the sum of the sensible enthalpy and the latent heat (ANSYS, 2009).

The conservation equations are linearized according to the implicit scheme with respect to the dependent variable and the result is a system of linear equations that can be solved simultaneously. Briefly, segregated implicit method calculates every single variable field considering all the cells at the same time. The code stores discrete values of each scalar quantity at the cell centre, the face values must be interpolated from the cell central values (Versteeg & Malalasekera, 2007).

2.5 Historical Data

At Alcoa Fjarðaál, the most important casting parameters are continuously registered and stored in a database. The registration frequency is determined by the variation in the casting parameters, predetermined standard deviation for each casting parameter assess the variation. If a casting parameter is stable, few measurements are stored but if the casting parameter suddenly becomes unstable, the storing frequency is increased. This is done to minimize the unnecessary storage in the database without affecting the quality of the measurements (Sigurðsson, 2012).

The measuring instruments used to monitor the process are thermometers, flow meters and sensors that detect height of aluminium alloy and speed of the conveyor belt. Figures 24 and 25 show examples of two measuring instruments. The thermometers are of the type K3 and PT100, the estimated error is ± 1,1°C. The flow meters are of the type Endress+Hauser Promag 50. Height sensors are of the type SIK DME3000 and the estimated error is ± 5mm. (Sigurðsson, 2012). All estimated errors were taken into account when processing data from the database.

Figure 24 : Thermometers, measuring the temperature of the aluminium alloy in tundish.

Figure 25 : Flow meter, measuring the cooling water rate to the molds.

The database was used to estimate the frequency of bleedouts. All stops at the HDC process were divided into categories and one of the category was bleedouts. The cases of each category were counted and with traditional percentage calculations, the ratio between categories were estimated. Casting times were also examined and average time calculated for each category. Whole years were compared, from January 1 to December 31. Based on this, the development in the HDC process can be evaluated, regarding to number of castings, casting time and bleedout frequency.

The database was used to estimate the effect of change between furnaces (CBF) on bleedouts. For each bleedout case, the time from the last CBF to a bleedout was examined. In consultation with Fjarðaál‘s HDC process engineer, it was decided how long after the CBF the bleedout could be directly linked to the CBF. The time from CBF was divided into categories and one of the categories was the time range in which bleedout could directly be linked to the CBF. With percentage calculations, the ration between categories was estimated. To assess whether each category was unusually high or unusually low, probability calculation were used. It was estimated that the distribution between categories were random and consequently all the categories would have the same weight. Since eight categories were used, the weight for each category should be 1/8 and null hypothesis was

presented as H0 : P_0 = 1/8 for each group. To test this null hypothesis Z-value was calculated for each group

$$Z = \frac{\hat{P} - P_0}{\sqrt{\frac{P_0 \cdot (1 - P_0)}{n}}} \quad (7)$$

where $\hat{P}$ is the actual weight for each group and n is the number of samples. For comparison $Z_{\alpha/2}$ was calculated. Calculation was based on significance requirement $\alpha = 0{,}05$, indicating 95% reliability of the comparison test. Obtained from Z-table $Z_{\alpha/2} = Z_{0{,}025} = 1{,}96$. The rejection region for the null hypothesis is $|Z| > Z_{\alpha/2}$. If the null hypothesis is rejected for a category, that category is unusually high or low and the weight cannot be estimated as 1/8 (Ross, 2009).

The database was used to investigate the casting parameters considered most important for the process. It was investigated whether these casting parameters showed a specific pattern the last hour before bleedout and then tried to find the cause for the bleedout. Based on this, causes for bleedouts were divided into categories and ratio between categories calculated. Thus it was possible to estimate which casting parameter is the most critical parameter in the process when it comes to bleedouts.

2.6 Cast Aluminium Alloys

Aluminum alloys have wide applications due to high strength, high toughness and light weight. High corrosion resistance, easy deformability and excellent machining properties, have made this material so popular in the industrial world (Y.Liu, 2009). Favorable properties of aluminum alloy for casting applications is low melting point, good fluidity, capability to control grain structure, good surface finish, low solubility of gases and ability to be strengthened by heat treatment. Despite all these advantages, disadvantages also exist, which are high shrinkage, susceptibility to hot cracking and low ductility (SubsTech, 2012).

To form a variety of casting alloys, Aluminium Associations of the United States classifies the casting aluminum alloys. Each cast alloy is designated by a four digit number. The first digit indicates the alloy group according to the major alloying element, as listed in table 1.
.,

Table 1 : Groups for cast aluminium alloys (SubsTech, 2012)

Group	Major alloying element
1xx.x	aluminium, 99,0% minimum
2xx.x	copper (4% - 4,6%)
3xx.x	silicon (5% - 17%) with added copper and/or magnesium
4xx.x	silicon (5% - 12%)
5xx.x	magnesium (4% - 10%)
7xx.x	zinc (6,2% - 7,5%
8xx.x	tin
9xx.x	others

For group 1xx.x the second two digits indicate the alloy purity, but in groups 2xx.x – 9xx.x the second two digits signify different alloys in the group. The last digit indicates the product form, 0 for casting and 1 or 2 for ingots (SubsTech, 2012).

Alcoa Fjarðaál has mostly been producing cast aluminum alloy 356.2 in the HDC casting machine, but marked conditions controls what is produced. A356.2 is one of the most versatile of 300 series (Al-Si-Mg) casting alloys. Due to excellent castability, weldability, high strength, pressure tightness and corrosion resistance, the A356.2 casting alloy is widely used for casting of high strength components in automotive, aerospace and military applications (Jorstad, Rasmussen, & Zalensas, 2001).

The chemical composition of A356.2 casting alloy can be seen in table 2. Each alloying element has its role in the chemical composition. For example, Si is added to impart additional fluidity in the melt to enable ease of castability, Mg is added to increase the strength of aluminium, Ti is added to refine the grain size of the primary Al phase and Sr is added to affect modification of the eutectic phase morphologies (Y.Liu, 2009).

Table 2 : Nominal chemical composition(wt%) of A356.2 casting alloy (Y.Liu, 2009).

Si	Mg	Fe	Cu	Mn	Zn	Sr	Ti
6,6-7,5	0,30-0,45	<0,12	<0,10	<0,05	<0,05	0,01-0,025	0,01-0,20

A356.2 casting alloy was used in the numerical model to simulate the HDC casting process at Alcoa Fjarðaáli. Thermophysical properties of A356.2 can be seen in table 3.

Table 3 : Thermophysical properties of A356.2 casting alloy (SubsTech, 2012).

Property	**Value**
Density	2680 kg/m3
Specific heat capacity	963 J/kg-°C
Thermal conductivity	167 W/m-°C
Viscosity	0.0013 kg/m-s
Heat of fusion	389000 J/kg
Liquidus temperature	613 °C
Solidus temperature	557 °C

3 Results from Case Studies

3.1 Measurements

3.1.1 Tundish – Temperature Distribution

Measurements were performed to examine the temperature distribution of the aluminium alloy in the tundishes. Figure 26 shows graphically the location of the measuring points. The red circles (points 1 and 6) denote points where thermometers are constantly collecting data in a database. The blue squares (points 2, 3, 4 and 5) denote new measuring points for comparison with points 1 and 6. The thermometer was dipped into the aluminium alloy at the same level as the outlet from the tundish, figure 2 (page 6) show the location of the thermometer in the tundish. Measurements were performed for three different days and the temperature distribution was even in all cases, the results can be seen in table 4. The flicker in the measurement device showed ± 0,5°C for each measurement, which is within the confidence limits.

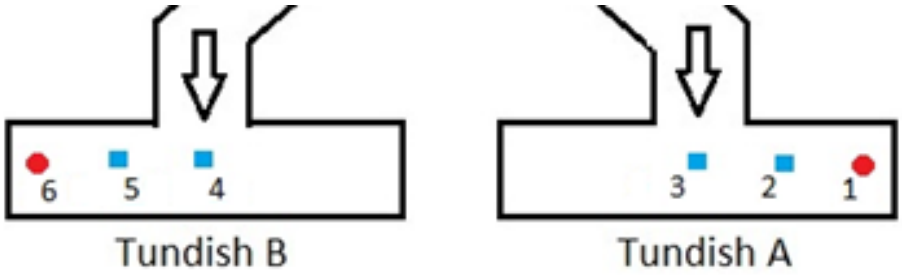

Figure 26 : Location of measurement points in tundishes. The arrows show the flow direction of the aluminium alloy. The figure is not in the right proportions.

Table 4 : Results from measurements in tundishes

Date	1	2	3	4	5	6
23.jan.12	671-672°C	671-672°C	671-672°C	670-671°C	670-671°C	670-671°C
15.feb.12	672-673°C	672-673°C	672-673°C	672-673°C	672-673°C	672-673°C
16.feb.12	670-671°C	670-671°C	670-671°C	669-670°C	669-670°C	669-670°C

From this it can be concluded that it is significant to have one thermometer in each tundish and having it located at the ends, such as points 1 and 6 in figure 26. It can be assumed that the temperature is the same for the entire tundish and all the alloyed bars at the same tundish have the same initial temperature.

3.1.2 Cooling Water – Temperature Difference

Measurements were performed to examine the temperature difference in the cooling water inside the molds. To get as accurate results as possible only outlets close to the intakes were measured. Four such outlets were examined, see locations in figure 27. It is believed that all bars are equally likely to bleed.

Figure 27 : Location of outlets measured, marked with blue squares. The arrow denotes casting direction. The figure is not in the right proportions.

The results show us that the temperature change of the cooling water in the molds is in the range 2,0°C – 2,2°C, see table 5. From this results it can be estimated that the average temperature change is 2,1°C.

Table 5 : Results from measurements at water outlets

Date	Intake	1	2	3	4	dT
23.jan.12	15,7°C	17,9°C	17,8°C	17,9°C	17,7°C	2,1°C
15.feb.12	16,1°C	18,1°C	18,0°C	18,2°C	18,1°C	2,0°C
16.feb.12	15,6°C	17,7°C	17,8°C	17,9°C	17,8°C	2,2°C

Knowing the amount of water flowing through the molds and the temperature change of the water in the molds, the heat transfer in the molds can me calculated. The value dT = 2,1°C was used in the numerical model.

3.1.3 Bars – Temperature Distribution

To understand what effect the cooling water has on the temperature distribution, measurements were performed for four different conditions as can be seen in table 6.

Table 6 : Conditions for cooling water

Condition	Water Temperature	Amount of water	Other variables
A	15°C	130 m^3/hour	constant
B	15°C	135 m^3/hour	constant
C	15°C	140 m^3/hour	constant
D	20°C	130 m^3/hour	constant

Average curve and range was calculated for each condition, see figure 28 for example. The average curve shows the average value of the measurements at each point. The range is shown with a maximum curve and minimum curve, which shows the maximum value and minimum value at each point. Figure 28 shows the results for condition A. The average curve and the minimum curve are almost straight lines. The maximum curve is fairly parallel to the other curves besides the flicker 22mm from the molds, see closer view in figure 29. The flicker is very obvious in the maximum curve but it is slightly visible in the other curves. It can also be seen that the range increases after the flicker and remains relatively stable after that. The average temperature 10mm from the molds is 112,4°C and 106mm from the molds it is 61,9°C. The range goes from 5,1°C up to 10,3°C.

The reason for this flicker is probably that the effect from the cooling water is strongest the first 20mm because of evaporation. According to the block flow diagram for this process, there is 0,012% evaporation of the cooling water (Fjarðaál, 2012). The heat transfer reaches its maximum where the cooling water boils (Grandfield & McGlade, 1996) (Zuidema, Katgerman, Opstelten, & Rabenberg, 2001). The ingots have the highest temperature when it comes out of the molds and the cooling water boils at first contact. It is reasonable to estimate that the effect from the evaporation ends around 10-20 from the molds, but then the heat transfer decreases and the temperature curves change their slope. Inaccuracy in the measurements can cause this flicker around this critical point where the effect from the evaporation ends. As mentioned above the evaporation is not very much or about 0,012%, which means that the change in the temperature curves should not be very visible.

The reason for the increased range is probably that further away from the molds the reliability of the cooling water reduces. The cooling water has been distributed and the bars receive different amount of cooling water, some bars gets more cooling than the other. Close to the molds there is much more even cooling and more likely that the bars receive the same amount of cooling water. Figure 30 shows how the water is distributed in actual casting.

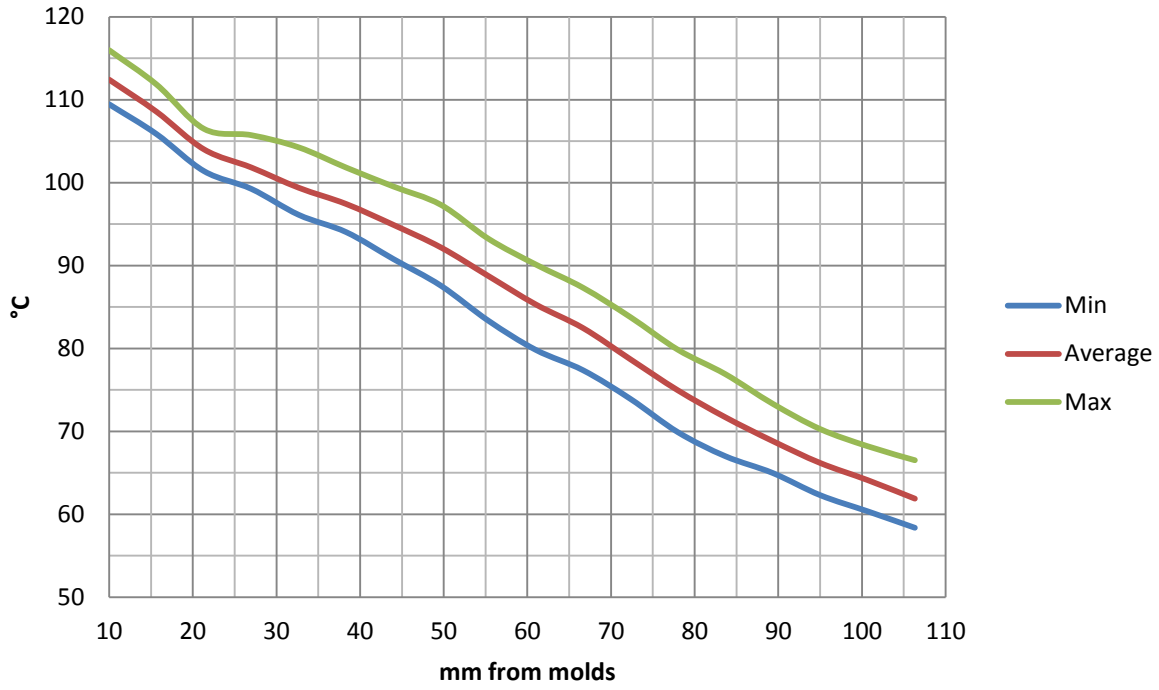

Figure 28 : Water temperature 15°C and cooling water rate 130 m3/h – Results for temperature distribution

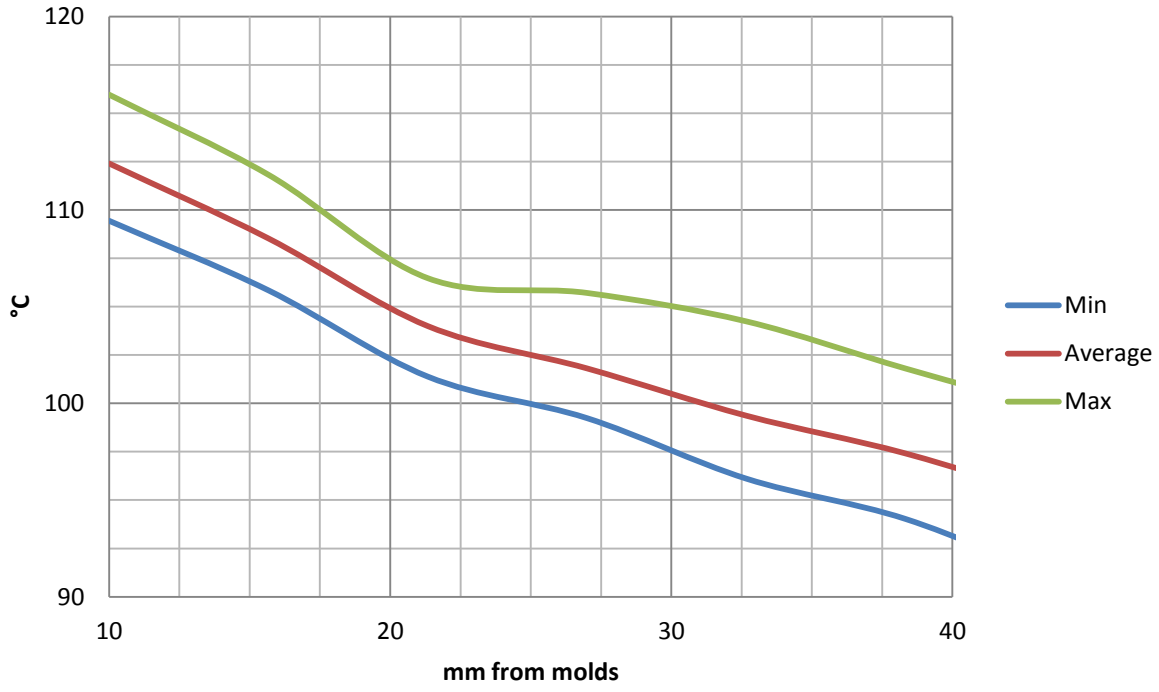

Figure 29 : Water temperature 15°C and cooling water rate 130 m3/h – Closer view of the flicker

Figure 30 : Water distribution during casting

Figure 31 shows the results for condition B. The average curve and the minimum curve are almost straight lines. The maximum curve is more unstable and there are flickers 16mm from the molds and 50mm from the molds. Both the flickers are slightly visible in the other curves, see closer view of the first flicker in figure 32. The previous flicker is probably because of the evaporation, but the later is probably just because of inaccuracies in the measurements. The range is rather narrow and unstable until 50mm from the molds, then it gets wider and more stable. It is likely that the effect from the cooling water is begining to decrease 50mm from the molds.

The average temperature 10mm from the molds is 108,4°C and 106mm from the molds it is 59,9°C. The range goes from 5,8°C up to 9,3°C.

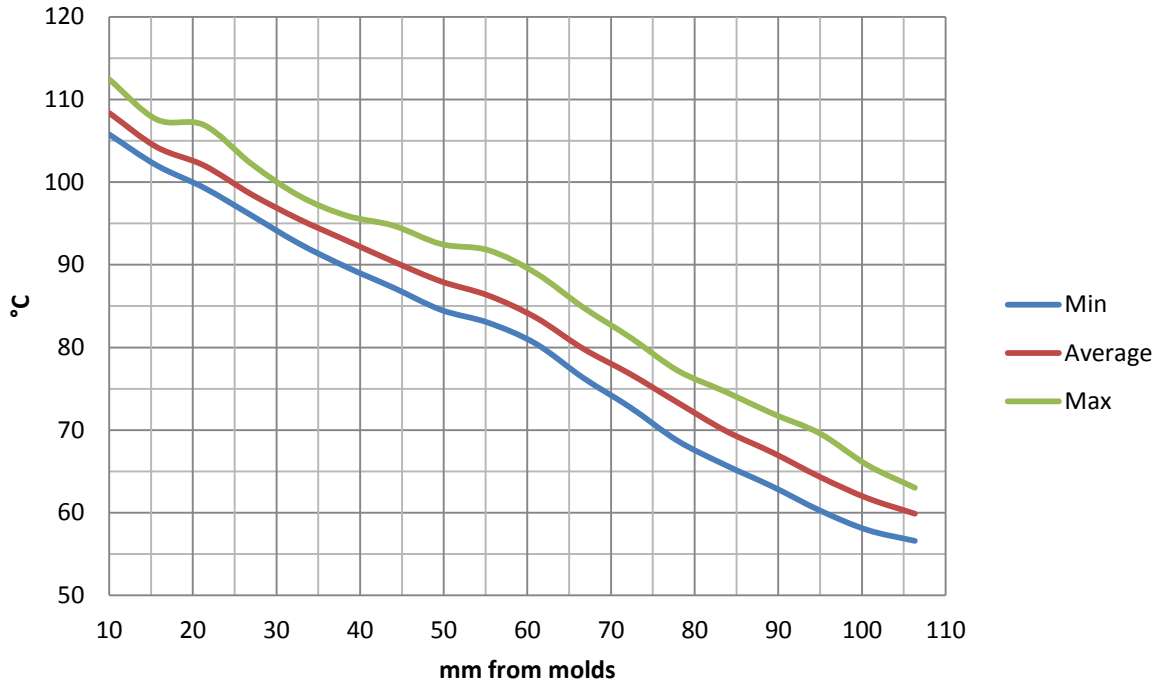

Figure 31 : Water temperature 15°C and cooling water rate 135 m3/h – Results for temperature distribution

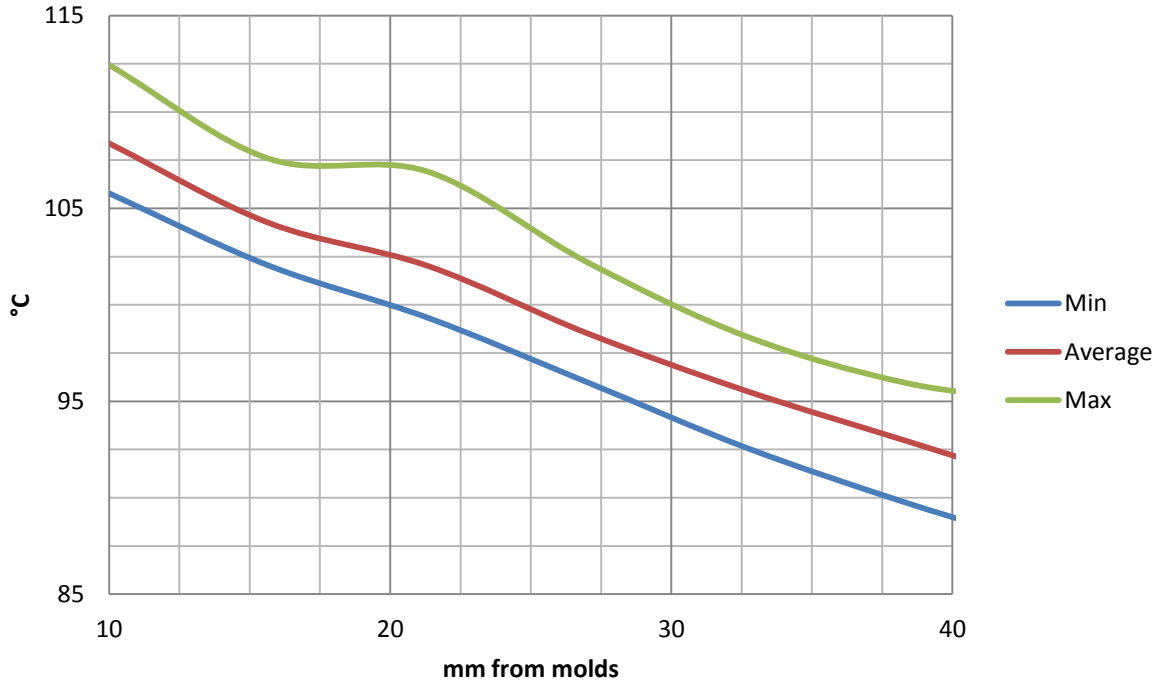

Figure 32 : Water temperature 15°C and cooling water rate 135 m3/h – Closer view of the first flicker

Figure 33 shows the results for condition C. All the curves are almost straight lines, but there are some small flickers in the minimum curve and the maximum curve. The flickers are probably because of inaccuracy in the measurements since those flickers seems to be random and does not appear in conditions A and B. The range is rather stable but 40mm from the molds the range increases a little bit and stays rather stable after that. As mentioned before the reason for the wider range is most likely because the effect from the cooling water decreases when the distance from the molds increases.

The average temperature 10mm from the molds is 104,1°C and 106mm from the molds it is 57,9°C. The range goes from 5,9°C up to 9,9°C.

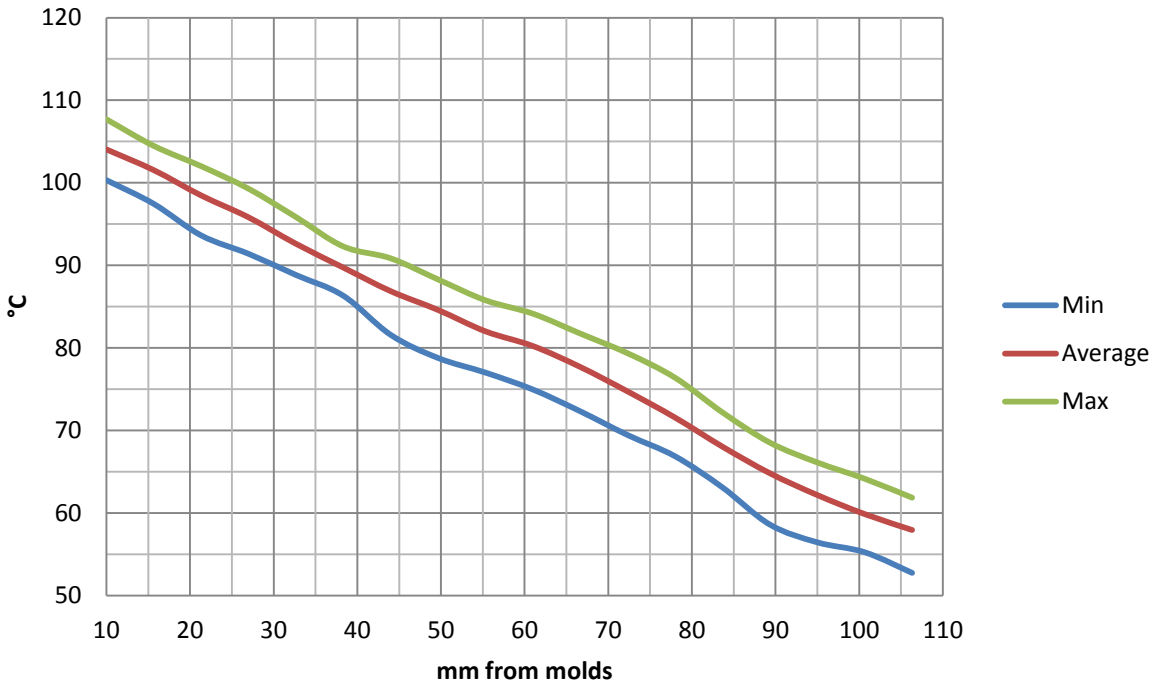

Figure 33 : Water temperature 15°C and cooling water rate 140 m3/h – Results for temperature distribution

Figure 34 shows the results for condition D. All the curves are almost straight lines, but there are some small flickers in all curves. The flicker 16mm from the molds is probably because of the evaporation in the cooling water, see closer view in figure 35. The other flickers are probably because of inaccuracy in the measurements since those flickers seems to be random and does not appear in conditions A, B and C at same locations. The range is rather stable but decreases slightly in the end.

The average temperature 10mm from the molds is 113,8°C and 106mm from the molds it is 65,3°C. The range goes from 6,1°C up to 9,8°C.

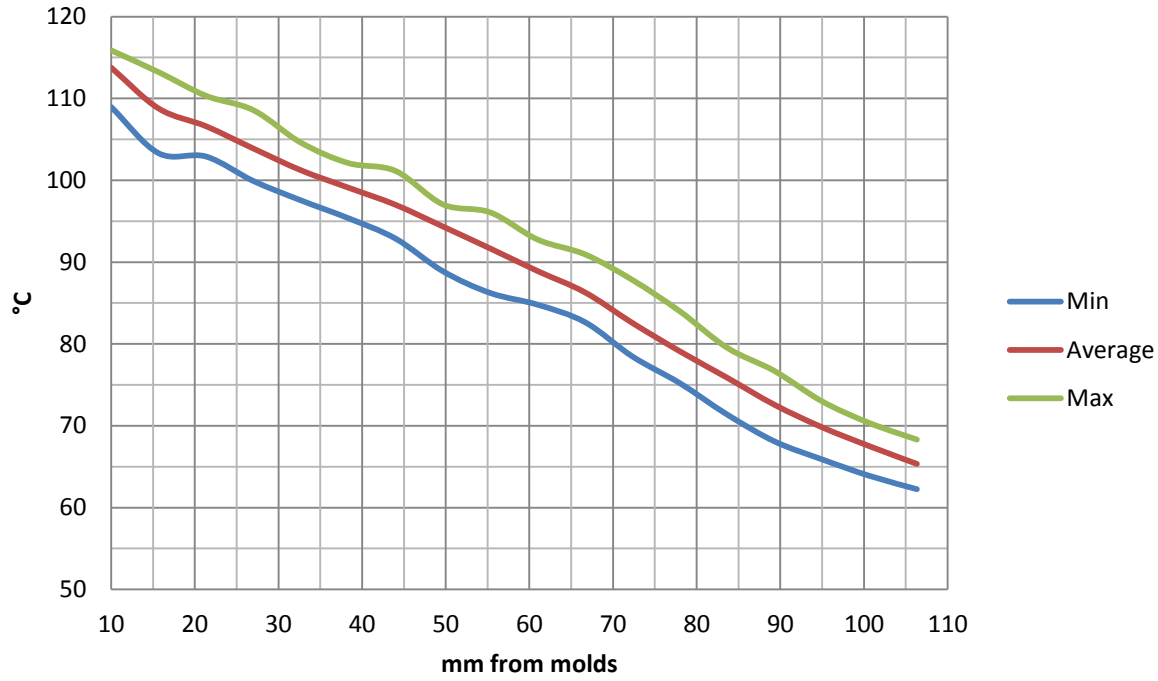

Figure 34 : Water temperature 20°C and cooling water rate 130 m3/h – Results for temperature distribution

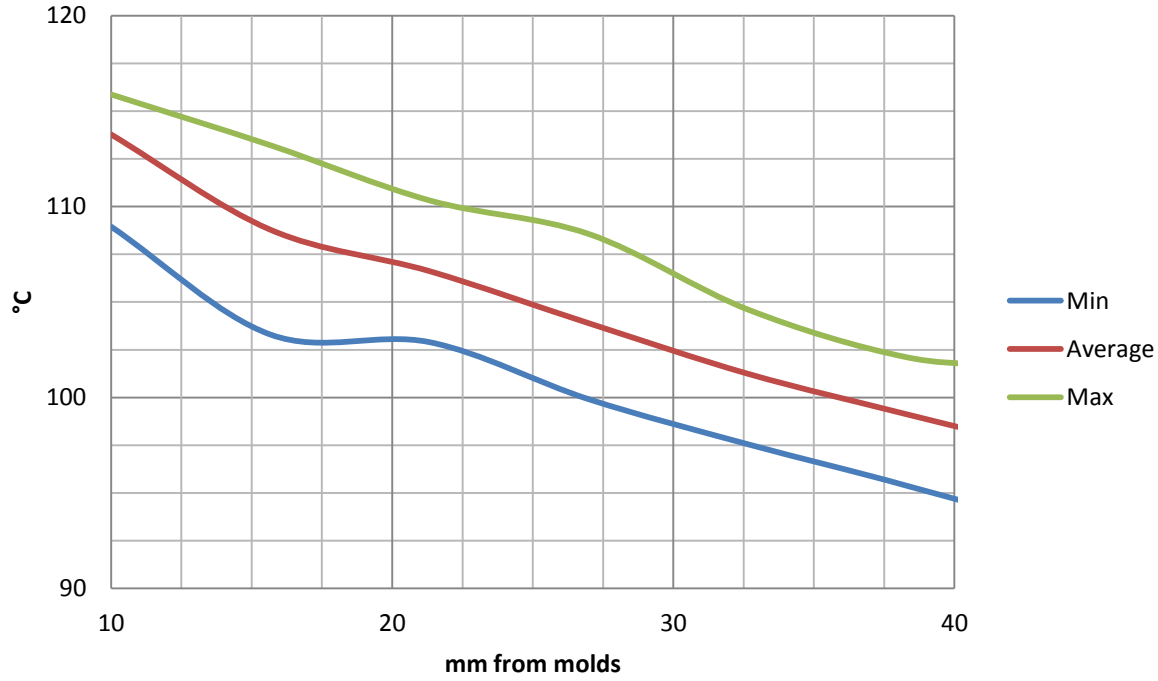

Figure 35 : Water temperature 20°C and cooling water rate 130 m3/h – Closer view of the flicker

For all conditions, except condition C, there is a flicker 15-20mm from the molds and it is most likely because of the evaporation that happens the first 20mm from the molds. The effect from the cooling water is strongest in the evaporation and then it decreases. It is interesting to know why there is no flicker for condition C, because it should be. It is probably because there is more amount of cooling water in condition C which causes more even cooling. In condition A this flicker is highly visible, but in condition B it is less visible and in condition C it is not visible. The main reason for this range is that it is a minor difference between ingots based on the location in the molds. The closer to the center of the mold the higher temperature.

Figure 36 shows the comparison for all conditions. Condition D has the highest temperature, which makes sense because in this condition the cooling water has the highest temperature. The higher temperature of the cooling water the less cooling. Conditions A, B and C shows clearly that the cooling effect increases in direct proportion to the increased amount of cooling water.

The difference between conditions A and D is 0,2-2°C the first 20mm from the molds, figure 37 shows closer view of the first 40mm. The difference increases however further away from the molds and ends at 4-5°C. This means that 5°C change in the cooling water temperature has negligible effect on the cooling, but 5°C change is an increase of 33% . The difference between conditions A and B is 4-5°C the first 55mm from the molds. The difference decreases suddenly 55mm from the molds and remains 1-2°C. The difference between conditions B and C is 3-5°C the first 60mm from the molds. The difference decreases suddenly 60mm from the molds and remains 1-2°C. This means that $5m^3$/hour change in the amount of cooling water has more effects on the cooling than the temperature of the cooling water. The relative change is also much less because $5m^3$/hour change in the amount of cooling water is around 4% change.

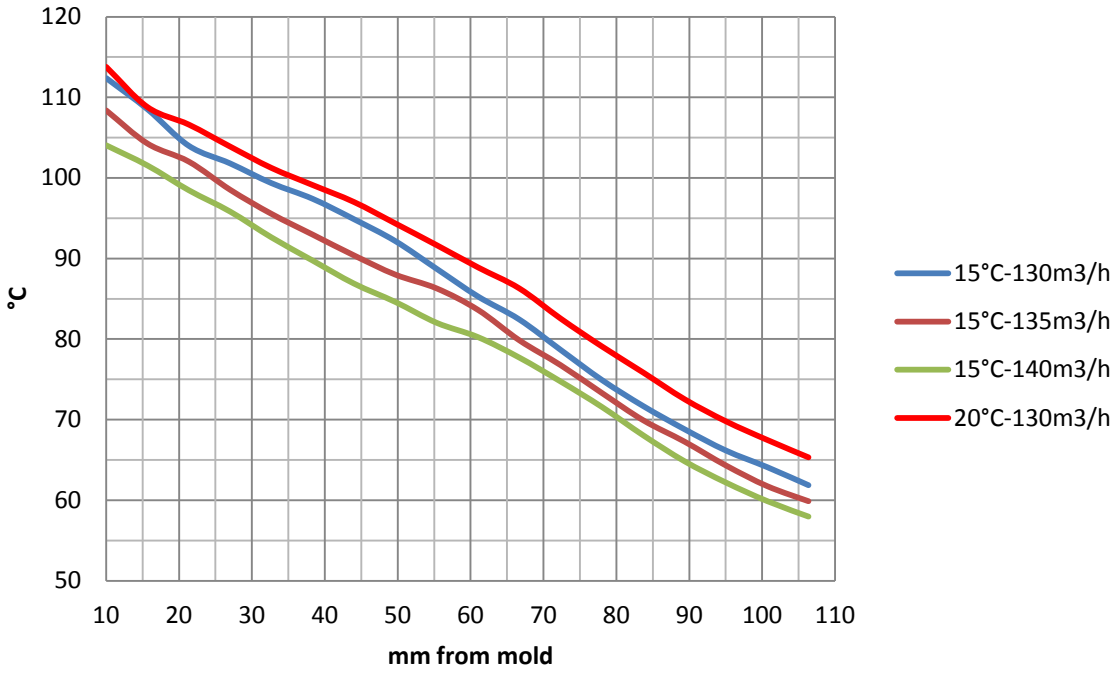

Figure 36 : Comparison for all conditions – temperature distribution

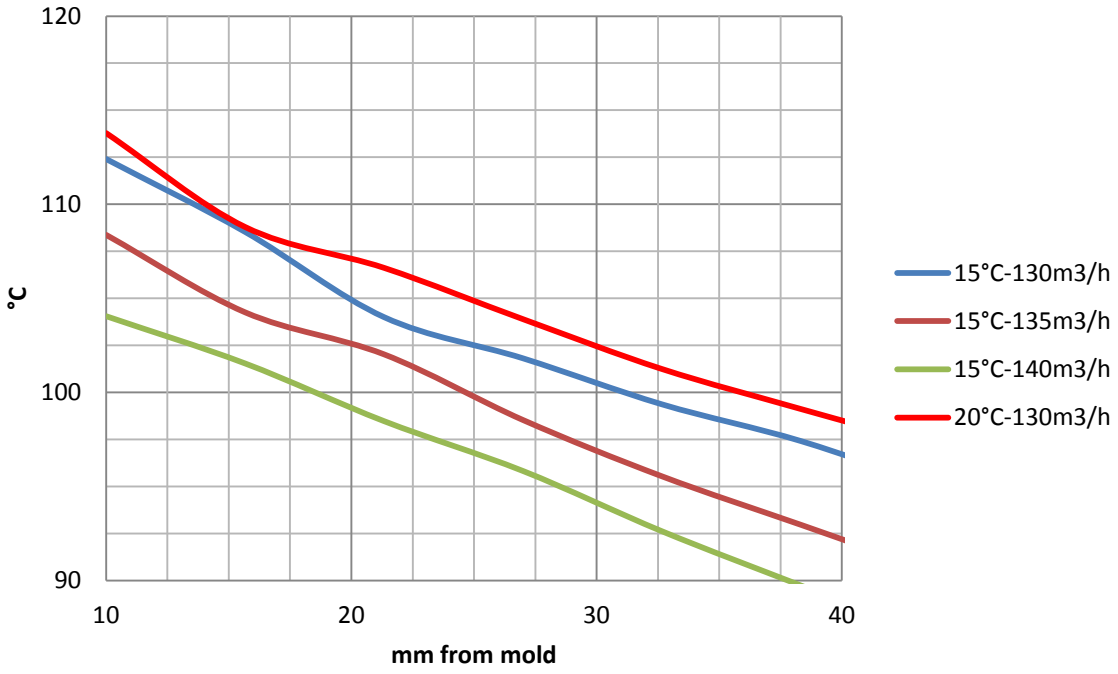

Figure 37 : Comparison for all conditions – closer view

These measurements shows that the amount of cooling water is much more critical parameter than the temperature of the cooling water. This can also be demonstrated with formula for convection heat transfer, see formula (1) in chapter 2.3. The heat transfer changes in proportion to the change in the amount of cooling water. Change in temperature of the cooling water affects only the specific heat capacity, the temperature change of the cooling water remains practically constant. For example, changing the temperature of water from 20°C to 15°C increases the specific heat capacity of 0,07%, see table for specific heat capacity of water (Engineering ToolBox, 2012)

3.2 Model Verification

3.2.1 2D Model for Comparison

Initially, two-dimensional numerical model in was designed Ansys Fluent and to verify the functionality of the model, known case from other study was simulated. The case used for comparison is presented in the paper of Krane and Vusanovic (Krane & Vusanovic, 2009). Figure 38 shows schematic figure of the physical model, which is designed to be similar to HDC casting of Mg alloys found in the model (Grandfield & Dahle, 2000). The alloyed bar is 300mm long, 80mm thick and the molds covers the first 45mm of the top and bottom surface. On the left side is a plate with no slip conditions and in the middle of that plate is a inlet with height 10mm. There is no heat flux from the plate, just the inlet. The cooling is divided into three zones: mold cooling zone h_1, air gap zone h_2 and secondary cooling with water impingement. The secondary cooling has two values, h_{top} and h_{bottom} and the ratio h_{top}/h_{bottom} has been defined as 1.7, found in the paper of Krane and Vusanovic. The inlet speed is defined as eight times the casting speed (Krane & Vusanovic, 2009).

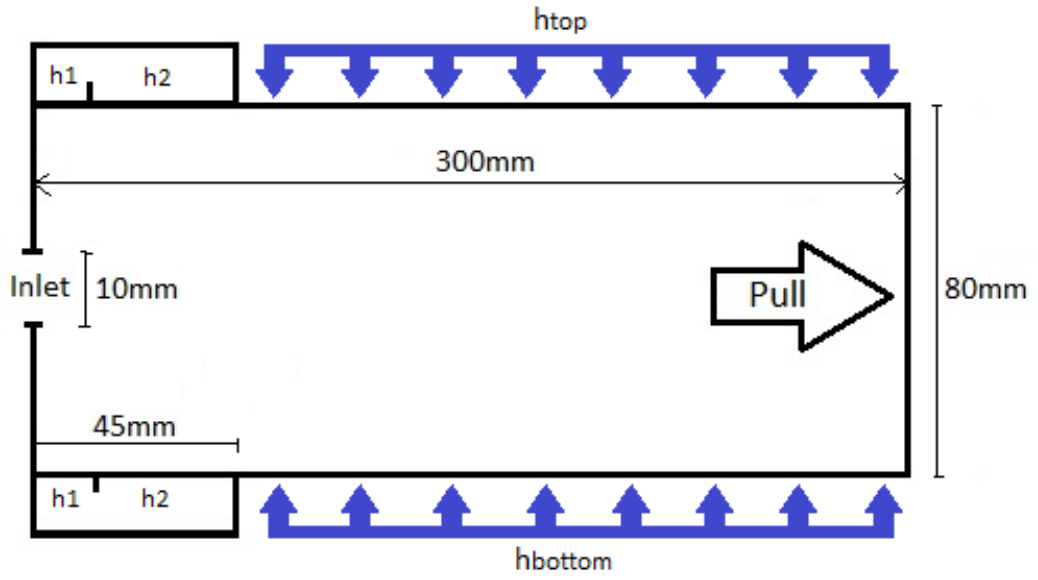

Figure 38 : Schematic figure of the case tested - horizontal direct chill casting (Krane & Vusanovic, 2009)

The case was tested for two different casting speeds. Values for the casting parameters can be seen in table 7.

Table 7 : Values for the casting parameters in the case

Variable	Value	Reference
h_1	150 W $m^{-2}°C^{-1}$	(Grandfield & Dahle, 2000)
h_2	1500 W $m^{-2}°C^{-1}$	(Grandfield & Dahle, 2000)
h_{top}	10000 W $m^{-2}°C^{-1}$	(Hamed & Akmal, 2005)
T_{inlet}	730 °C	(Krane & Vusanovic, 2009)
$V_{casting}$ - 1	300 mm/min	(Krane & Vusanovic, 2009)
$V_{casting}$ - 2	210 mm/min	(Krane & Vusanovic, 2009)

Krane and Vusanovic used the alloy Al-4,5 wt-%Cu , which is comparable to cast aluminium alloy A201.0. Thermophysical properties of the cast aluminium alloy A201.0 can be seen in table 8.

Table 8 : Thermophysical properties of cast aluminium alloy A201.0 (SubsTech, 2012).

Property	Value
Density	2800 kg/m^3
Specific heat capacity	963 J/kg-°C
Thermal conductivity	121 W/m-°C
Viscosity	0.0013 kg/m-s
Heat of fusion	389000 J/kg
Liquidus temperature	649 °C
Solidus temperature	571 °C

Figures 39 and 40 show the results from Ansys Fluent. These are almost the same pictures as in the paper from Krane and Vusanovic. The depth of the mushy zone decreases with decreasing casting speed, causing faster solidification. Inside the molds, thin shell is formed next to the walls. When leaving the mold, faster cooling begins, and the bar freezes all the way to the core. In the comparison, the solidus lines and the liquidus lines have similar locations and the depth of the mushy zone is the same.

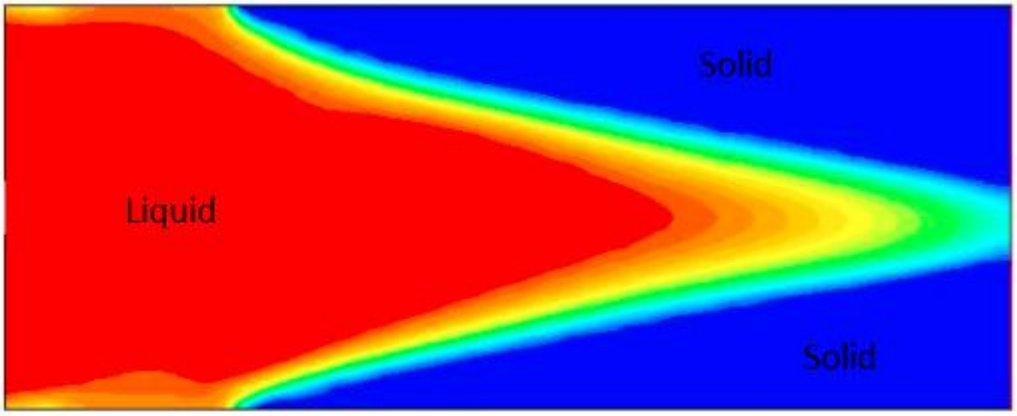

Figure 39 : Casting speed 1 – results from Ansys Fluent.

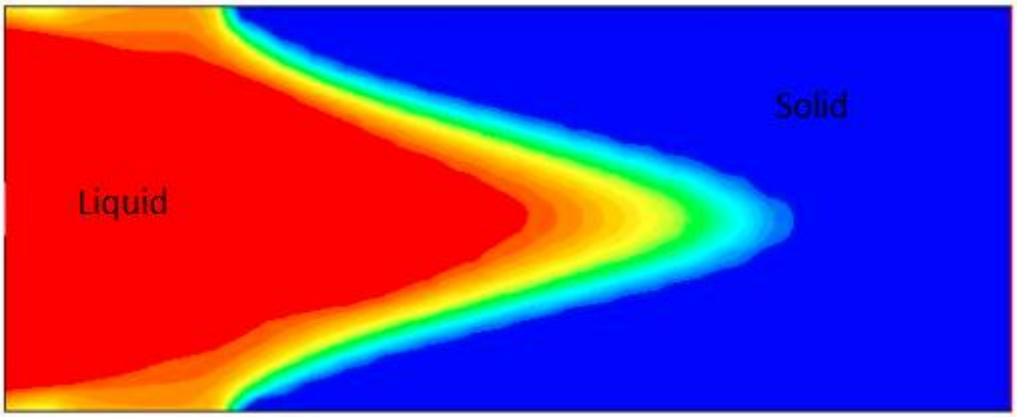

Figure 40 : Casting speed 2 – results from Ansys Fluent

It can be said that the simulation confirms that the functionality of the model is similar. Therefore it is assumed that the Ansys Fluent model constructed in this study returns realistic results.

3.2.2 Mesh Comparison

Different meshes were tested, started with rough mesh and then it was refined until enough accuracy was achieved. The goal was to have as few cells as possible, without affecting the quality of the results. Figures 41 - 44 show the four meshes that were tested, looking at the symmetry surface. Mesh 1was rather rough with little bit denser mesh close to the cooling zones. Mesh 2 was the same as mesh 1, except cells was increased where solidification occurred. It is important to increase cells in important zones where changes are fast, it leads to more accuracy. Mesh 3 was the same as mesh 2 except cells was increased close to inflow pipe walls. It is important to have more cells close to walls because of friction. Mesh 4 was the same as mesh 1 except each cell was divided into more cells.

Figure 41 : Mesh 1 – Rough mesh with little bit denser mesh close to the cooling zones.

Figure 42 : Mesh 2 – Same as mesh 1 except cells was increased where solidification occurs.

Figure 43 : Mesh 3 – Same as mesh 2 except cells was increased close to inflow pipe walls.

Figure 44 : Mesh 4 – Same as mesh 1 except each cell was divided into more cells.

To compare these meshes, they were all tested for the same case. Temperature curve was plotted along the top surface of the bar and it compared for all the meshes. When the temperature curve stopped changing between meshes the correct accuracy was achieved. Then it was clear that more fine mesh would not yield better result. Figure 45shows the comparison of the temperature curves. Meshes 1, 2 and 3 all gave different results. Meshes 3 and 4 gave the same results, the curve for mesh 3 is behind the curve for mesh 4.

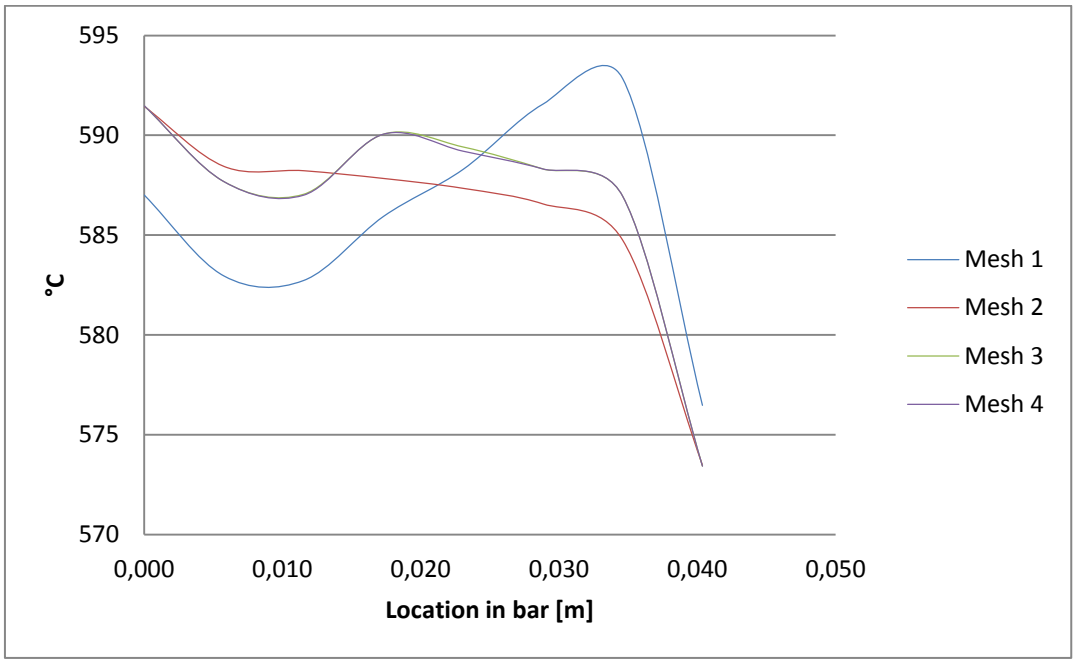

Figure 45 :Comparison between meshes.

From this comparison it was assumed that mesh 3 gives results with the same accuracy as mesh 4. Mesh 3 has approximately 50000 cells and mesh 4 has approximately 70000 cells. The less cells the fewer calculations for the numerical model, so mesh 3 was chosen to be the optimum mesh.

3.2.3 Heat Transfer Coefficients

Heat transfer in the numerical model was defined by heat transfer coefficients (denoted by *h*), heat transfer coefficient was defined for each cooling surface. Heat transfer coefficient indicates how much heat is transferred away per square meter to reduce the temperature by 1°C, the unit is W/m^2-°C.

Heat transfer coefficients in the primary cooling, inside the molds, were obtained from measurements on the cooling water, see chapter 3.1.2. By knowing the temperature decrease of the cooling water inside the molds and the cooling water rate, the heat transfer

coefficients can be calculated. Zone 1 was defined as the first 10mm of the mold and zone 2 was the rest of the mold. Zone 1 is where the alloyed bar is in direct contact to the mold and zone 2 is where there is an air gap between the alloyed bar and the mold, because of shrinkage.

Heat transfer coefficients for secondary cooling, where the cooling water injects directly on the bars, were obtained by using the numerical model to simulate the temperature curve on the surface of the bars. This temperature curve was obtained by measurements, see condition A in chapter 3.1.3 (figure 28). Condition A is defined as the normal state in the casting process. In figure 46 the location of the temperature curve is shown in the cross section but the curve is plottet along the casting direction. To be able to simulate the temperature curve, secondary cooling was divided into 6 cooling zones with 6 different heat transfer coefficients. Different values were tested for the heat transfer coefficients until the simulation of the temperature curves were acceptable.

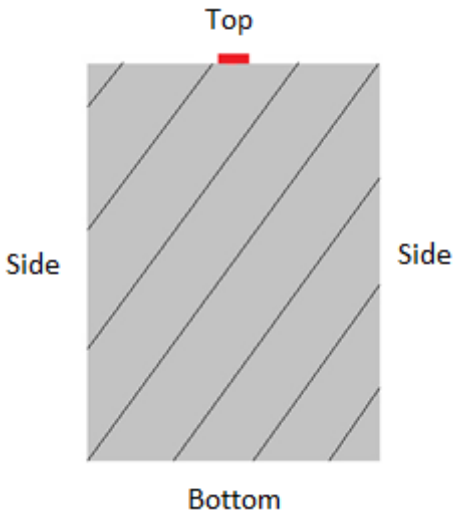

Figure 46 : Cross section of a bar, the red line denotes location of the temperature curve.The surfaces of the bar are marked into the figure; top, bottom and sides.

Figure 47 shows how the cooling zones were defined in the model. These cooling condition were applied to all cooling surfaces; bottom, top and sides of the bar. Heat transfer coefficients h1 and h2 belong to the primary cooling and are located inside the molds. Heat transfer coefficients h3, h4, h5, h6, h7 and h8 belong to the secondary cooling and are located outside the molds.

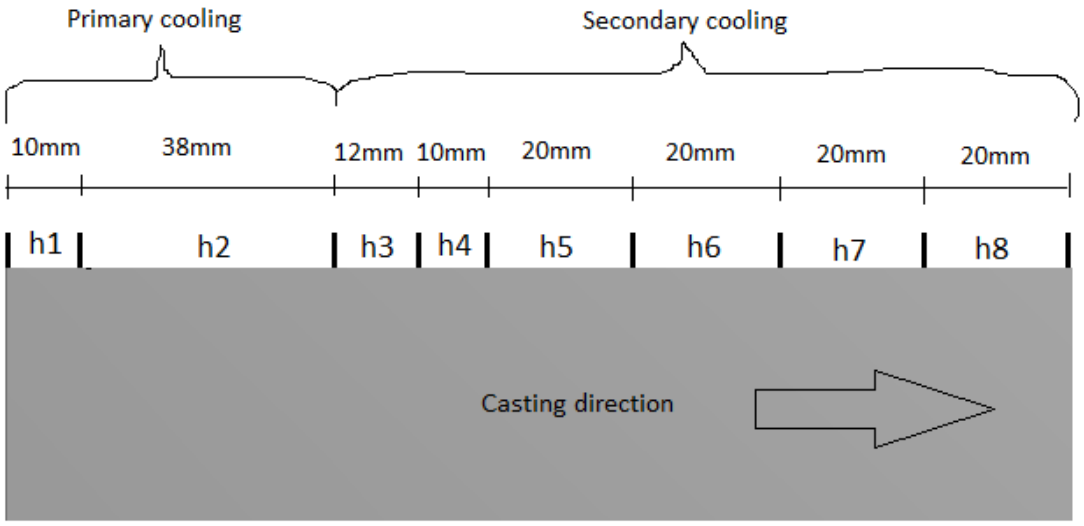

Figure 47 : Cooling distribution in the numerical model. These conditions were applied to all cooling surfaces of the bar; bottom, top and sides.

Figure 48 shows the simulation. The goal was to simulate a curve that would fit between the maximum curve and the minimum curve from the measurements mentioned earlier.

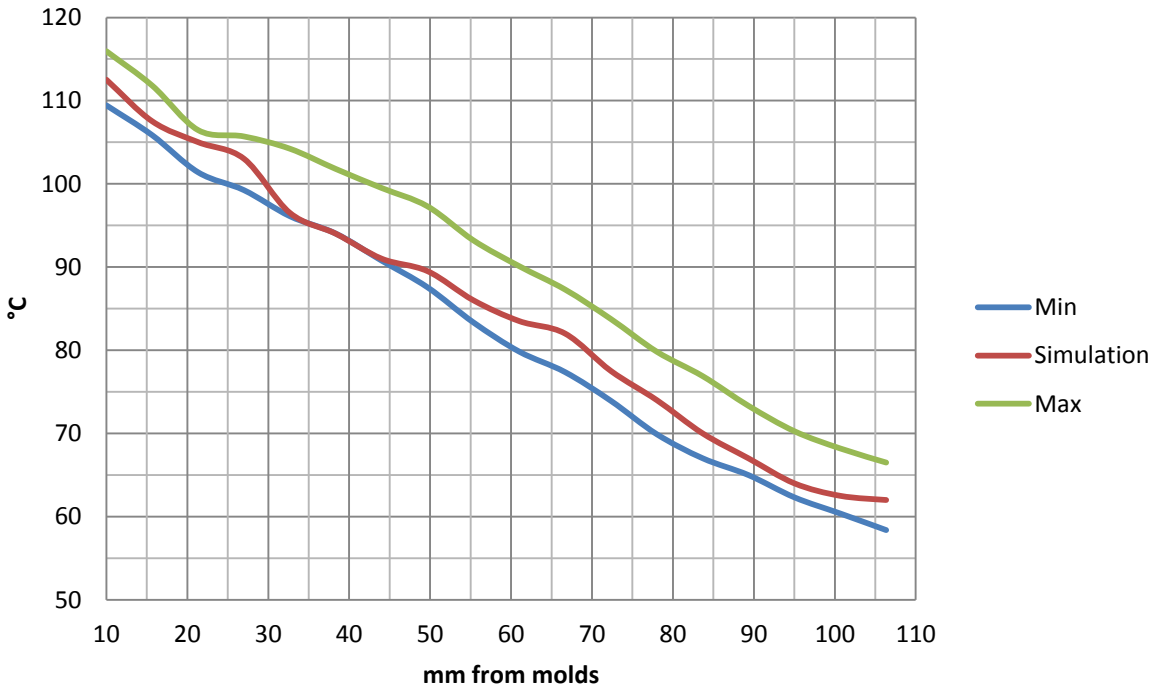

Figure 48 : Simulation of the temperature curve.

Table 9 shows the conditions used for this simulation along with the results for the heat transfer coefficients.

Table 9 : Conditions used for simulation and results for heat transfer coefficients

Parameter	**Value**
Temperature of aluminium alloy	675°C
Casting speed	360 mm/min
Cooling water rate	130 m^3/hour
Cooling water temperature	15°C
Heat transfer coefficient - h1	3000 W/m^2-°C
Heat transfer coefficient - h2	600 W/m^2-°C
Heat transfer coefficient - h3	90000 W/m^2-°C
Heat transfer coefficient - h4	60000 W/m^2-°C
Heat transfer coefficient - h5	39000 W/m^2-°C
Heat transfer coefficient - h6	26000 W/m^2-°C
Heat transfer coefficient - h7	19000 W/m^2-°C
Heat transfer coefficient - h8	19000 W/m^2-°C

These results show clearly how the secondary cooling is major compared to the primary cooling. As mentioned before, a thin shell is formed in the primary cooling so the bar can leave the mold without bleeding and then the secondary cooling finish the solidification process (Nadella, Eskin, & Katgerman, 2006). It is very interesting to see how fast the cooling changes in the secondary cooling. Figure x shows the value of the heat transfer coefficient as a function of distance from the molds. Right up to the molds the cooling reaches its maximum, 90000 W/m^2-°C, where the cooling water boils, this is quite consistent with studies from others (Grandfield & McGlade, 1996) (Zuidema, Katgerman, Opstelten, & Rabenberg, 2001). Approximately 60mm from the molds, the heat transfer coefficient has decreased by 79%. As can be seen in figure 49 these collection points can be approximated by 3. order polynomial. This approximation curve shows more clearly how the coefficient decreases.

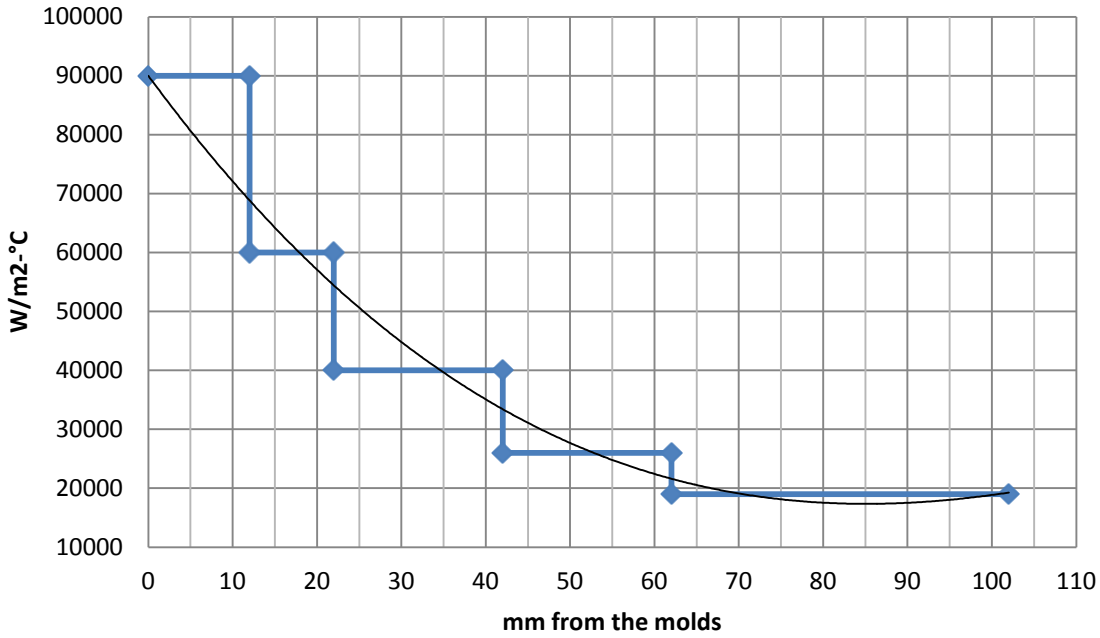

Figure 49 : Heat transfer coefficient in the secondary cooling. Blue lines denote simulation values and black curve denote approximation through the points with 3.order polynomial.

After this simulation, the model was able to simulate current state at Fjarðaál fairly accurately.

3.2.4 Flow Through the Pipe

The model takes into account the flow and wall resistance. Figure 50 shows the velocity of the aluminium alloy in the flow direction. It can be seen that there is resistance from the walls of the inflow pipe and the flow is not even. It can be seen that the flow is reversed in the inside the bar where the liquid fraction is 1.

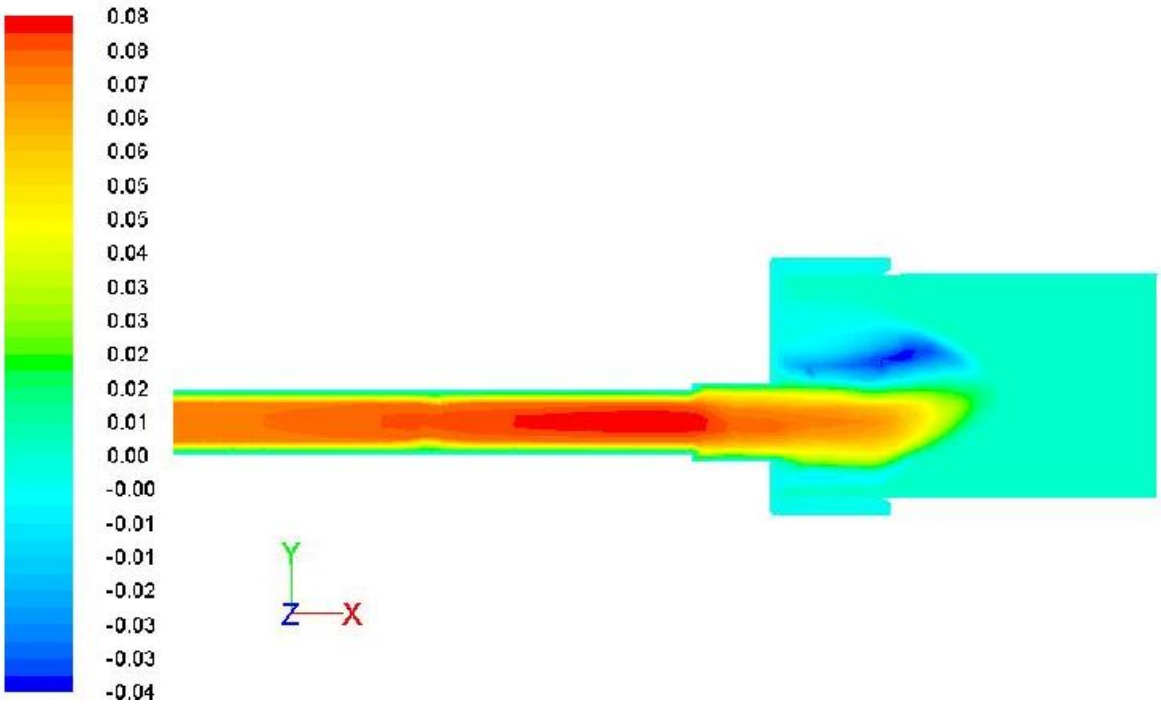

Figure 50 : Velocity of the aluminium alloy in the x-direction (flow direction).

3.3 Model Test

3.3.1 Simulation of Normal State

The model was used to simulate the normal state. The heat transfer coefficients found in chapter 3.2.3 were used. Table 10 shows values for casting parameters in normal state.

Table 10 : Values for casting parameters in normal state.

Parameter	**Value**
Temperature of aluminium alloy	675°C
Casting speed	360 mm/min
Cooling water rate	130 m^3/hour
Cooling water temperature	15°C

Figures 51 shows the temperature distribution in a bar in normal state.

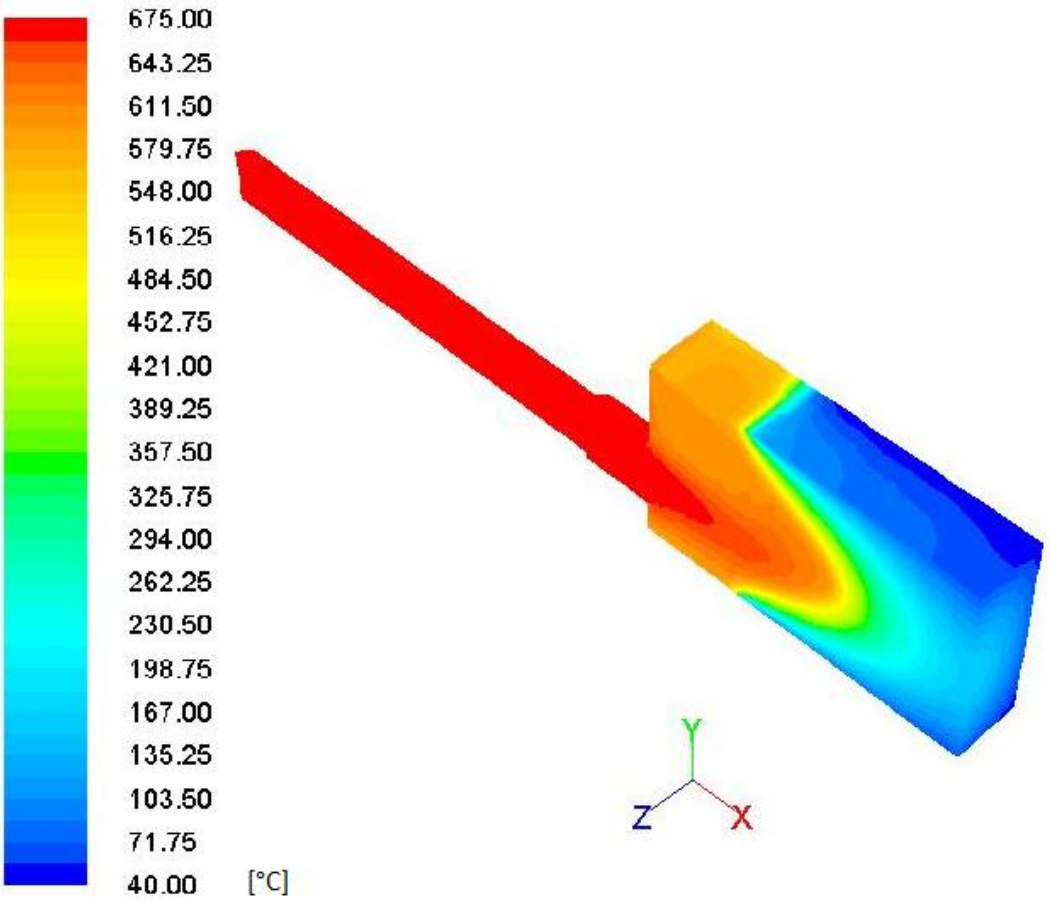

Figure 51 :Isometric view of temperature distribution in a bar – normal state.

It was focused on examining solidification to analyse bleedouts. Figures 52 and 53 show the solidification process.

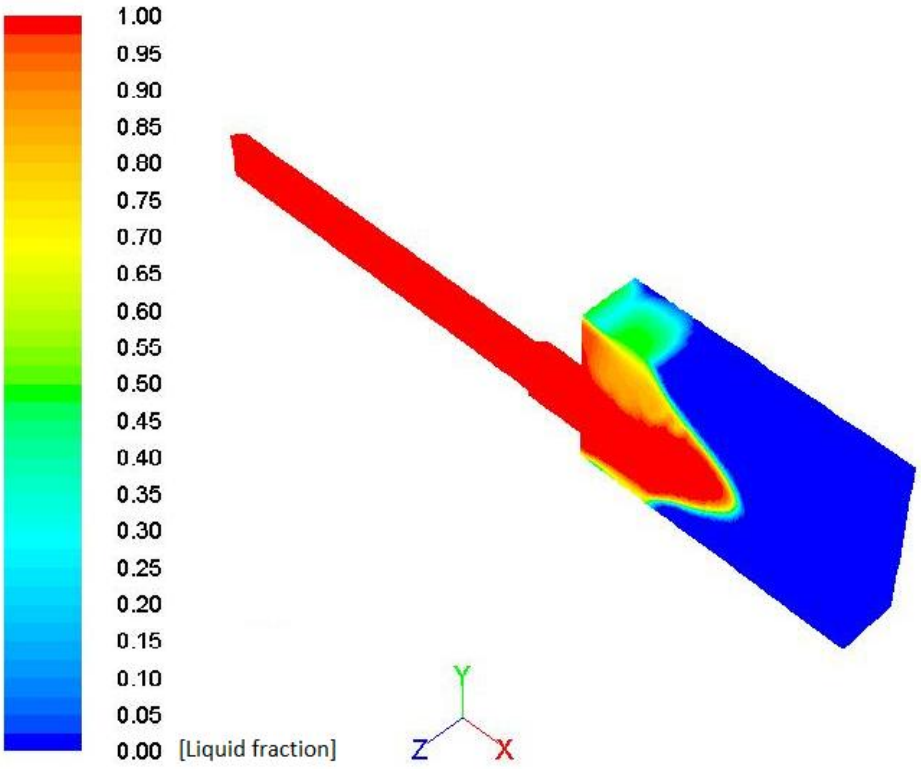

Figure 52 : Isometric view of solidification in a bar – normal state.

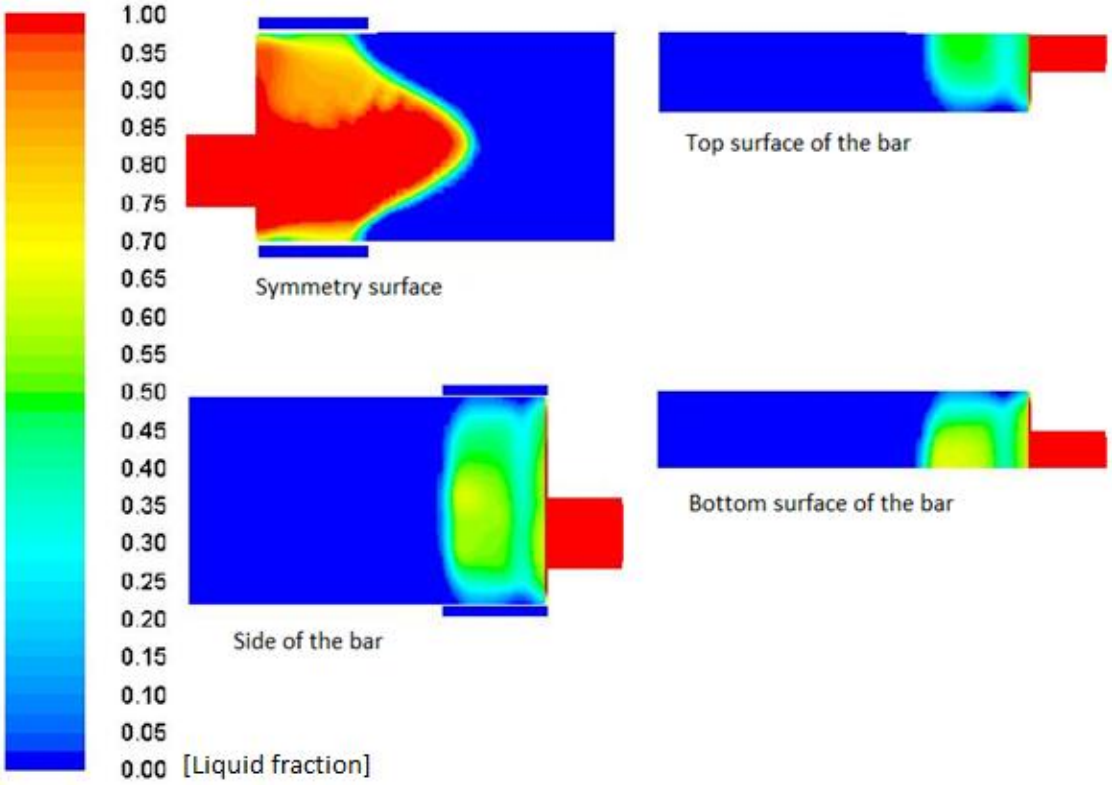

Figure 53 :2D views of solidification in a bar – normal state. In the symmetry view and the side view, location of molds is shown.

To see better inside the bar, two cross-sections were taken through the bar as can be seen in figure 54. Section 1 is horizontal plane through the middle of the inflow pipe and along the bar. Section 2 is vertical plane located the end of the molds.

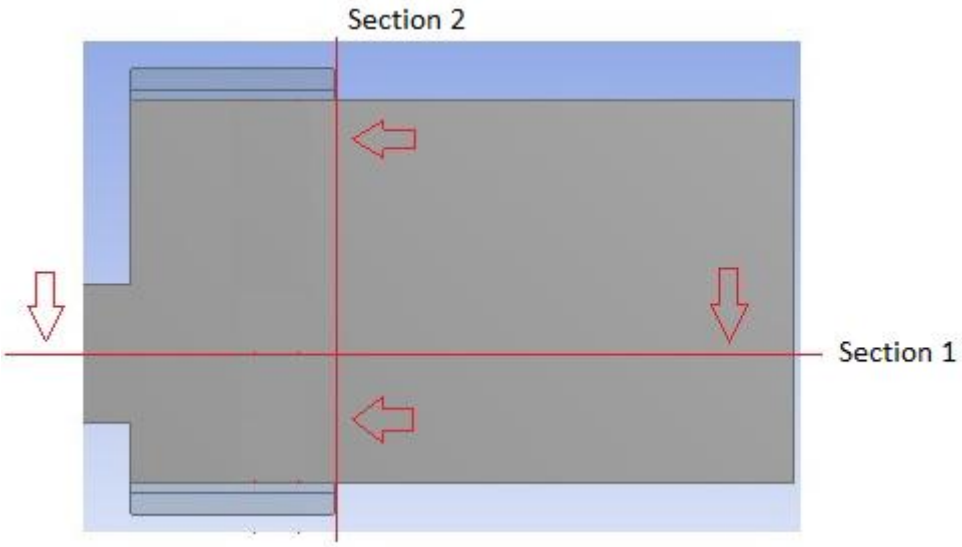

Figure 54 :Cross-sections through the bar.

Figures 55 and 56 show the cross-sections.

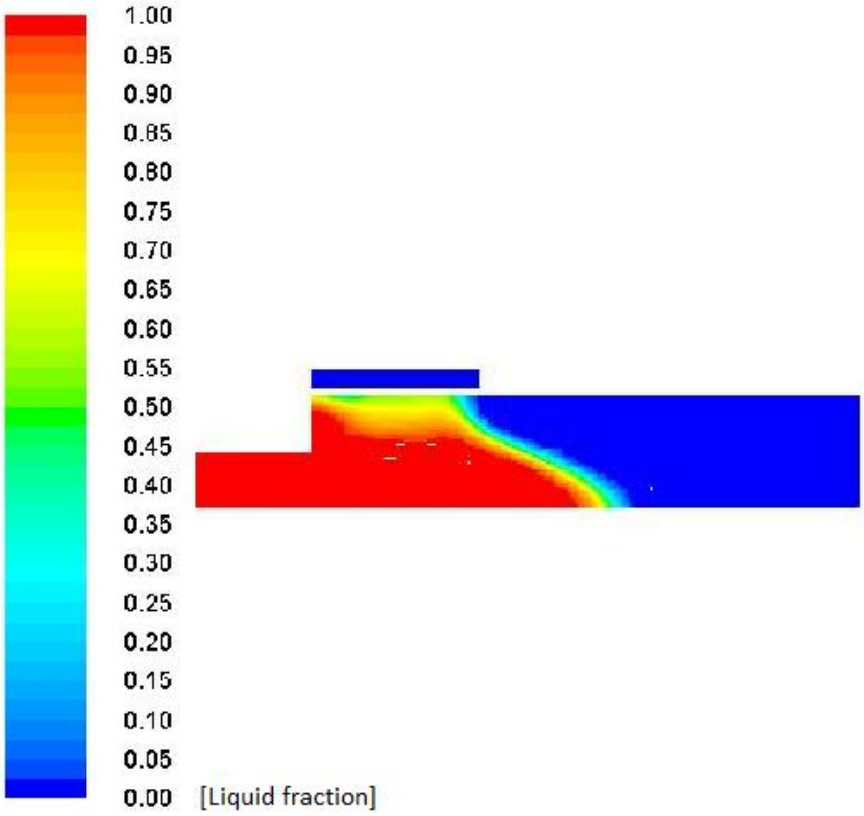

Figure 55 : Section 1, showing solidification in normal state.

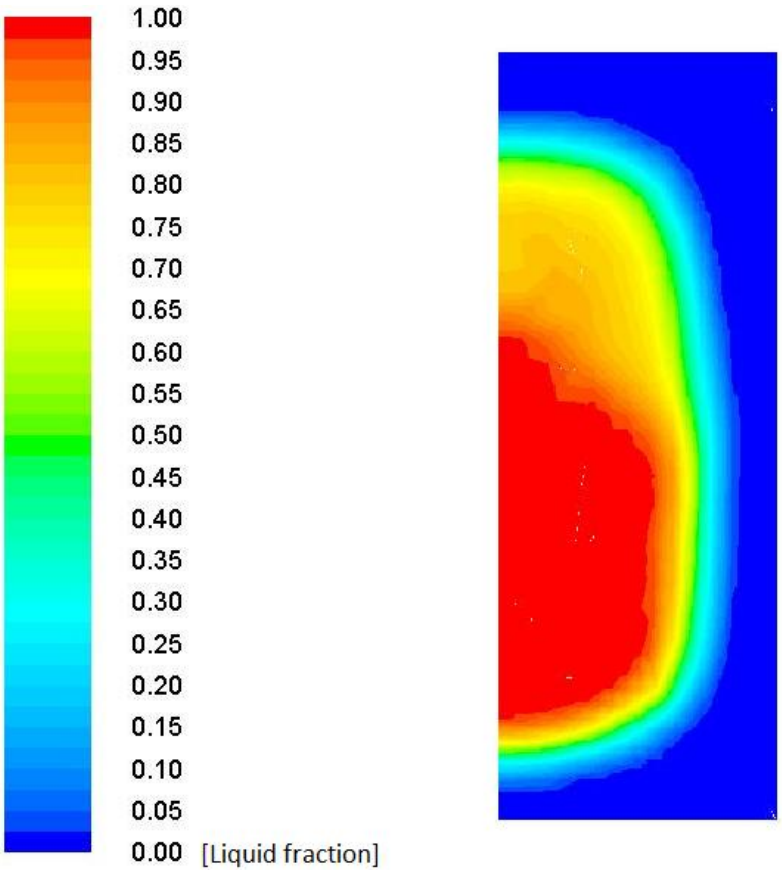

Figure 56 : Section 2, showing solidification in normal state.

According to these figures from the numerical model, there is good balance in the casting process and no bleedout. Solidification seems to be rather rapid and before the bar leave the mold, the solidification has worked quite well into the center. Keeping this condition stable should prevent bleedouts. The greatest risk of bleedouts should be closest to the inflow, it is in the bottom surface or on the sides. The minimal risk of bleedout is in the top surface because of distance from the inflow. Section 2 in figure 56 shows that the shortest way for the liquid to melt itself though the solid metal is toward the bottom surface or the sides. To see this more closely, curves were plotted along the length of the bar close to the inflow. Figure 57 shows the location of the curves from the inflow. Curves c1 and c6 were at the surface, curves c2 and c5 were 5mm under the surface and curves c3 and c4 were 10mm under the surface.

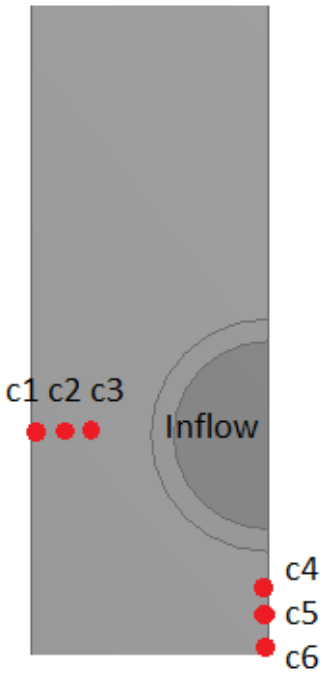

Figure 57 : Locations of curves plotted along the length of the bar

Figures 58 and 59 show the curves c1, c2, c3,c4, c5 and c6. These curves show the liquid fraction in the casting direction. The liquid fraction on the surface was 0,4 – 0,6 the first 35mm and then it drops to zero. In both cases the liquid fraction reaches zero at the surface at the moment the bar leaves the mold. It is interesting to see how the liquid fraction increases in position 10mm. That is when the air gap is formed between the bar and the wall of the mold because of shrinkage, resulting in lower cooling. The liquid begin to melt through the solid in position 10mm until in position 35mm when the secondary cooling begin to affect. The liquid fraction is much higher 5mm under the surface. It starts at 1 and decreases slowly until in position 35mm, then it drops to zero few millimeters outside the mold. The liquid fraction 10mm under the surface is around 0,55 – 0,85 when the bar leaves the mold and reaches zero 10mm outside the mold. These curves shows clearly the effect of the secondary cooling. When the liquid fraction is low enough when the bar leaves the mold, the secondary cooling handles the solidification. When the liquid fraction is not low enough when the bar leaves the mold, bleedout is likely to occur. How low the liquid fraction needs to be is not known. From these curves it can be shown that the liquid fraction is relatively higher below the inflow. This indicates that the cooling on the bottom surface is less than on the side. Therefore it is most likely that bleedout would occur through the bottom surface.

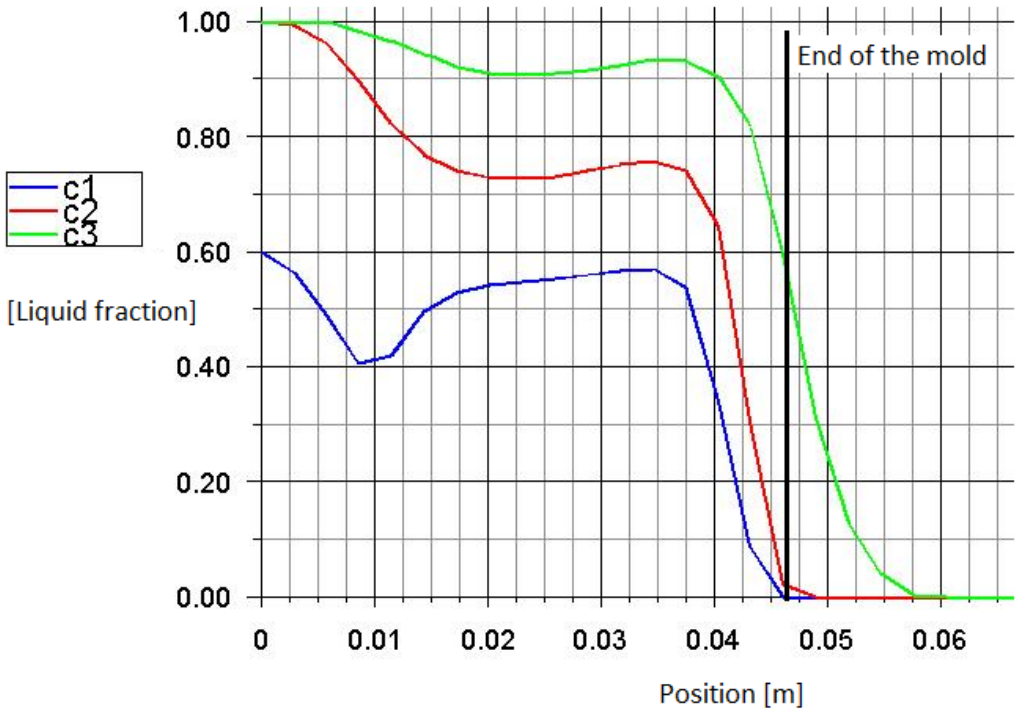

Figure 58 :Liquid fraction beside the inflow in normal state. C1 was at the surface, c2 was 5mm under the surface and c3 was 10mm under the surface.

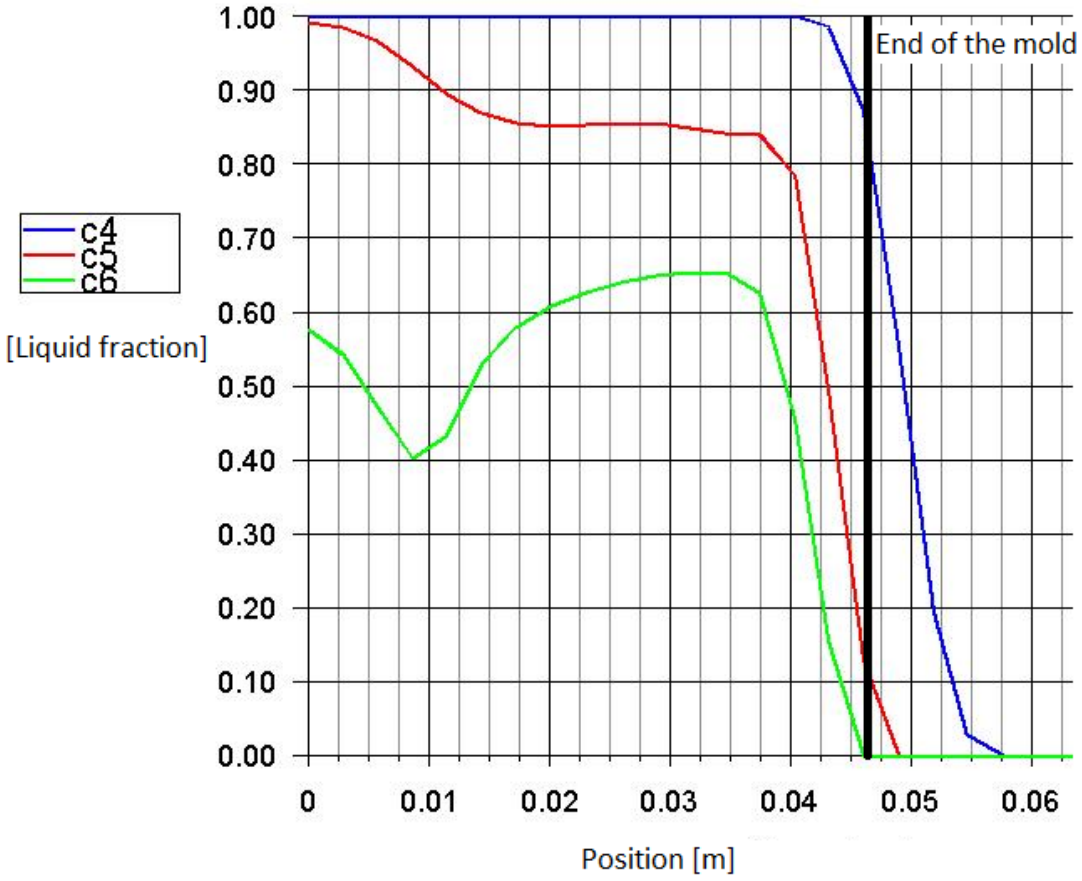

Figure 59 : Liquid fraction below the inflow in normal state. c6 was at the surface, c5 was 5mm under the surface and c4 was 10mm under the surface.

3.3.2 Bleedout test - Increased Temperature

The model was used to examine the effects of increasing the temperature of the aluminium alloy, keeping other casting parameters fixed. The temperature was increased by 50°C, table 11 shows values for the casting parameters.

Table 11 : Values for casting parameters, increased temperature.

Parameter	Value
Temperature of aluminium alloy	725°C
Casting speed	360 mm/min
Cooling water rate	130 m^3/hour
Cooling water temperature	15°C

Figures 60 – 64 show temperature distribution and solidification in a bar for increased temperature.

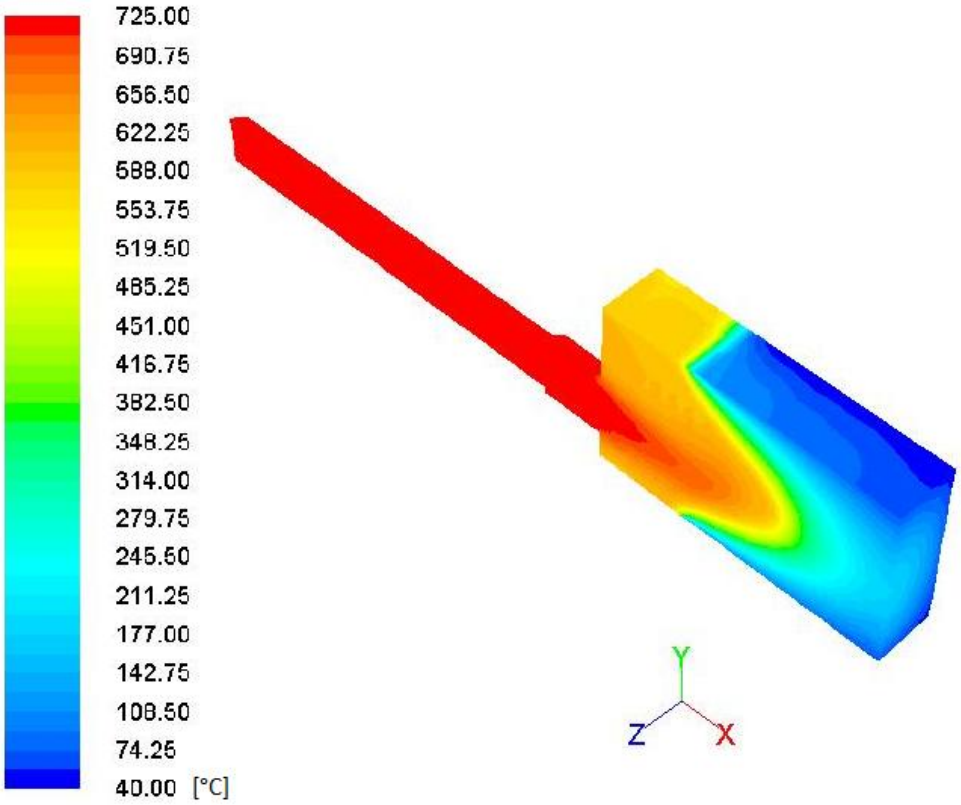

Figure 60 : Isometric view of temperature distribution in a bar – increased temperature.

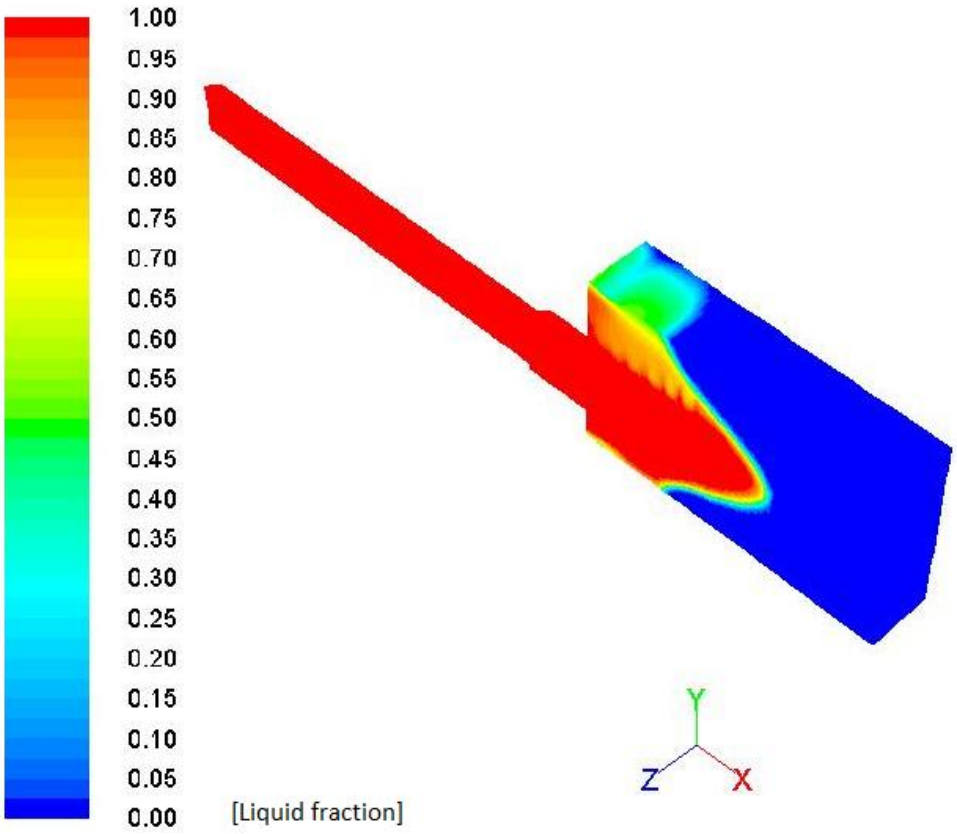

Figure 61 : Isometric view of solidification in a bar – increased temperature.

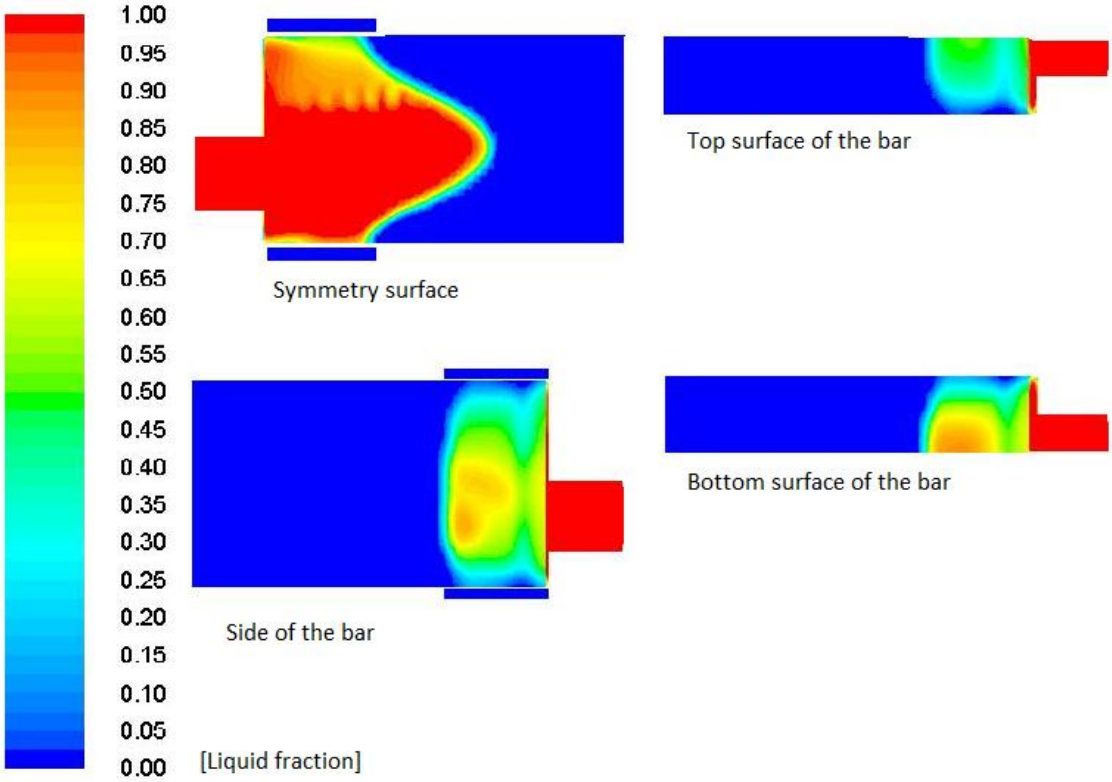

Figure 62 : 2D views of solidification in a bar – increased temperature. In the symmetry view and the side view, location of molds is shown.

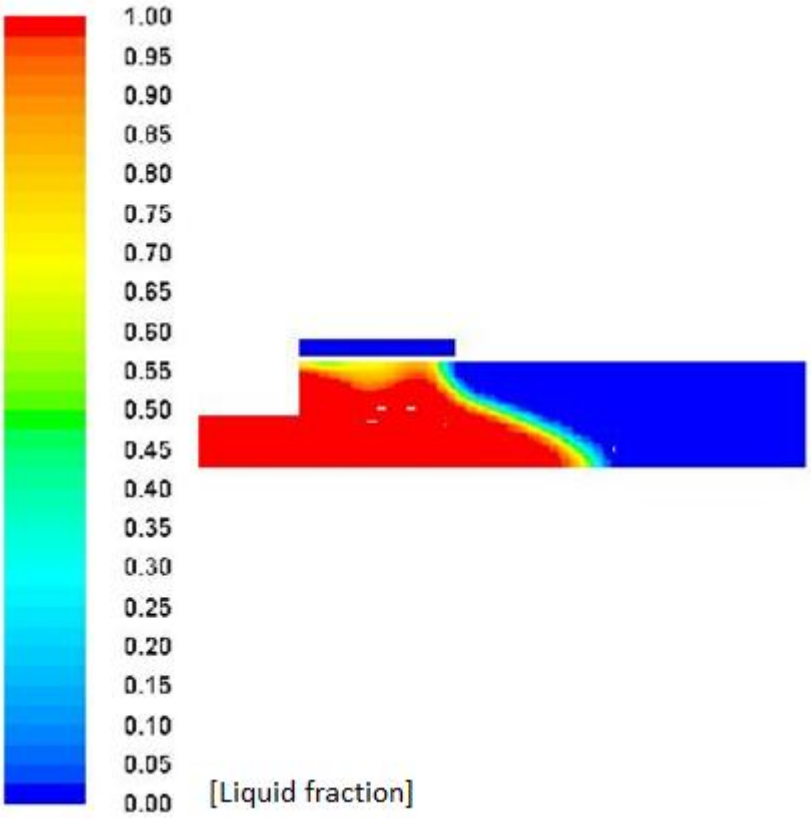

Figure 63 : Section 1, showing solidification – increased temperature.

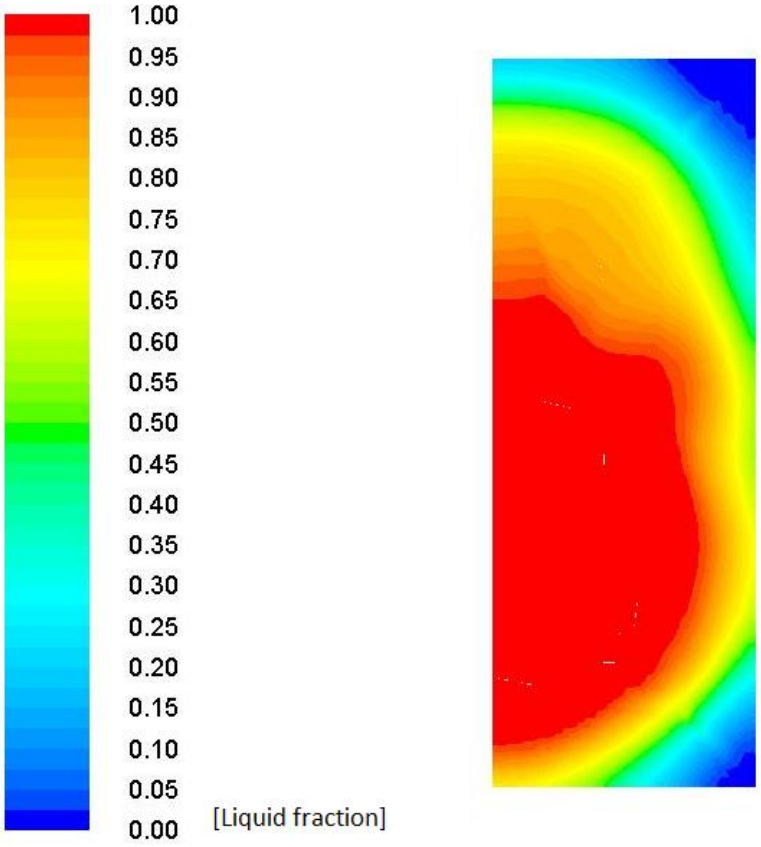

Figure 64 : Section 2, showing solidification – increased temperature.

In this case there are probably bleedouts both at the bottom surface and at the sides. Figure 63 show that the liquid is beginning to melt through the solid metal toward the side and the liquid fraction at the surface is 0,7-0,9. Figure 64 shows the same for the bottom surface, the liquid is beginning to melt through the solid metal toward the bottom surface and the side. The liquid fraction at the surface is 0,7-0,9 and there is no solidification shell around the bar. The liquid fraction is zero just in the corners of the bar.

Figures 65 and 66 show liquid fraction beside the inflow and below the inflow. It can be seen that when the bar leave the mold the liquid fraction on the surface is more than zero. The liquid fraction 5mm under the surface is 0,3 – 0,5 when the bar leaves the mold. In both cases, 5mm under the surface the liquid fraction is 1 only 10mm before the bar leaves the mold, as well as the liquid fraction is 0,8 – 0,9 on the surface. This leads to a bleedout both at the bottom surface and at the sides. For this temperature increase in the reality in this casting process, it is certain that bleedouts occur (Sigurðsson, 2012). These results indicate that the model gives quite reasonable results.

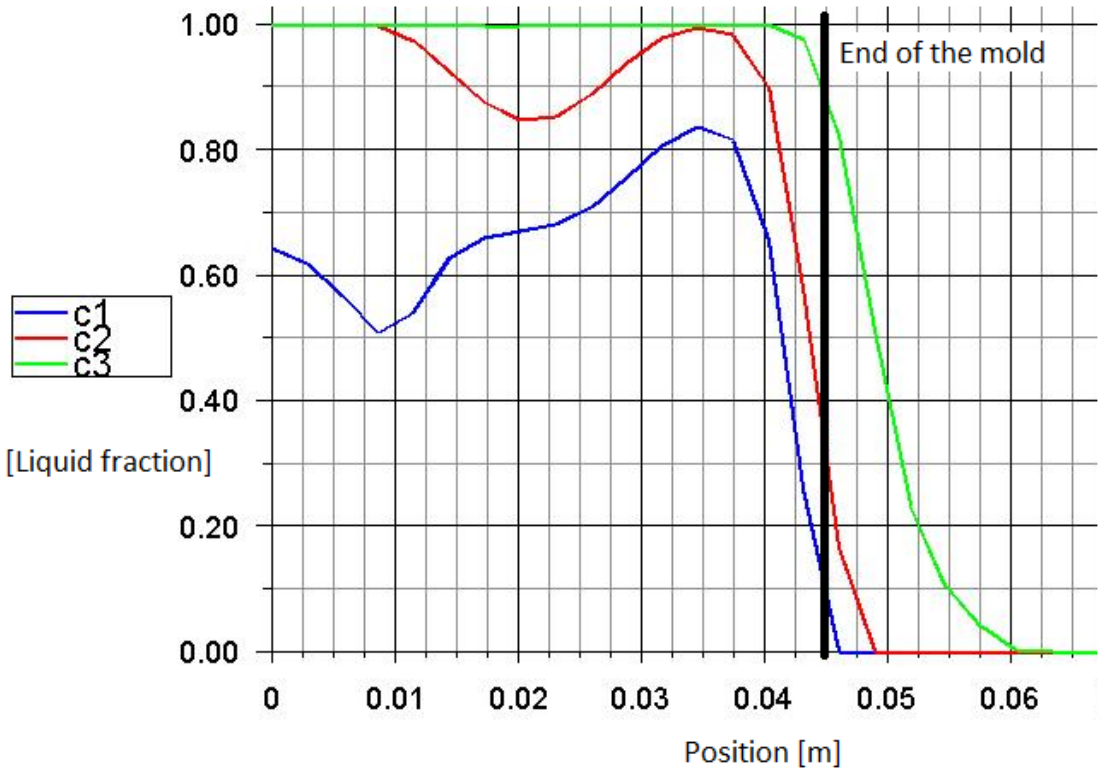

Figure 65 : Liquid fraction beside the inflow – increased temperature. C1 was at the surface, c2 was 5mm under the surface and c3 was 10mm under the surface.

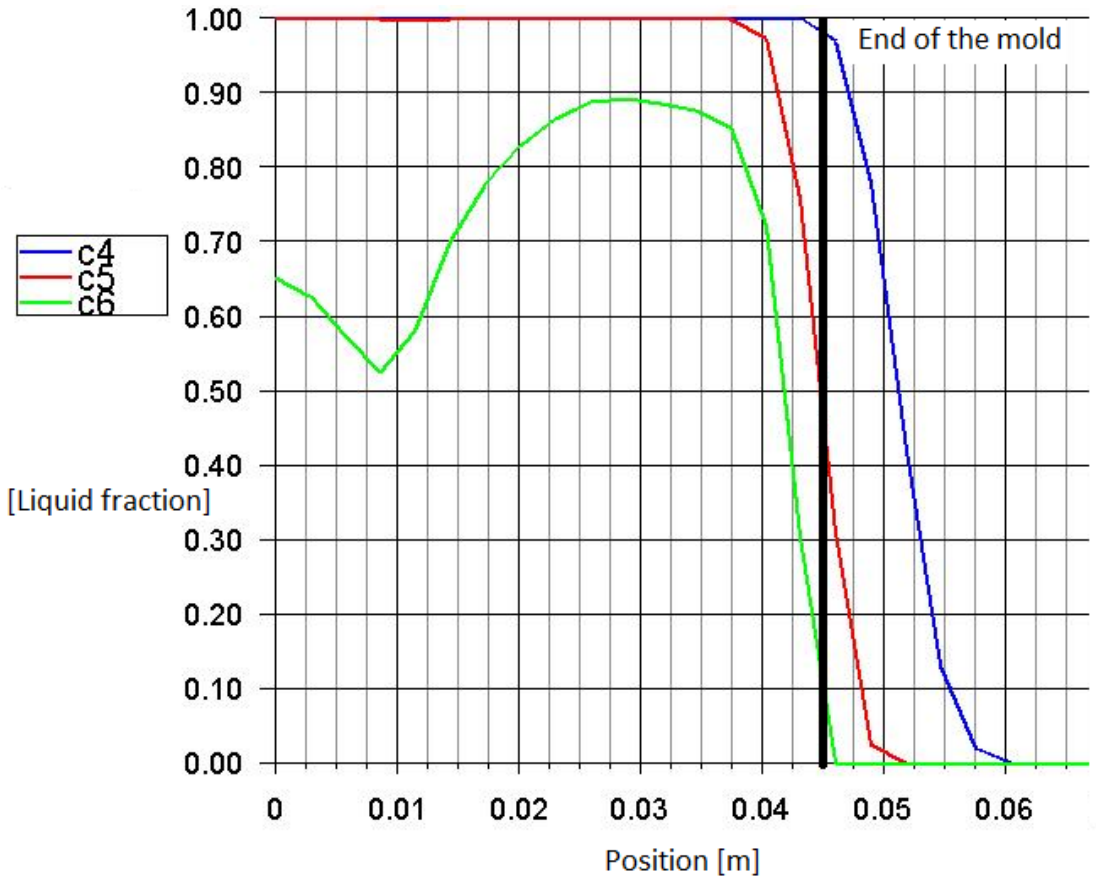

Figure 66 : Liquid fraction below the inflow – increased temperature. c6 was at the surface, c5 was 5mm under the surface and c4 was 10mm under the surface.

3.3.3 Bleedout test - Decreased Temperature

The model was used to examine the effects of decreasing the temperature of the aluminium alloy, keeping other casting parameters fixed. The temperature was decreased by 50°C, table 12 shows values for the casting parameters.

Table 12 : Values for casting parameters, decreased temperature.

Parameter	**Value**
Temperature of aluminium alloy	625°C
Casting speed	360 mm/min
Cooling water rate	130 m^3/hour
Cooling water temperature	15°C

Figures 67 – 71 show temperature distribution and solidification in a bar for decreased temperature.

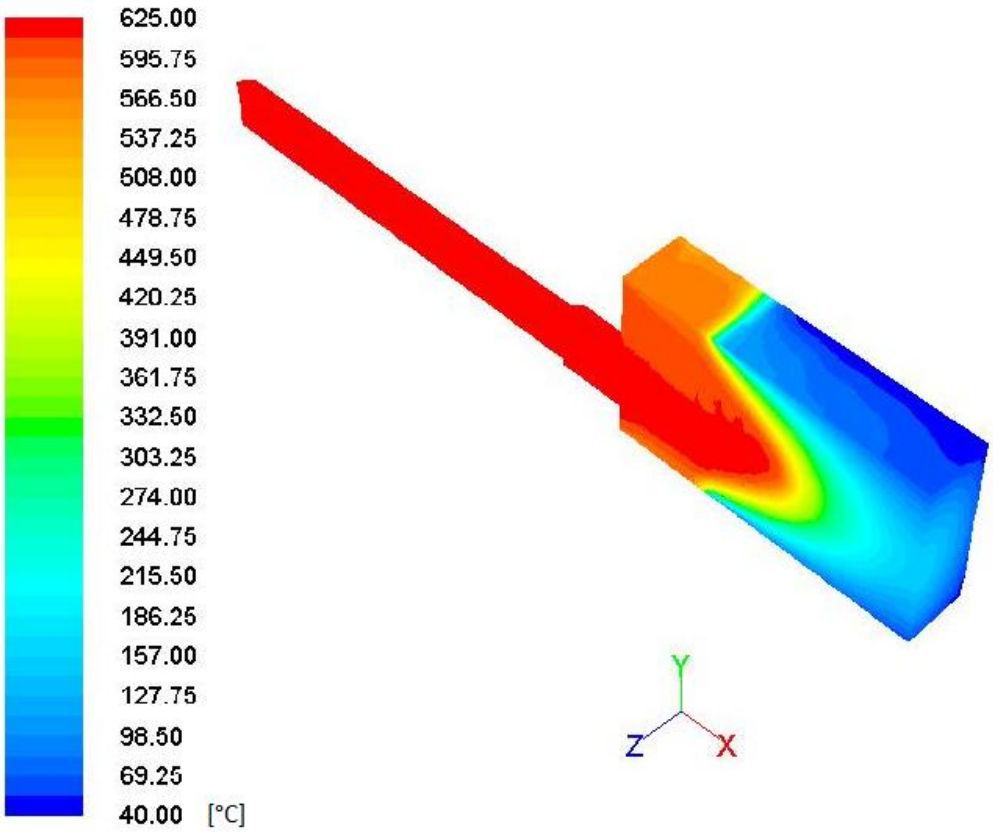

Figure 67 : Isometric view of temperature distribution in a bar – decreased temperature.

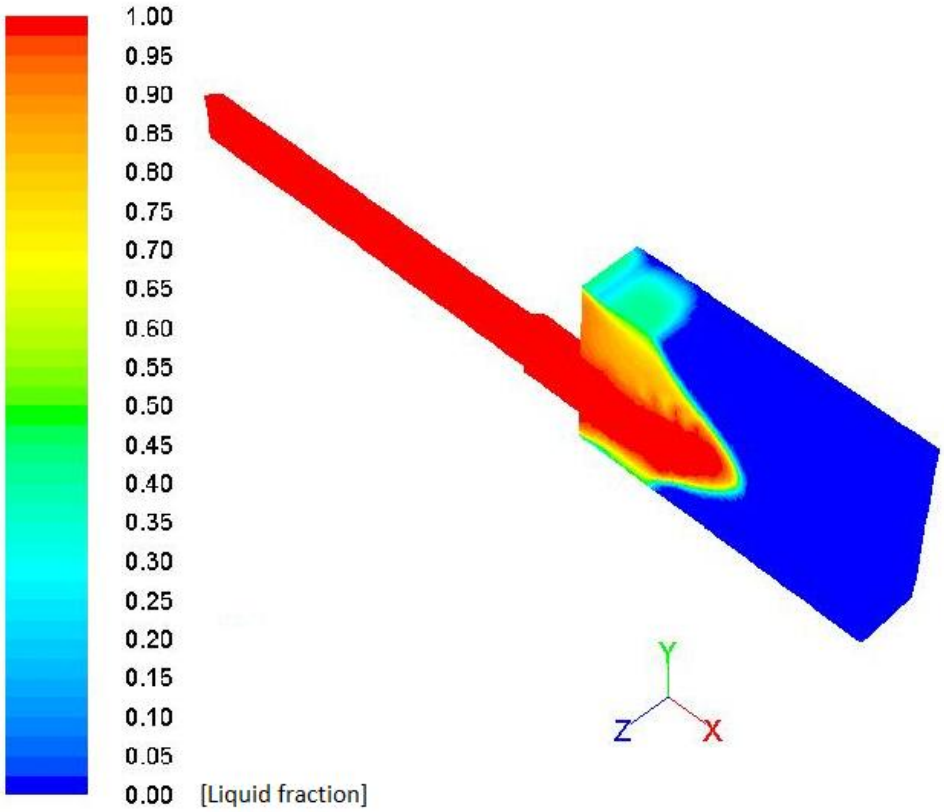

Figure 68 : Isometric view of liquid fraction in a bar – decreased temperature.

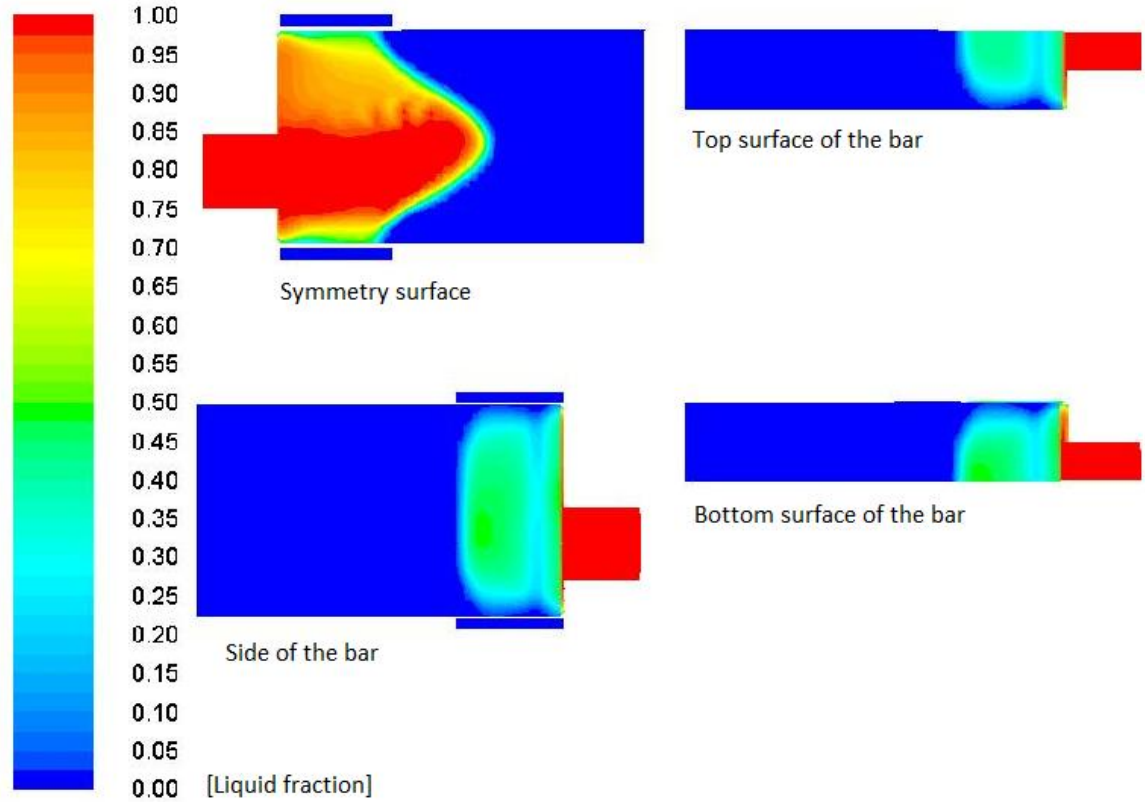

Figure 69 : 2D views of solidification in a bar – decreased temperature. In the symmetry view and the side view, location of molds is shown.

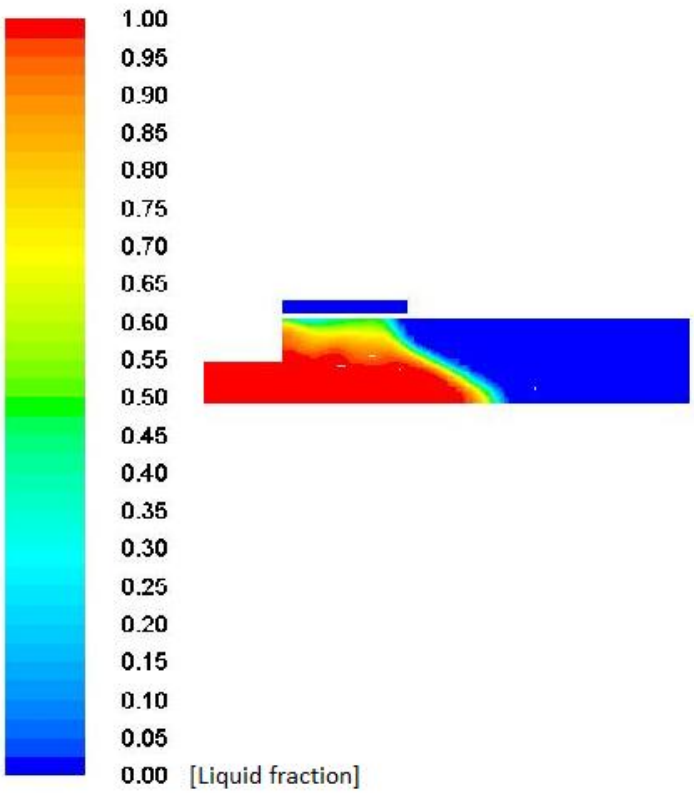

Figure 70 : Section 1, showing solidification – decreased temperature.

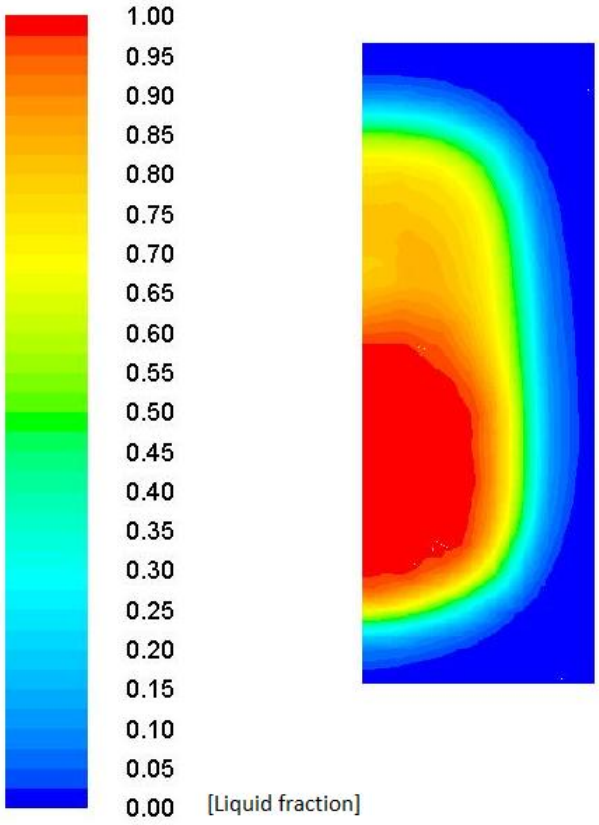

Figure 71 : Section 2, showing solidification – decreased temperature.

In this case the solidification is greater than in the normal state case. The initial temperature of the aluminium alloy is lower and the temperature needs to be reduced by fewer degrees to reach the solidification. Figure 71 shows that the mushy zone is larger and the liquid zone is smaller than in the normal state case.

Figures 72 and 73 show liquid fraction beside the inflow and below the inflow. It can be seen that when the liquid fraction on the surface reach zero 5mm before the bar leaves the mold. The liquid fraction 5mm under the surface is around 0,05 when the bar leaves the mold. The liquid fraction never reaches for these curves, it just decreases. In the normal state case the liquid fraction began in 1, both 5mm under the surface and 10mm under the surface. Here the solidification is very fast and probably too fast, the bar can get stuck. The flow from the pipe and into the mold needs to be free, here the fast solidification and the low liquid fraction up against the walls in the mold causes inertia and adhesion. For this temperature decrease in the reality in this casting process, it is certain that bars get stuck followed by bleedout (Sigurðsson, 2012). These results indicate that the model gives quite reasonable results.

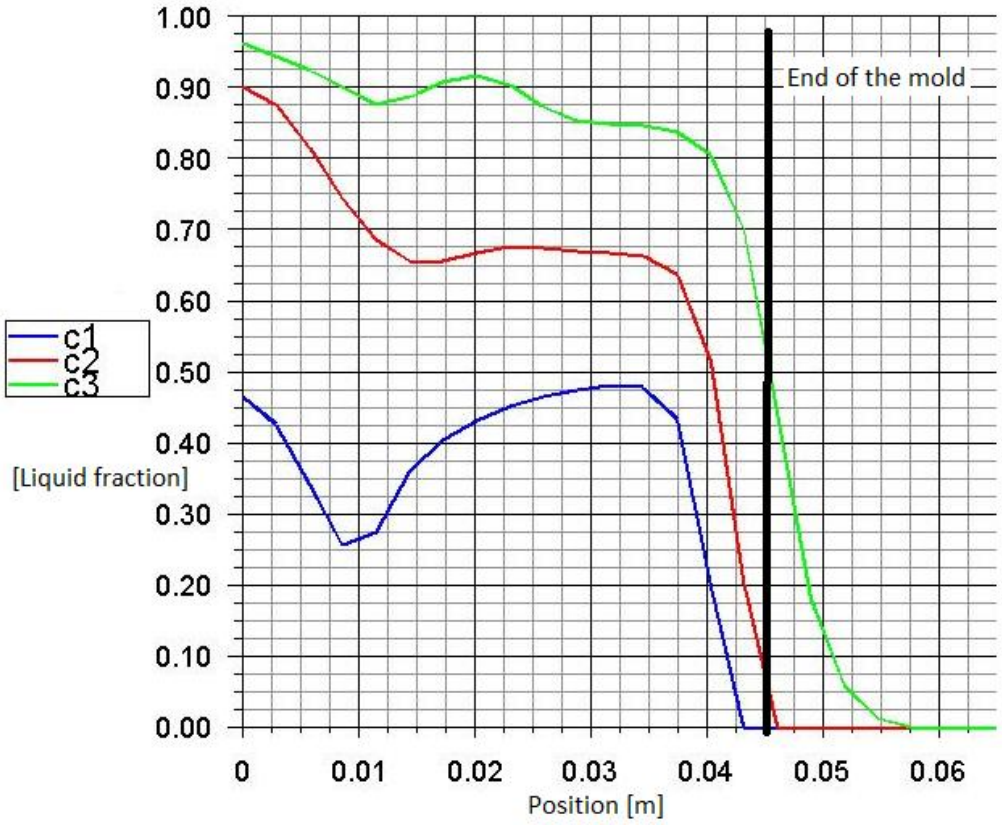

Figure 72 : Liquid fraction beside the inflow – decreased temperature. C1 was at the surface, c2 was 5mm under the surface and c3 was 10mm under the surface.

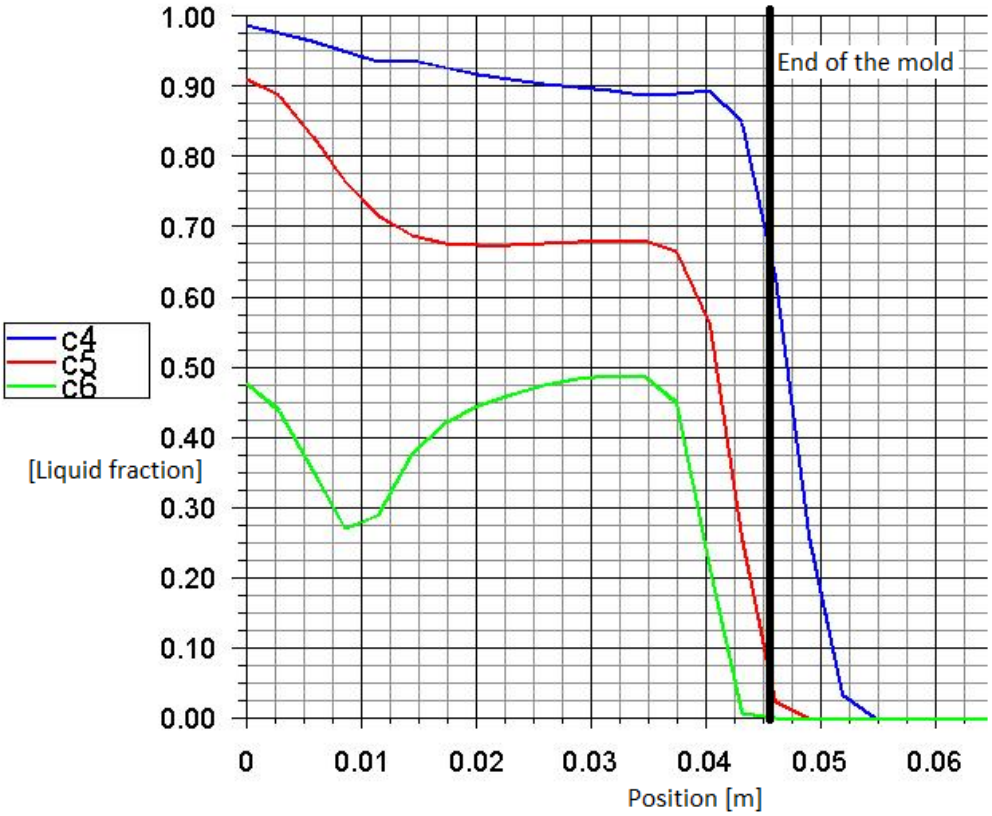

Figure 73 : Liquid fraction below the inflow – decreased temperature. C6 was at the surface, c5 was 5mm under the surface and c4 was 10mm under the surface.

3.4 Analysis of Historical Data

3.4.1 Bleedouts

Bleedouts for the years 2009-2011 were analysed (Fjarðaál, 2012). Productivity of the horizontal direct chill casting machine (HDC) has been increasing from the year 2009 but in 2009 the production of ingots began and it takes time to balance the production process. Already in 2010 the process have been improved and the total casting time had increased by over 1200%. Increase between years 2010 and 2011 was 35%, which is also very good. This is illustrated graphically in figures 74 and 75.

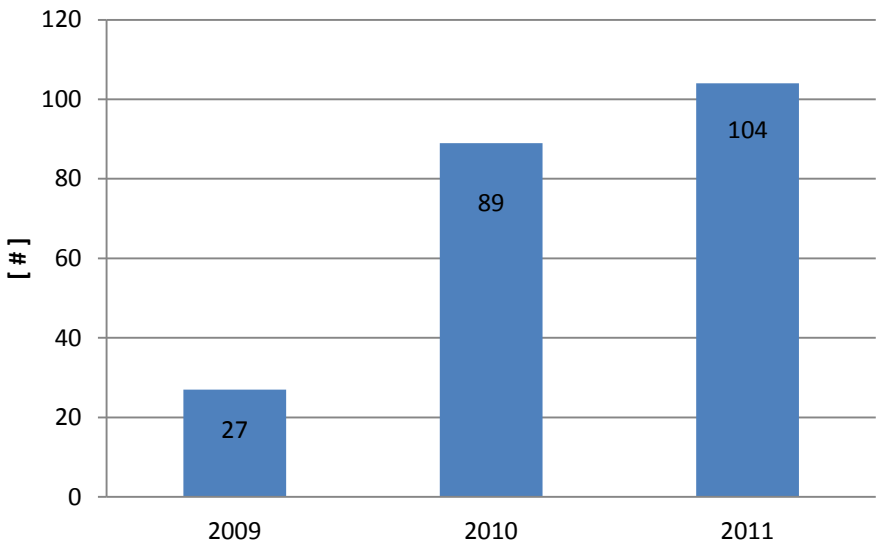

Figure 74 **:** *Total number of castings per year at Fjarðaál.*

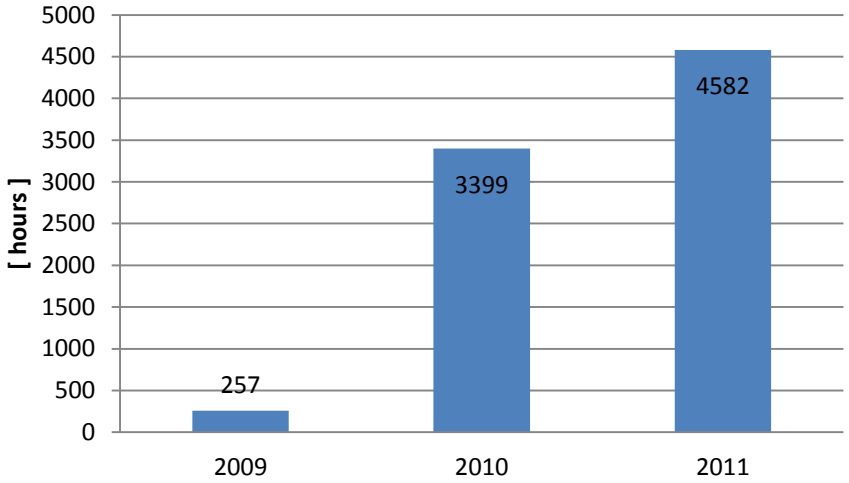

Figure 75 : Total casting time per year at Fjarðaál.

Stops at the HDC casting machine were divided into three categories, as can be seen in table 13.

Table 13 : Categories for stops at the HDC casting mashine.

Category	**Definition**
Controlled stop	Predetermined stop - No critical failure in the casting process
Bleedout	Necessery to stop casting process - One or more ingots bleed
Other	Necessery to stop casting process - Some failure in casting process

The first year there were many different problems in the casting process that resulted in many short castings, see figure 75. In 2010 was already more balance in the process but bleedouts had become the main problem. The same can be seen in 2011 but the number of castings had increased and each casting last longer. There is relative increase in controlled stops between years 2010 and 2011 as well as bleedouts reduces slightly. The goal is that most stops are controlled stops.

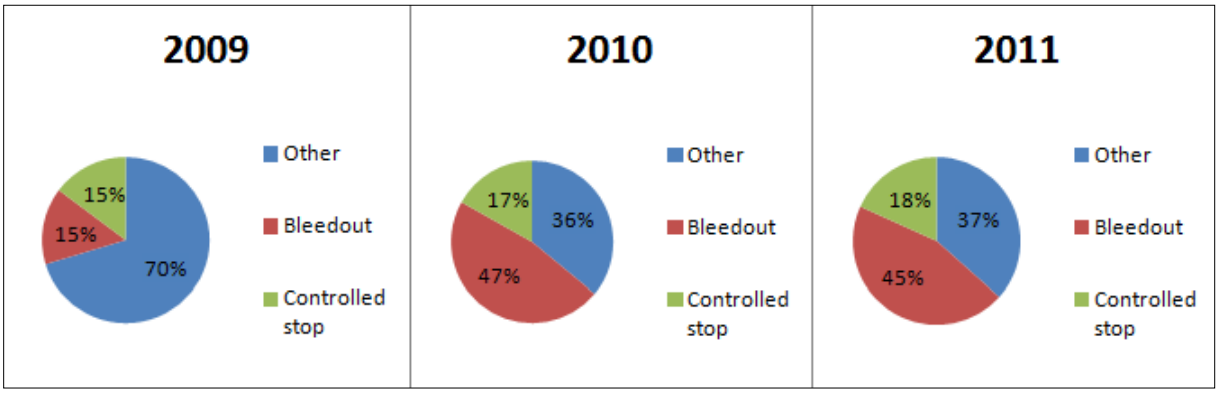

Figure 76 : Stops at the HDC casting machine – Ratio between categories

As can be seen in figure 77 the longest castings achieve when the stops are controlled, since no problems have occured in the casting process. The shortest castings are when equipment fails or when other unexpected problems occur in the casting process.

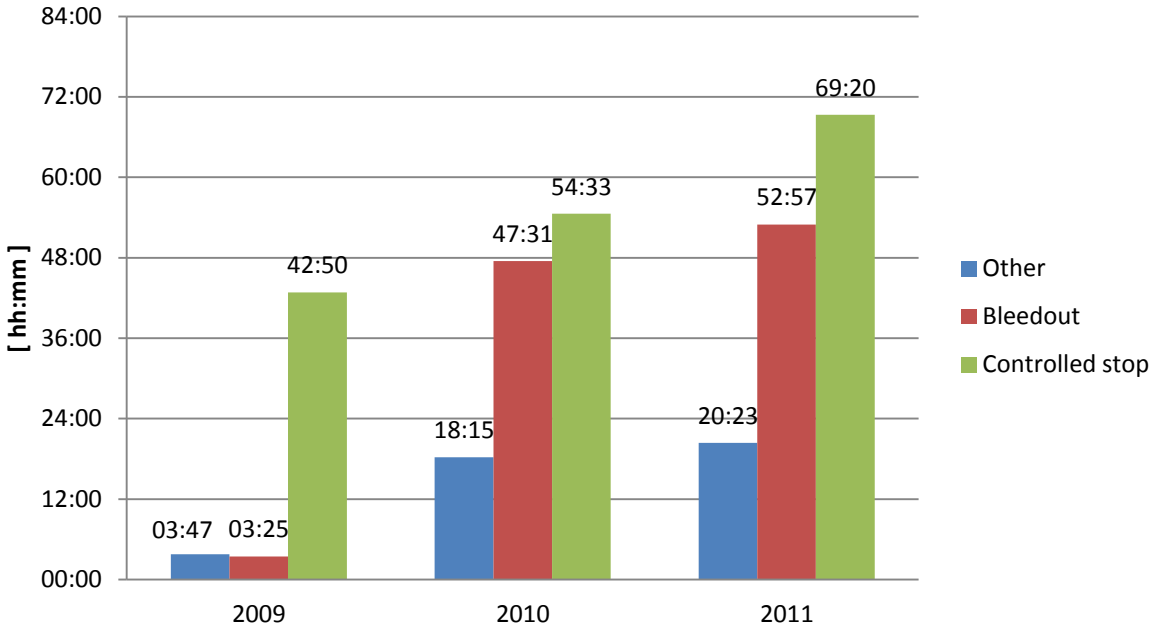

Figure 77 : Average casting time for the years 2009-2011

Bleedouts are the the most frequent unique problem in this casting process. The category „other“ is more extensive and applies to the rest of the casting process, from furnaces to packing machines that finalize the final product. To achieve higher performance and more stable operation, it needs to put more emphasis on analysing why bleedouts occurs and prevent it. Other problems such as failure in equipment are more convenient to deal with.

3.4.2 Change Between Furnaces

Change between furnaces for the years 2010 and 2011 were analysed (Fjarðaál, 2012). Critical conditions can occur in change between furnaces (CBF) and therefore correlation between CBF and bleedouts in the alloyed bars was investigated. The length of time from the last CBF until a bleedout occurred was examined. If less than one hour passes from CBF until bleedout occurs, it can be assumed that the CBF could have caused the bleedout. If more than hour passes, it is estimated that the CBF has been successful and will not cause bleedout directly. Unsuccessful CBF characterized by inconsistency between furnaces, but the most important parameters are the chemical composition and the temperature of the alloy (Sigurðsson, 2012). To facilitate the processing, the time from CBF was divided into 8 intervals, as can be seen in table 14.

Table 14 : Intervals – Time from change between furnaces

Interval	Time from CBF [h:mm]
Int 1	0:01 - 1:00
Int 2	1:01 - 2:00
Int 3	2:01 - 3:00
Int 4	3:01 - 4:00
Int 5	4:01 - 5:00
Int 6	5:01 - 6:00
Int 7	6:01 - 7:00
Int 8	7:01 - 8:00

Figure 78 shows results for the year 2010. In most cases less than 1 hour passed from CBF (Int 1) until bleedout occurred, or in 21,6% of the cases. In second most cases 2-3 hours passed from CBF (Int 3) until bleedout occurred, or 16,2% of the cases. Otherwise it was fairly equally distributed but the average for all the intervals was 12,5% and the standard devitation was 4,6%. Int 1 was the only interval which was more than one standard deviation above the average. No category was more than one standard deviation below the average.

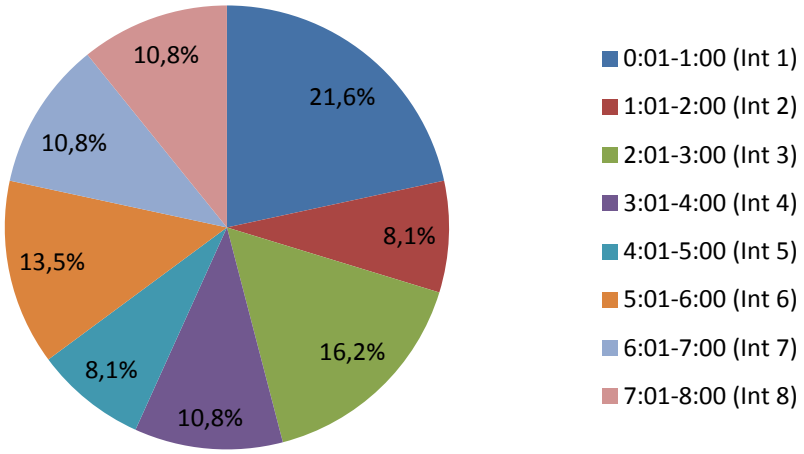

Figure 78 : The year 2010 – Time from change between furnaces.

Figure 79 shows results for the year 2011. In most cases less than 1 hour passed from CBF (int 1) until bleedout occurred, or 22,2% of the cases. Otherwise it was fairly equally distributed but the average for all the intervals was 12,5% and the standard deviation was 5,9%. Int 1 was the only interval which was more than one standard deviation above the average. Int 5 and Int 7 are more than one standard deviation below the average.

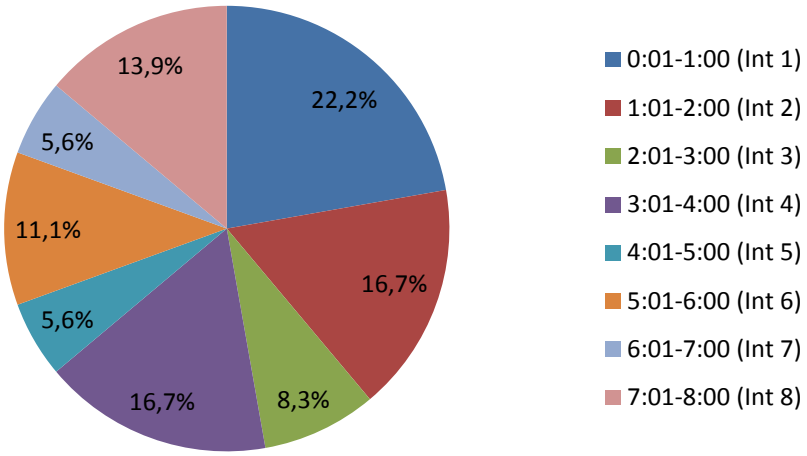

Figure 79 : The year 2011 – Time from change between furnaces

Figure 80 shows results for both the years. In most cases less than 1 hour passed from CBF (Int 1) until bleedout occurred, or 21,9% of the cases. Otherwise it was fairly equally distributed but the average for all the intervals was 12,5% and the standard deviation was 4,5%.

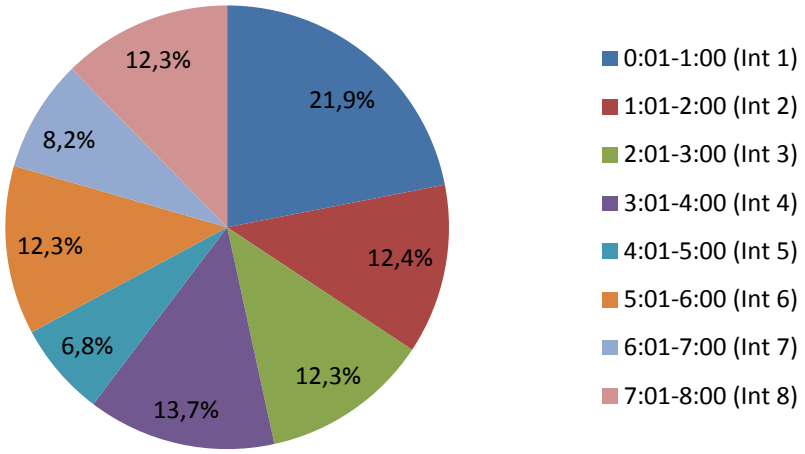

Figure 80 : Total results for years 2010 and 2011 – Time from change between furnaces

To estimate whether Int 1 was unusually high compared to other intervals, probability calculations were used to test the null hypothesis that all intervals have the same weight. Null hypothesis was that all intervals should have the weight 1/8 = 12,5%. Under normal circumstances the distribution should be random and weight between intervals equal. Table 15 shows results for the probability calculations. The table show the actual weight and expected weight for each category, together with the deviation. The second lowest row show the Z-value calculated for the null hypothesis and the lowest row show whether the null hypothesis is qualified for relevant category. The Z-value used for comparison was 1,96, obtained from significance requirement 0,05. If the absolute value of Z calculated was higher than 1,96 then the null hypothesis was rejected, see description of the calculation method in chapter 2.5.

Table 15 : Results for probability calculations

	Int 1	**Int 2**	**Int 3**	**Int 4**	**Int 5**	**Int 6**	**Int 7**	**Int 8**
Actual weight	21,9%	12,4%	12,3%	13,7%	6,8%	12,3%	8,2%	12,3%
Expected weight	12,5%	12,5%	12,5%	12,5%	12,5%	12,5%	12,5%	12,5%
Deviation	9,4%	-0,1%	-0,2%	1,2%	-5,7%	-0,2%	-4,3%	-0,2%
Z-value	2,43	-0,03	-0,06	0,32	-1,46	-0,05	-1,12	-0,04
Null hypothesis	No	Yes	Yes	Yes	Yes	Yes	Yes	Yes

The results of this probability test was that all intervals are within the confidence limits expect Int 1. Int 1 is unusually high and cannot be classified as being equal to other intervals. Most bleedouts occurs less than hour after change of furnace, therefore it can be concluded that change of furnace has direct effect on bleedouts.

Based on data from the database, all casting parameters seemed to be stable during CBF except the temperature of the aluminium alloy (Fjarðaál, 2012). Figure 81 shows traditional temperature distribution during CBF. Yellow and pink curves show temperature in the furnace launder, green and cyan curves show temperature in the tundishes. Every 8 hours (approximately) the yellow and pink curves switch, it is when switching between furnaces. It can be shown that each time when it is switched between furnaces, temperature change occurred in the tundishes. Red circles mark temperature decrease and blue circle mark temperature increase. The temperature decrease can be up to 20-25°C.

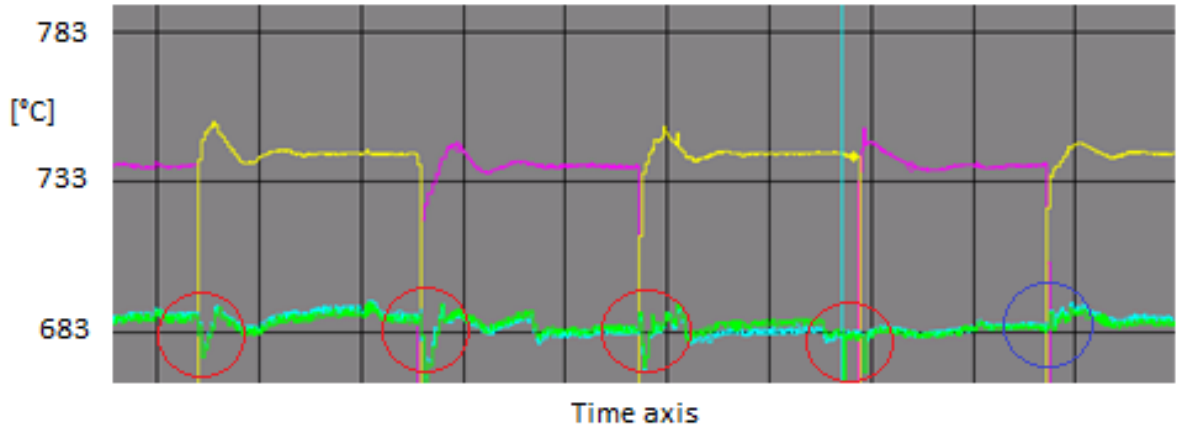

Figure 81 : Temperature of the aluminium alloy. Green and cyan curves show temperature in the tundishes, yellow and pink curves show temperature in the furnace launder Red circles mark temperature decrease, blue circle mark temperature increase (Fjarðaál, 2012).

Thus instability can certainly create problems for the casting process. Most bleedouts, or 21,9% of cases, occurred less than hour after CBF.

3.4.3 Casting Parameters

Correlation between instability of casting parameters and bleedouts was examined. All bleedouts and all controlled stops from the year 2011 were examined and it compared (Fjarðaál, 2012). The most important casting parameters for the casting process were analysed which was the temperature of the aluminium alloy, amount of cooling water and the casting speed.. Instability in these parameters can cause problems for the casting process, other casting parameters are considered less important (Sigurðsson, 2012) (Nadella R. , Eskin, Du, & Katgerman, 2007). The temperature of the cooling water was not examined since measurements (chapter 3.1.3) showed that this parameter has little impact on the cooling process.

Charts were used to analyse instability in the casting parameters, the last 1 hour of each casting was examined. The analysis revealed that the casting speed and the amount of cooling water were always stable, figures 82 and 83 show examples of its stability when bleedout occurs. The casting speed is fixed at certain value which is easy to control and the same applies to the amount of cooling water, it is fixed at certain value although with some noise which is normally ± 0,5 m3/hour.

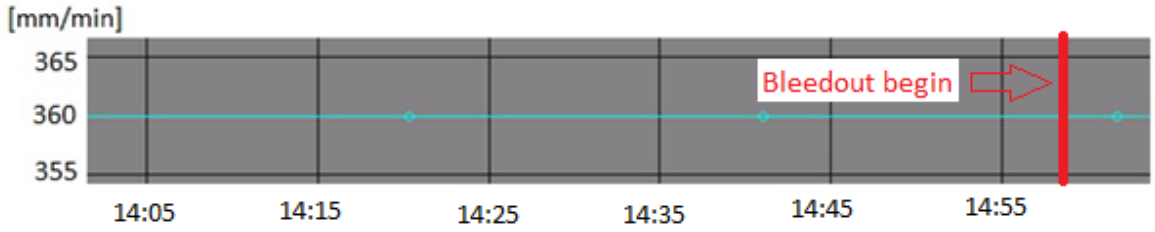

Figure 82 : Bleedout where the casting speed is stable (Fjarðaál, 2012)

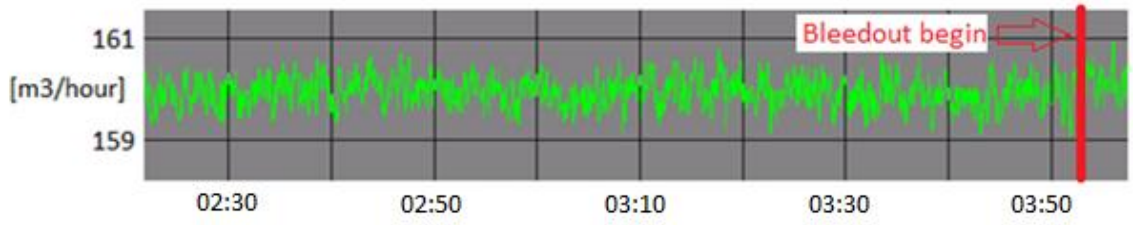

Figure 83 : Bleedout where the amount of cooling water is stable (Fjarðaál, 2012)

This suggests that bleedouts could not have occurred because of instability in the casting speed or the cooling water rate. Both in bleedout cases and cases without bleedouts, these two parameters were stable. These parameters varies by castings, figure 84 shows bleedout cases and figure 85 shows cases without bleedouts, the last hour of each casting. The cooling water rate was similar in both cases, 130 m^3/hour and 160 m^3/hour was most commonly used. The average for bleedout cases was 146 m^3/hour and the average for cases without bleedouts was 148 m^3/hour. This distribution indicates that the value of the cooling water rate is not causing bleedouts. Other studies have shown that the cooling water rate is the parameter that has minimal effect on bleedouts (Gariepy & Caron, 1991). The casting speed was similar in both cases, most common values were between 330 mm/min and 360 mm/min. The average for bleedout cases was 344 mm/min and the average for cases without bleedouts was 337 mm/min. This is not much difference but this may indicate that lower casting speed reduces the likelihood of bleedouts. Other studies have shown that severity of bleedouts increases with the casting speed (Nadella, Eskin, & Katgerman, 2006).

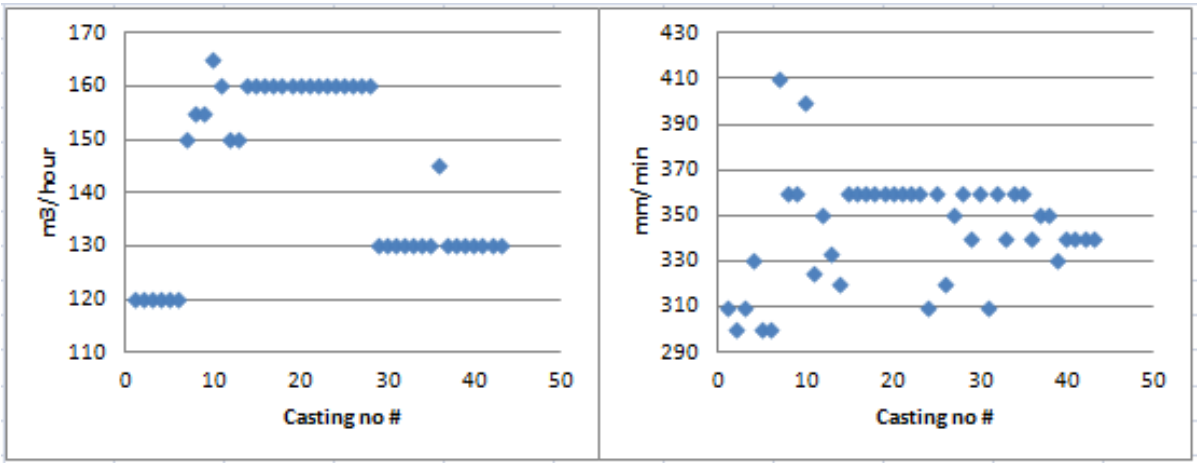

Figure 84 : Bleedout cases, value of the casting parameters the last hour of each casting. The chart to the left show different values for the cooling water rate and the chart to the right show different values for the casting speed (Fjarðaál, 2012).

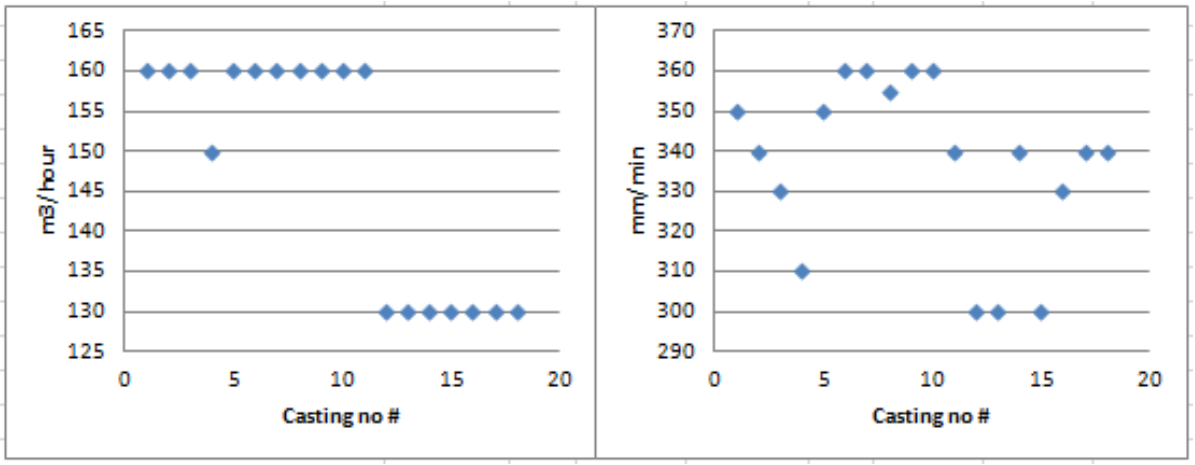

Figure 85 : Cases without bleedout, value of the casting parameters the last hour of each casting. The chart to the left show different values for the cooling water rate and the chart to the right show different values for the casting speed (Fjarðaál, 2012).

The temperature of the aluminum alloy turned out to be the only unstable casting parameter. In the bleedout cases it was clearly more instability than in cases without bleedouts. Figures 86 and 87 show the instability the last hour in each casting. These figures show the upper and lower limit for fluctuations. The average value for bleedout cases was 675°C, lower limit 670°C and upper limit 680°C, so total range of 10°C for fluctuations. The average value for cases without bleedout was 675°C, lower limit 673°C and upper limit 677°C, so total range of 4°C for fluctuations. The maxinum change in temperature in bleedout cases was decrease of 24°C. The maximum change in temperature in cases without bleedouts was increase of 2,5°C. It is interesting that the mean value is the same for both cases but there is much more stability in cases without bleedouts. The total range in bleedout cases was 655°C – 697°C. The total range in cases without bleedout was 668°C-682°C.

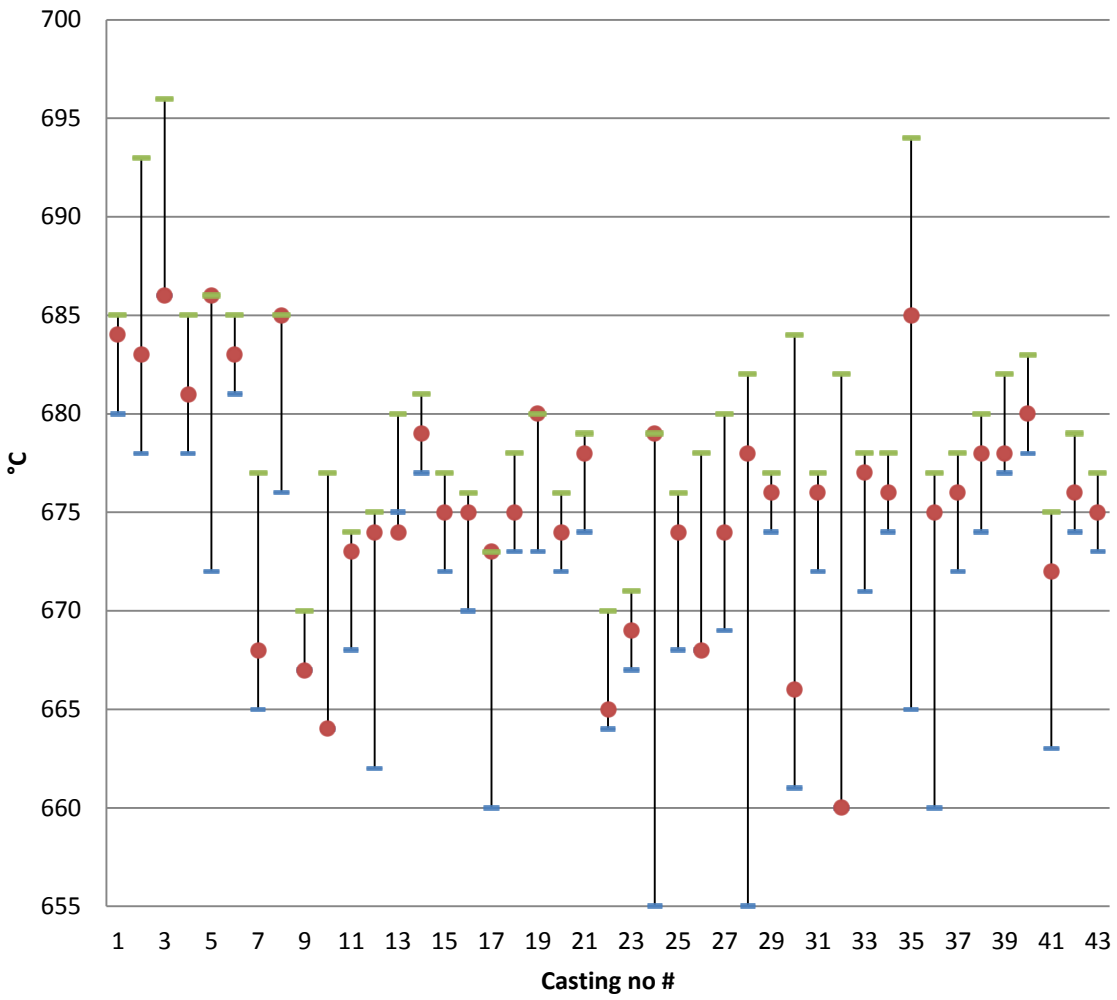

Figure 86 : Bleedout cases, the last hour of each casting. Red dots denote the values 1 hour before the end of casting, green and blue lines show upper and lower limits for fluctuations during the last hour (Fjarðaál, 2012).

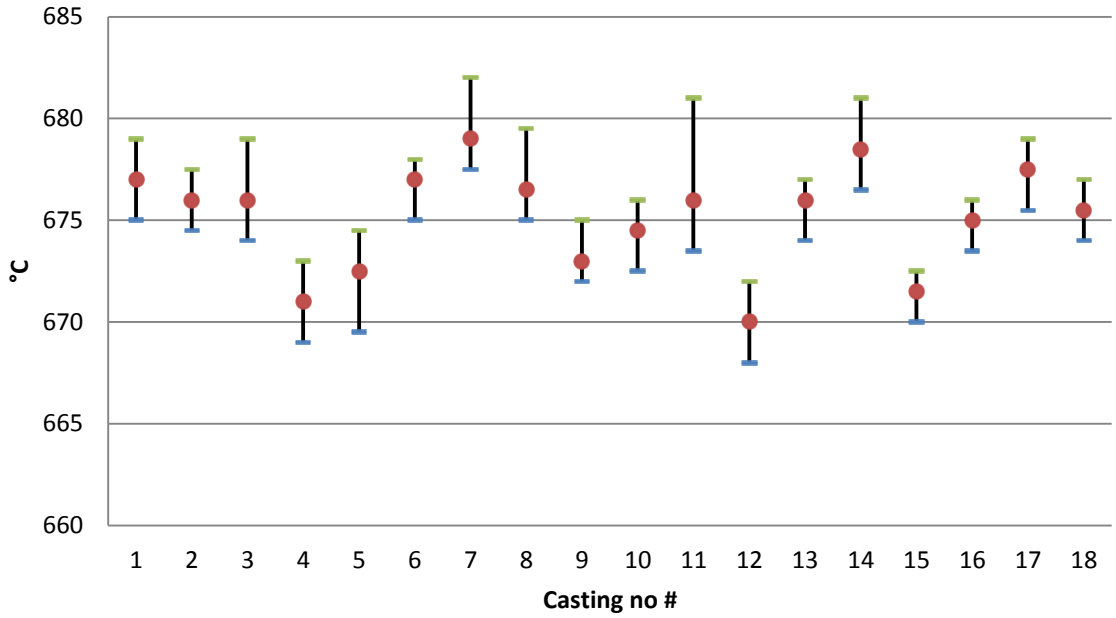

Figure 87 : Cases without bleedout, the last hour of each casting. Red dots denote the values 1 hour before the end of casting, green and blue lines show upper and lower limits for fluctuations during the last hour (Fjarðaál, 2012).

To investigate the correlation between unstable temperature and bleedouts, maximum range for fluctuations in temperature was defined. Each bleedout case was examined and if the temperature would reach that limit, the fluctuation was defined as cause for the bleedout. Causes for bleedouts were divided into three categories as can be seen in table 16. The temperature is considered stable if the fluctuations were inside the given range and there is some other, known or unknown, cause for the bleedout. If the temperature reaches the upper limit, increased temperature is considered as cause for the bleedout and if the temperature reaches the lower limit, decreased temperature is considered as cause for the bleedout. When the temperature is too low, the aluminium alloy freezes too early and the pipe into the mold can get clogged. When pipe gets clogged either all flow stops or the pipe is semi-closed, which means that aluminium alloy flows through but no alloyed bar will be formed in the mold. When the temperature is too high, the alloyed bar is unable to form sufficiently thick shell in the primary cooling and the hot aluminium alloy melts through the shell before the bar leaves the mold.

Table 16 : Correlation between temperature and bleedouts - categories

Category	Definition
Temp. decrease	Temperature of the aluminium alloy had decreased abnormally
Temp. increase	Temperature of the aluminium alloy had increased abnormally
Within range	Temperature of the aluminium alloy is stable, there is other cause

Three conditions were examined for the upper and lower limit of the temperature as can be seen in table 17. The temperature value 1 hour before stop was defined as the initial value and certain maximum change in temperature for the last hour was defined.

Table 17 : Conditions for maximum allowed temperature change in tundishes

Condition	Maximum allowed temperature change
1	Initial value ± 2°C (cf. the calculated range for cases without bleedouts)
2	Initial value ± 5°C
3	Initial value ± 10°C

Figure 88 shows the results for condition 1, defined as ±2°C maximum change in the temperature. In 48,8% of cases, the temperature reached the lower limit and the bleedout occured because of decreased temperature of the aluminum alloy. In 34,9% of cases, the temperature reached the upper limit and the bleedout occurred because of increased temperature of the aluminium alloy. In 16,3% of cases the temperature was within the given range and temperature was considered stable. In total 83,7% of cases the instability in the temperature caused the bleedout which is very high percentage. Indeed, the temperature range is rather narrow (4°C).

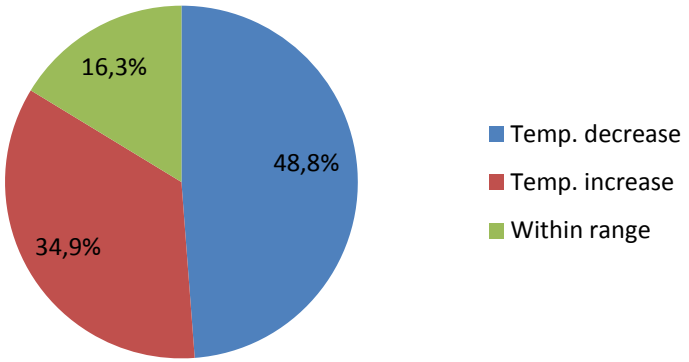

Figure 88 : Condition 1(Initial value ± 2°C) – Ratio between categories

Figure 89 shows the results for condition 2, defined as ±5°C maximum change in the temperature. In 30,2% of cases, the temperature reached the lower limit and the bleedout occured because of decreased temperature of the aluminum alloy. In 23,3% of cases, the temperature reached the upper limit and the bleedout occurred because of increased temperature of the aluminium alloy. In 46,5% of cases the temperature was within the given range and temperature was considered stable. In total 53,5% of cases the instability in the temperature caused the bleedout. Since the temperature range is rather wide (10°C), it must be said that 53,5% is pretty high percentage. Great instability is in the temperature.

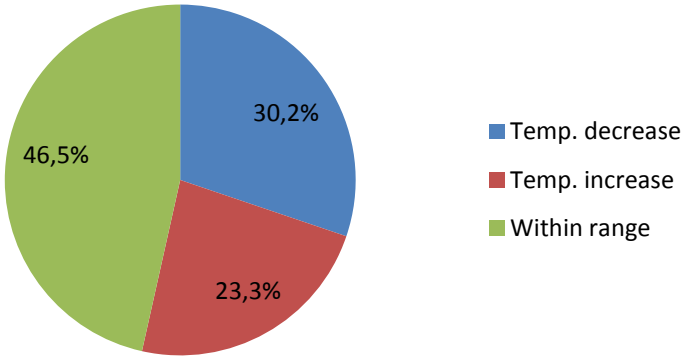

Figure 89 : Conditions 2 (Initial value ± 5°C) – Ratio between categories

Figure 90 shows the results for condition 3, defined as ±10°C maximum change in the temperature. In 18,6% of cases, the temperature reached the lower limit and the bleedout occured because of decreased temperature of the aluminum alloy. In 18,6% of cases, the temperature reached the upper limit and the bleedout occurred because of increased temperature of the aluminium alloy. In 62,8% of cases the temperature was within the given range and temperature was consider stable. In total 37,2% of cases the instability in the temperature caused the bleedout. Since the temperature range is very wide (20°C), it must be said that 37,2% is very high percentage. It would be normal if all temperature fluctuations were inside these range. Great instability is in the temperature.

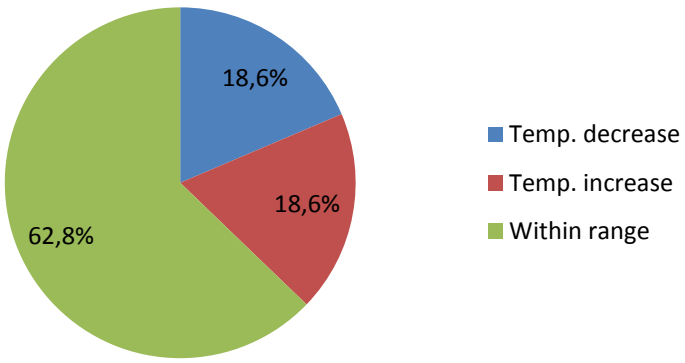

Figure 90 : Condition 3 (Initial value ± 10°C) – Ratio between categories

The results from these three conditions show that there is great instability in the temperature of the aluminium alloy. This leads to that this casting parameter is critical for bleedouts. This parameter is stable in cases without bleedouts and unstable in bleedout

cases. Other parameters are stable both in bleedout cases and cases without bleedouts. Considerable uncertainty is in the evaluation at what time point the bleedout begin. It can be difficult to read from the graphs and realise what changes causes bleedouts. As can be seen above high percentage of the bleedouts occurs when all three casting parameters are stable. It is estimated that the initial value of the temperature (value 1 hour before stop) is the mean value and upper and lower limits are derived from that. If the mean value is shifted and the same upper and lower limits are used, it could cause different results. Since the results are so crucial, it is not expected to have major impact.

To support this analysis, height of aluminium alloy in launder were examined. When bleedout occurs, unusually large amount of aluminium alloy flows from the tundish and thus the height of aluminium alloy in launder suddenly decreases. Graph for height in launder shows sudden decrease and then sudden increase shortly afterwards. That is when the flow from the furnace is increased to reach the correct height of aluminium alloy in launders. Increased flow from the furnace results also in temperature increase in the tundishes due to reduced resident time of the metal in the launder and consequently reduced heat loss.

Figure 91 shows example when the aluminium alloy temperature is stable in a bleedout case. It can be seen that the fluctuation is around ± 2°C before the bleedout occurs. Height of the aluminium alloy in launder indicates at what point bleedout began. When the bleedout begin, the height in the launder suddenly decrease and starts to increase again. The temperature suddenly increase in both tundishes but more in the tundish where the bleedout is which in this case is was tundish A. No visible signs can be seen in the temperature before the bleedout begin. If looked very closely the slope of the graph slopes very slightly downward. This case was defined with stable temperature.

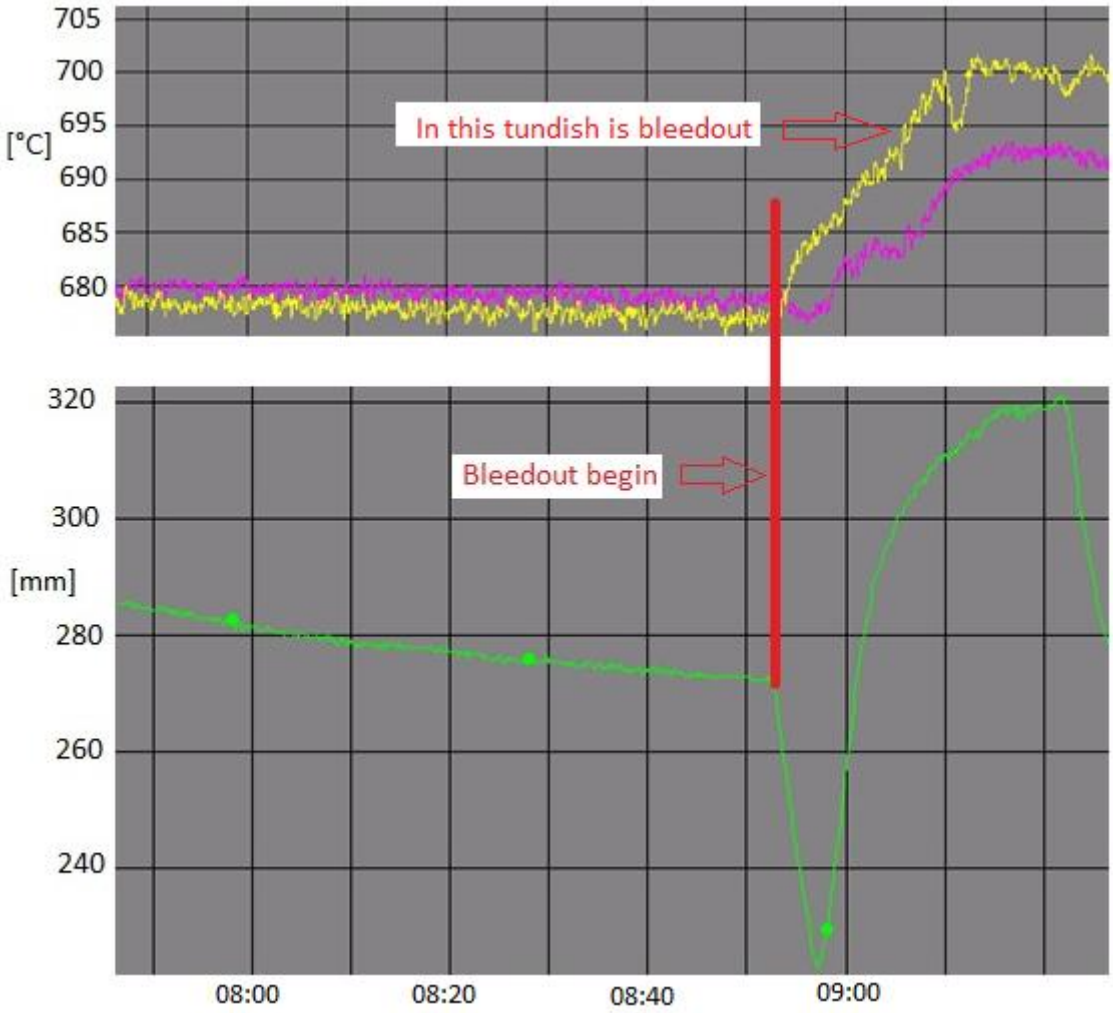

Figure 91 : Bleedout where the temperature of the aluminium alloy is stable - Upper chart is the temperature of the aluminium alloy, yellow is tundish A and pink is tundish B. Lower chart is height of aluminium alloy in the launder (Fjarðaál, 2012)

Figures 92 and 93 show examples when the temperature of the aluminium alloy is increasing before bleedout. In figure 41 the increase is more than 12°C and in figure 42 the increase is around 4°C.

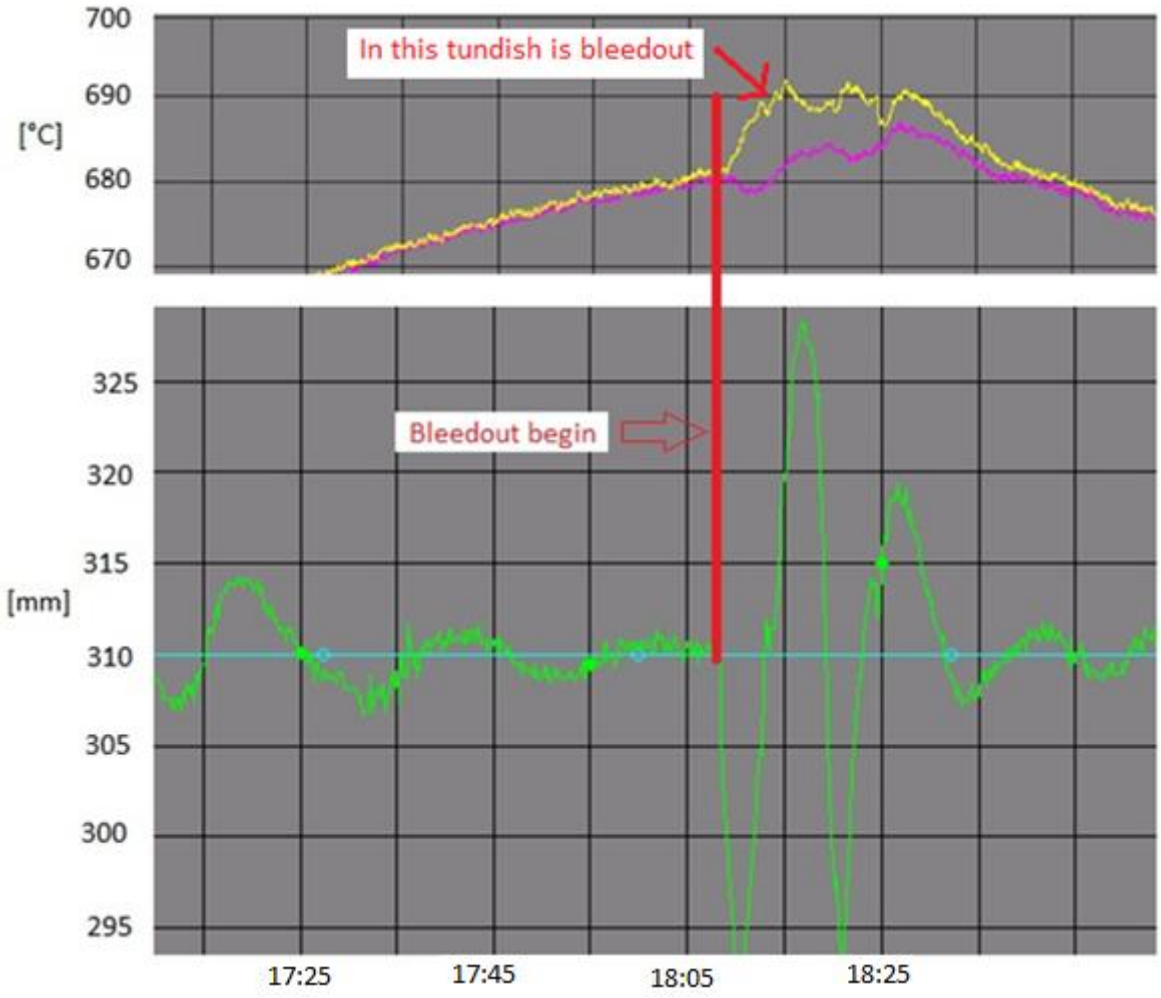

Figure 92 : Bleedout where the temperature of the aluminium alloy is increasing – Upper chart is the temperature of the aluminium alloy, yellow is tundish A and pink is tundish B. Lower chart is height of aluminium alloy in the launder (Fjarðaál, 2012)

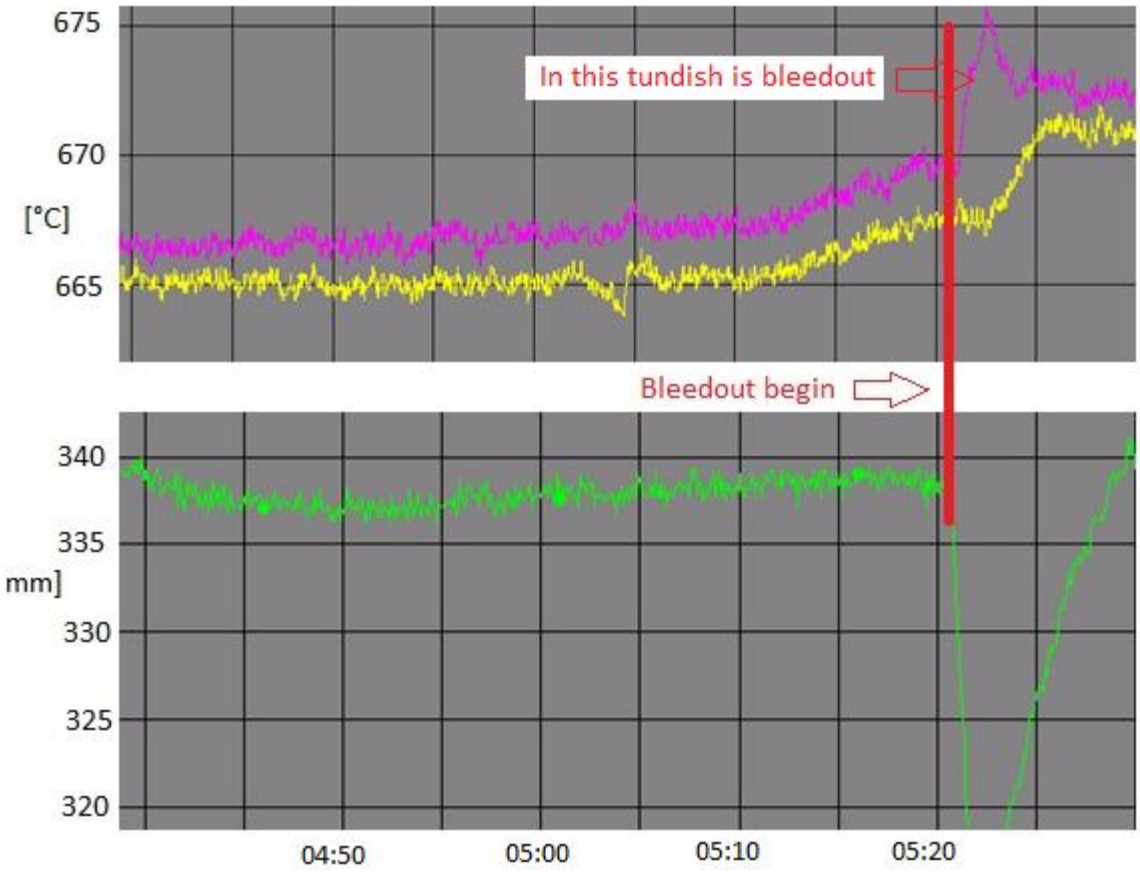

Figure 93 : Bleedout where the temperature of the aluminium alloy is increasing – Upper chart is the temperature of the aluminium alloy, yellow is tundish A and pink is tundish B. Lower chart is height of aluminium alloy in the launder (Fjarðaál, 2012)

Figures 94 shows bleedout case where the cause for the bleedout is temperature drop during furnace exchange, but the temperature decreases by more than 20°C and then increases again by more than 20°C in 30 minutes. Such a fluctuation causes problems in the casting process which leads to a bleedout. When the temperature drops, the flow from the furnace is increased to increase the temperature again. Previous temperature is reached again but the temperature keeps falling and finally bleedout occurs. This figure shows well how long the time it can takes for the bleedout to occur after the problem begin, in this case 45 minutes after the furnace exchange.

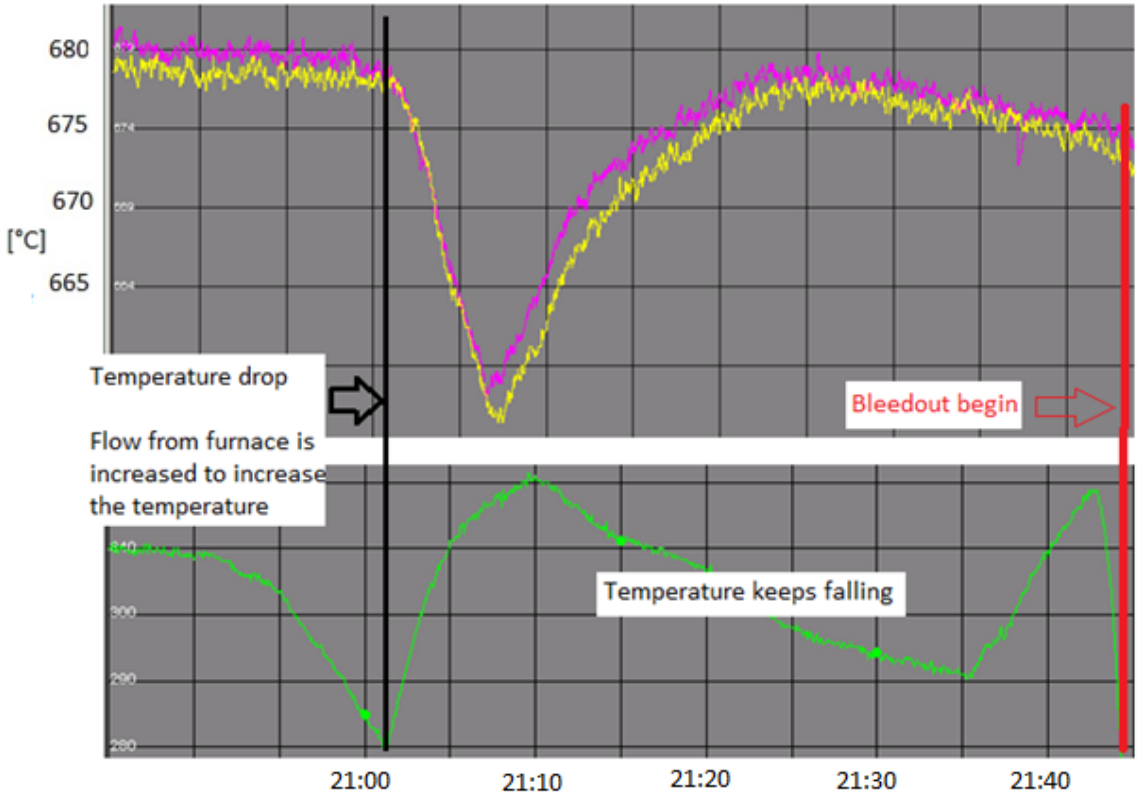

Figure 94 : Bleedout because of temperature drop during furnace exchange – Temperature of the aluminium alloy, yellow is tundish A and pink is tundish B (Fjarðaál, 2012)

Figure 95 shows example when the temperature of the aluminium alloy is decreasing before bleedout, the decrease is around 6°C.

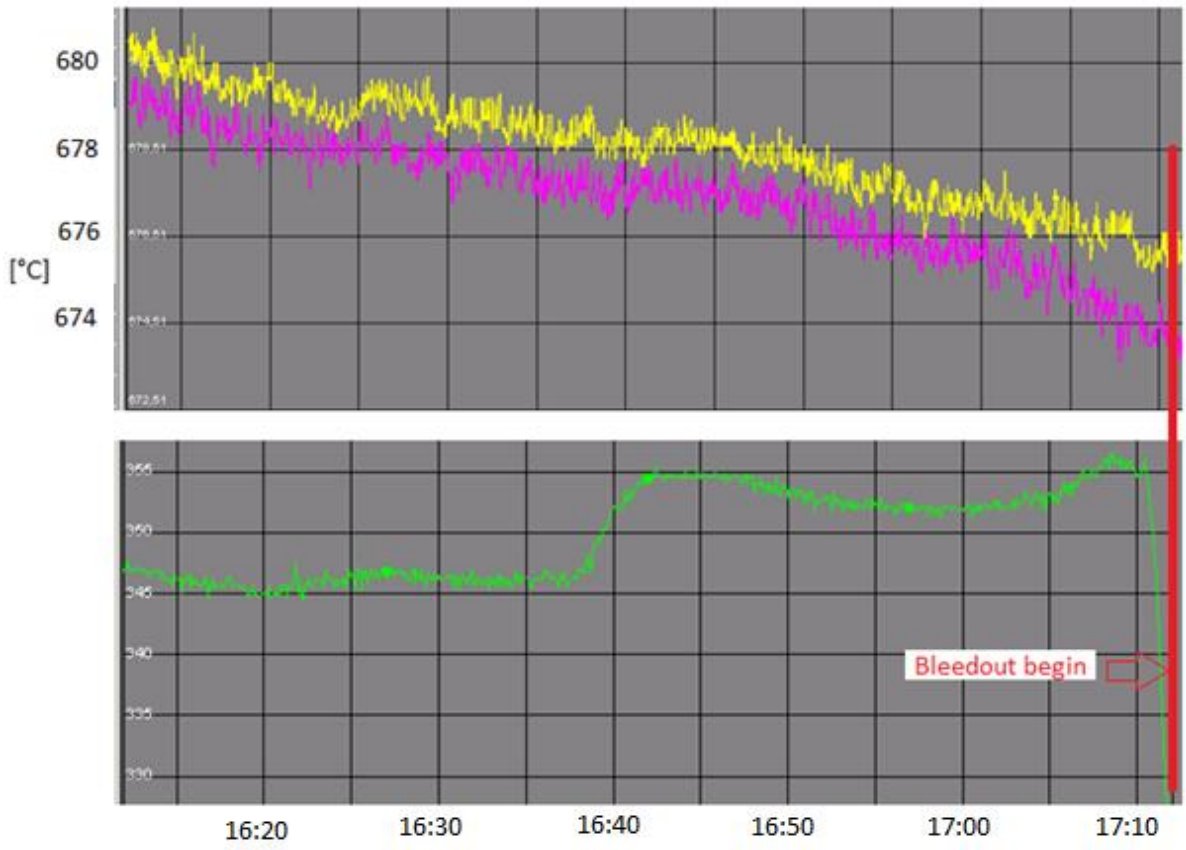

Figure 95 : Bleedout example 5 – Temperature of the aluminium alloy, yellow is tundish A and pink is tundish B (Fjarðaál, 2012)

This research shows that the temperature of the aluminium alloy is critical parameter in this casting process. The control limits needs to be clearer and to reduce or prevent bleedouts, greater stability needs to be achieved. Casting speed and cooling water rate are not showing any indication of bleedouts.

4 Conclusions

The focus of this study was to analyse which casting parameter is most critical for the solidification process and construct a complete numerical model of the solidification process. The study showed that the temperature of the aluminium alloy is the most critical casting parameter in the process. By measurements it was possible to construct a complete numerical model which simulates the current state in the casting process.

When examining the historical data, bleedouts was proved to be the biggest unique problem in the casting process. In most cases in the years 2010 and 2011, the reason for stops at the HDC casting process were bleedouts or in 45% - 47% of all cases. In 36% - 37% of cases there were other problems in the process causing stops and in 17% - 18% of cases was stopped by natural causes (ordinary castings) that is, no problems were encountered. Bleedout castings are on average shorter than ordinary castings and turnaround after bleedout takes longer than turnaround after ordinary castings. It is clear that bleedouts are causing production loss and the up time of the machine is shorter than it should be. To increase the performance of the machine, it needs to prevent bleedouts or reduce the number of cases.

When examining the correlation between bleedouts and change between furnaces (CBF), revealed that in 21,9% of cases bleedout occurred less than hour after CBF. It is considered that if bleedout occur less than hour after CBF, it can possibly be linked together (Sigurðsson, 2012). Under normal circumstances it should be a random distribution when bleedout occurs. Based on random distribution, in 13,5% of cases bleedouts should occur less than hour after CBF. Probability calculations showed that 21,9% is too high percentage and it cancels the theory that this is random distributed. It seems to be that it is possible to link part of the bleedouts to CBF. The difference between 21,9% and 13,5% is 8,4% and then it can be estimated that 8,4% of all bleedouts are caused by CBF. There are two things that can go wrong during CBF, it is wrong temperature of the aluminium alloy and wrong chemical composition of the aluminium alloy. Although this is not high percentage of all bleedouts, it needs to be considered how it is possible to increase the reliability of CBF and prevent those 8,4% bleedouts to occur.

Cooling water rate and casting speed were proved to be stable casting parameters, both in bleedout castings and ordinary castings. The temperature of the aluminium alloy however, was very unstable casting parameter. In bleedout castings the temperature fluctuations were throughout the range of 655°C – 697°C and the average was 675°C ± 5°C. In ordinary castings the temperature fluctuations were throughout the range of 668°C – 682°C and the average was 675°C ± 2°C. In bleedout castings the temperature is more unstable and the fluctuations are high. Today the permissible tolerance for the temperature of the aluminium alloy is ± 5°C and it is difficult to maintain it. To prevent bleedouts, these tolerance needs to be narrower and greater stability must be achieved. It would be desirable to set a target for permissible tolerance of ± 2°C.

To construct the numerical model, measurements were performed on the casting process. Temperature of the aluminium alloy in the tundishes was proved to be equally distributed. This indicates that all the bars in each tundish have the same initial temperature but it was thought that the bars in the middle of each tundish had higher initial temperature because of the inflow of alloy to the tundish. Based on these measurements it can be assumed in

the numerical model that all bars are similar and all bars have the same probability of bleedout. Measurements showed that the cooling water increases by 2,1°C inside the molds, so the heat transfer inside molds can be calculated. These numbers were used in the numerical model to simulate the primary cooling. Based on measurements on the temperature distribution at the surface of the bars, the cooling water rate was proved to be more important for the cooling capacity than the temperature of the cooling water. The heat transfer inside the molds changes in the same proportion as the cooling water rate. However, changing the temperature of the cooling water by 5°C causes 0,07% of change in the heat transfer inside the molds. When the cooling water leaves the mold, 5°C decrease in the cooling water causes 5°C decrease at the surface of the bar. These changes will not occur until 10-20mm from the molds.

To verify the functionality of the numerical model, the model was tested on known case. Comparison was made between the results and it showed that the calculations in the model are correct. Tests on the model indicates that the simulation of current state is successful. The cooling in the model is correct, both primary cooling and secondary cooling. It was tested to generate bleedout, both with too high temperature and too low temperature, and it worked.

According to this study the main cause for bleedouts is the instability in the temperature of aluminium alloy in the tundishes. Further studies should be done on the temperature and examined why the temperature is so unstable. It has been showed that in 8,4% of cases the instability can be linked to the change between furnaces. It is very low percentage and it would be worthy to see why the other 91,6% of cases occurs. By investigating the reason for this instability it is possible to prevent it and at the same time prevent bleedouts or reduce it significantly. The work procedure for the change between furnaces should be investigated to see why there is inconsistency between the furnaces.

The numerical model can be very useful in further studies. It can be used to do sensitivity analysis for the casting parameters and to find the optimum value for each casting parameter based on certain given situation. For example, it could be examined how possibly the performance of the process can be increased. By increasing the casting speed, which casting parameters needs to be changed to maintain the same solidification conditions. The numerical model can also be used to test new aluminium alloys. By changing the thermophysical properties, it is needed to find new values for the casting parameters to maintain the same solidification conditions. The model assumes the same cooling capacity so this is mostly about the correlation between the casting speed and the temperature of the aluminium alloy.

References

ANSYS. (2009). *ANSYS FLUENT 12.0 Theory Guide.* ANSYS Inc.

Dawood, A. (2001). Improving horizontal direct chill casting. *Proceedings of the Australian Asian Conference on Aluminium Cast House Technology*, (pp. 275-283).

Engineering ToolBox. (2012, -). Retrieved April 2012, from www.engineeringtoolbox.com: http://www.engineeringtoolbox.com/water-thermal-properties-d_162.html

Fjarðaál. (2012). *Database of Alcoa Fjarðaál*. Retrieved January 2012, from Database.

Fjarðaál, A. (2011, August). Fjarðaálsfréttir. *4.edition* , p. 15.

Gariepy, B., & Caron, Y. (1991). Light metals. *TMS* (pp. 961-971). Warrendale [PA]: Roy Elwin L.

Grandfield, J., & Dahle, A. (2000). *Modeling of casting and solidification processes 1999.* Seoul Hanrimwon.

Grandfield, J., & McGlade, P. (1996). *Mater Forum* , 20:29-51.

Hamed, M., & Akmal, M. (2005). Int. J. *Material production technology* , 184-198.

Holman, J. (2002). *Heat Transfer 9.edition.* New York: McGraw Hill.

Jorstad, J., Rasmussen, W., & Zalensas, D. (2001). Aluminium cast technology, 2nd Edition. Des Plaines, Il, USA.

Krane, M. J., & Vusanovic, I. (2009). Macrosegregation in horizontal direct chill casting of aluminium slabs. *Materials Science & Technology, vol25* , 102-107.

Nadella, R., Eskin, D. G., Du, Q., & Katgerman, L. (2007). Macrosegregation in direct-chill casting of aluminium alloys. *Progress in Materials Science 53* .

Nadella, R., Eskin, D., & Katgerman, L. (2006). *Material Science Forum* , 519-521 : 1841-1846.

Ross, S. M. (2009). *Probability and statistics for engineers and scientists.*

Sigurðsson, Á. (2012). An interview with Ásgrímur Sigurðsson, Process engineer, from Alcoa Fjarðaál. Tel: +354 470 7700.

SubsTech. (2012). *SubsTech*. Retrieved April 2012, from www.substech.com: http://www.substech.com/dokuwiki/doku.php?id=cast_aluminum_alloys&DokuWiki=d404e75606031f9bf1386610391719ad

Suyitno, Eskin, D. G., & Katgerman, L. (2006). Structure observation related to hot tearing of Al-Cu billets produced by direct-chill casting. *Material Science & Engineering A 420* , 1-7.

Suyitno, Kool, W. H., & Katgerman, L. (2004, September). Finite Element Method Simulation of Mushy Zone Behavior during Direct-Chill Casting of an Al-4.5 Pct CU Alloy. *Metallurgical and Materials Transactions, volume 35A* , pp. 2917-2926.

Versteeg, H. K., & Malalasekera, W. (2007). *An Introduction to COMPUTATIONAL FLUID DYNAMICS, The Finite Volume Method.* Harlow: Pearson Education Limited.

Wertli, T. (1986). Horizontal continuous casting technology in the eighties, Metallurgia 53. 192-194.

Y.Liu, G. (2009). *Effect of Ageing heat Treatment on the Hardness and Tensile Properties of Aluminium A356.2 Casting Alloy, Master's thesis.* Hamilton, Ontario: McMaster University.

Zhao, Z., Cui, J., Dong, J., & Zhang, B. (2007). Effect of low-magnetic field on microstructures and macrosegregation of horizontal direct chill casting 7075 aluminium alloy. *Journal of Materials Processing Technology 182* , 185-190.

Zuidema, J., Katgerman, L., Opstelten, I., & Rabenberg, J. (2001). Light metals. *TMS* (pp. 873-878). Warrendale [PA]: Anjier JI.